Thèse de Junheng Shi, Université de Lille, 2018

SHANGHAI INSTITUTE OF OPTICS AND FINE MECHANICS,
UNIVERSITY OF CHINESE ACADEMY OF SCIENCES
AND
LABORATOIRE PHLAM,
UNIVERSITÉ LILLE 1, FRANCE

DOCTORAL THESIS

Quantum Temporal Imaging

Author:
Junheng SHI

Supervisors:
Prof. Shensheng HAN
Prof. Mikhail I. KOLOBOV

A thesis submitted in fulfillment of the requirements for the degree of Doctor of Philosophy

August, 2018

© 2018 Tous droits réservés.

lilliad.univ-lille.fr

© 2018 Tous droits réservés.

lilliad.univ-lille.fr

Thèse de Junheng Shi, Université de Lille, 2018

Declaration of Authorship

I, Junheng SHI, declare that this thesis titled, "Quantum Temporal Imaging" and the work presented in it are my own. I confirm that:

- This work was done wholly or mainly while in candidature for a research degree at this University.
- Where any part of this thesis has previously been submitted for a degree or any other qualification at this University or any other institution, this has been clearly stated.
- Where I have consulted the published work of others, this is always clearly attributed.
- Where I have quoted from the work of others, the source is always given. With the exception of such quotations, this thesis is entirely my own work.
- I have acknowledged all main sources of help.
- Where the thesis is based on work done by myself jointly with others, I have made clear exactly what was done by others and what I have contributed myself.

Signed:

Date:

© 2018 Tous droits réservés.

lilliad.univ-lille.fr

© 2018 Tous droits réservés.

lilliad.univ-lille.fr

"It then becomes clear and certain to him that he does not know a sun and an earth, but only an eye that sees a sun, a hand that feels an earth; that the world around him is there only as representation, in other words, only in reference to another thing, namely that which represents, and this is himself."

Arthur Schopenhauer

© 2018 Tous droits réservés.

lilliad.univ-lille.fr

© 2018 Tous droits réservés.

lilliad.univ-lille.fr

Thèse de Junheng Shi, Université de Lille, 2018

SHANGHAI INSTITUTE OF OPTICS AND FINE MECHANICS,
UNIVERSITY OF CHINESE ACADEMY OF SCIENCES
AND
LABORATOIRE PHLAM,
UNIVERSITÉ LILLE 1, FRANCE

Abstract

Doctor of Philosophy

Quantum Temporal Imaging

by Junheng SHI

Temporal imaging, like its spatial counterpart, is rooted in the combination of a simple and universal concept - linear system, or even a shift-invariant linear system with an useful tool - Fourier analysis. The first aim of this thesis to show this nature of temporal imaging by the operator algebra we developed. That a variety of temporal imaging systems are just combinations of a few operations.

However, as an imaging theory, gaining a perfect understanding of its nature is only half of the journey, the final purpose should be to serve an application. For this thesis, this purpose is to explore the application of temporal imaging in quantum domains. Because despite the popularity of classical temporal imaging with various applications such as in ultrafast signal processing, applying temporal imaging to manipulate nonclassical light is far from being well-established. There are two major jobs to be done.

First, to expand its territory such as finding new applications for existing techniques or discovering new schemes with better performance for applications needed. For this purpose, we try to use the existing four-wave mixing based time lenses on nonclassical light such as broadband squeezed light to see whether the squeezing property is still preserved. And we propose a new time lens based on counter-propagating Bragg-scattering, we show that it has better performances than other nonlinear process based time lenses.

Second, to establish an evaluation system to accurately, or even quantitatively assess the performances of existing schemes, in this particular case, different types of time lens and to study the aberrations that deteriorate the performances. For this purpose, we use the impulse response of a linear system as a tool to evaluate the resolutions of various time lenses for quantum temporal imaging and we study the restrictions of quantum temporal imaging on resolution and quantum field of view due to the preservation of quantum properties and phase matching conditions.

© 2018 Tous droits réservés.

lilliad.univ-lille.fr

© 2018 Tous droits réservés.

lilliad.univ-lille.fr

Thèse de Junheng Shi, Université de Lille, 2018

Acknowledgements

Some people grow up twice in their lives, first time as children and teenagers, second time as PhD candidates. There is simply too much to try and to learn that without the help from others, it would be impossible for me to finish this journey. I give them my most sincere gratitude.

I am grateful to both my thesis advisors for their expertise, guidance and support, Professor Mikhail I. Kolobov and Professor Shensheng Han. Professor Kolobov was always calm and patient to teach no matter how slow I was to follow, his knowledge is significant to my research and he spent a lot of time and efforts refining my writings for each of my publications. Professor Han was always supportive and concerned with my research. He went to great length to help me as much as he could. He gave me many precious advices even to this day I could remember clearly.

I would like to thank Dr. Giuseppe Patera for his tremendous help during my stay in France, not only in research, but also in life, in administration stuff. He never hesitated to help or discuss when I went to him. I was so lucky to have a supervisor like him. It's a pity he was not able to attend my PhD defense.

I wish to thank Dr. Youzhen Gui for early-stage guidance and pushing me to work harder, she was a good example herself.

I also wish to thank Dr. Dmitri B. Horoshko for the educational discussions we had and the inspirations I received.

How can I skip my best friends in the university, Tobias lipfert and Alexey Tikan. Thanks for the physics club every Sunday and the adventures every Friday evening. Thank you so much for drinking my beer and finishing my sentence:) Those were the best memories I had in France. Hope they are doing great.

And I owe a great deal of thanks to all the friends that I had in France, to Aurélien and Bea, who painted my days with colors; to Lamyae, Mardia, Eva and Raouf who shared the office with me, who offered much more help than I could ask; to Katharina, Anya, Julien, Ajay, Cherlene, Yanting, Morten, Antoine for all the happy time we spent together.

I shall thank my Chinese friends in the Chinese version of this thesis.

Most of all, I would like to express my gratitude to my parents. It was only the elapse of time that made me realize how much love and support they have offered me without asking for return.

Finally, I pay my tributes to those who ignited sparks into the darkness of this absurd world and shed light on my thought and heart, Arthur Schopenhauer, Karl Marx, Kenji Miyazawa, Ludwig von Beethoven and Lu Xun.

© 2018 Tous droits réservés.

lilliad.univ-lille.fr

© 2018 Tous droits réservés.

lilliad.univ-lille.fr

Thèse de Junheng Shi, Université de Lille, 2018

Contents

© 2018 Tous droits réservés.

lilliad.univ-lille.fr

Thèse de Junheng Shi, Université de Lille, 2018

© 2018 Tous droits réservés.

lilliad.univ-lille.fr

Thèse de Junheng Shi, Université de Lille, 2018

List of Figures

© 2018 Tous droits réservés.

lilliad.univ-lille.fr

Thèse de Junheng Shi, Université de Lille, 2018

© 2018 Tous droits réservés.

lilliad.univ-lille.fr

Thèse de Junheng Shi, Université de Lille, 2018

List of Tables

© 2018 Tous droits réservés.

lilliad.univ-lille.fr

© 2018 Tous droits réservés.

lilliad.univ-lille.fr

Dedicated to my parents,
Xiaoqiu CHEN & Shiwang SHI.

© 2018 Tous droits réservés.

lilliad.univ-lille.fr

© 2018 Tous droits réservés.

lilliad.univ-lille.fr

Thèse de Junheng Shi, Université de Lille, 2018

Chapter 1

Introduction

1.1 Organization of the Thesis

In Chapter 2, we show mathematically the concept of space-time duality by deriving the equations for Fresnel diffraction and Group velocity dispersion. Then we develop the operator algebra for temporal imaging. We define four operators and derive the commutation relations between each other. After that, we use this approach to obtain various classical temporal imaging systems.

In chapter 3, we first give the quantum treatment of four-wave mixing (FWM) processes including PC FWM and PP FWM and counter-propagating FWM. Then we visit the multimode squeezing, starting by reviewing the concepts of single-mode coherent state and squeezed state and by deriving the temporal fluctuation of light we show the presence of shot noise and how to produce broadband squeezed light. In the end, we combine all the preparations to calculate the effect of different FWM time lenses on broadband squeezed light.

Chapter 4 is devoted to examine the resolution and field of view (FOV) in quantum temporal imaging. We begin by obtaining the sum-frequency generation (SFG) time lens because it's the main tool to show the causes of aberrations. Based on the concept of linear system, we derive the impulse response and the definition of resolution for temporal imaging before we use them to evaluate a variety of time lenses including a brand new scheme with a promise of better performance. Finally we examine the restrictions on quantum temporal imaging including the restriction on the pump bandwidth and on resolution and FOV.

Chapter 5 focuses on how quantum temporal imaging scheme would affect the nonclassical property of single photons produced by single-photo source by comparing the normalized second order correlation function and squeezing spectrum.

1.2 Contributors of the Work

The work presented in this thesis is done by the author himself under the supervision of Prof. Mikhail I. Kolobov, Dr. Giuseppe Patera from PhLAM, Université Lille 1 and Prof. Shensheng Han from Shanghai Institute of Optics and Fine Mechanics, Chinese Academy of Sciences except for the topic on restrictions on quantum temporal imaging which was done in collaboration also with Dr. Dmitri B. Horoshko.

© 2018 Tous droits réservés.

lilliad.univ-lille.fr

© 2018 Tous droits réservés.

lilliad.univ-lille.fr

Thèse de Junheng Shi, Université de Lille, 2018

Chapter 2

Classical Temporal Imaging

2.1 Space-Time Duality

The development of optics goes through the development of physics itself. Starting from Newton's Corpuscular theory of light, to the wave theory by Huygens and Fresnel, to electromagnetic theory which was inspired by Faraday and established by Maxwell, reaching the land of wave-particle duality thanks to the early founders of quantum mechanics, every time optics moves forward, it pushes forward the boundary of physics. But it does not mean that the old territories should be deserted and forgotten. The wave theory of light based on Fresnel's works, shone in the nineteenth century, even in the age when the kingdom of classical optics is dominated by Maxwell's equations, combined with Fourier analysis used for possessing signals, could sprout a new branch – Fourier optics[23]. That is because unless the permittivity of the medium a wave passes depends on position or the size of the confinement in space is comparable to the wavelength of a wave which induce coupling between the various components of the electric field, otherwise what we obtained from Maxwell's equations remains a scalar theory, in other words, a linear system. For a physical phenomena with the property of linearity, its physical quantities could be modeled as system inputs (called stimuli) and system outputs (called response) and the response resulted from many stimuli equals to the sum of the responses resulted from each individual stimuli. Needless to say, Fourier analysis is a perfect tool to deal with linear system since complex-exponential functions are the eigenfunctions for the Linear Shift-Invariant (LSI) system such as Fresnel diffraction. It is thanks to this tool that enables the characterization and manipulation of spatial wavefront and Fourier spectrum including scaling, Fourier transform and filtering etc.

On the other side, the invention and development of laser in the late twentieth century gave birth to the short and ultrashort pulse with many advantages such as high peak power, short duration and long coherence time. Its wide ranges of applications in physics pushes people to find better ways of processing it[11, 13, 22, 55, 60, 65, 67, 72, 73] .

The stage had been set and the story began with the discovery of space-time duality.

2.1.1 Fresnel Diffraction

We skip the derivation from Maxwell's equations to Fresnel diffraction which contains a series of approximations. The only approximation should not be neglected is

© 2018 Tous droits réservés.

lilliad.univ-lille.fr

Thèse de Junheng Shi, Université de Lille, 2018

the paraxial approximation.

When a light wave is traveling in free space (diffraction) and its frequency is independent of its position, it satisfy the Helmholtz equation

$$(\nabla^2 + k^2)\mathbf{E}(x, y, z) = 0 \tag{2.1}$$

where the wavenumber $k = \frac{2\pi}{\lambda}$, z axis is the direction of the propagation, λ is the wavelength.

According to the paraxial approximation, we could separate the fast-varying exponential factor

$$\mathbf{E}(x, y, z) = \mathcal{E}(x, y, z)\mathrm{e}^{\mathrm{i}kz} \tag{2.2}$$

where $\mathcal{E}(x, y, z)$ is the slowly varying envelope respect to z axis.

Put Eq.(2.2) back to Eq.(2.1) and neglect the term $\frac{\partial^2}{\partial z^2}\mathcal{E}(x, y, z)$ according to the paraxial approximation, we could obtain

$$\frac{\partial}{\partial z}\mathcal{E}(x, y, z) - \frac{\mathrm{i}}{2k}\left(\frac{\partial^2}{\partial x^2} + \frac{\partial^2}{\partial y^2}\right)\mathcal{E}(x, y, z) = 0 \tag{2.3}$$

which is called Paraxial Helmholtz equation.

Fourier transform Eq.(2.3) with respect to x and y ($x \to k_x$; $y \to k_y$) we obtain

$$\widetilde{\mathcal{E}}(\xi, k_x, k_y) = \widetilde{\mathcal{E}}(0, k_x, k_y)\mathrm{e}^{-\mathrm{i}\frac{\xi}{2k}(k_x^2 + k_y^2)} \tag{2.4}$$

where the propagation distance $\xi = z - z_0$, z_0 is the starting location of the propagation.

As you could see, Fresnel diffraction is equivalent to multiplying the initial angular spectrum with a quadratic phase factor with respect to spatial frequency.

2.1.2 Group Velocity Dispersion

Now let's turn to Group Velocity Dispersion(GVD) under the quasi-monochromatic approximation.

A linear-polarized plane wave is presumed to pass through a dispersive medium along z-axis. The electric field in x and y axes do not depend on z and t and therefore could be neglected. It satisfies the wave function.

$$(\frac{\partial^2}{\partial z^2} - \frac{1}{c^2}\frac{\partial^2}{\partial t^2})E(z, t) = \mu_0\frac{\partial^2}{\partial t^2}P^L(z, t) \tag{2.5}$$

$$P^L(z, t) = \epsilon_0\int_0^\infty \mathrm{d}t'\ R^{(1)}(t')E(z, t - t') \tag{2.6}$$

where ϵ_0 is the vacuum permittivity, μ_0 is the vacuum permeability, $R^{(1)}(t)$ is the response function of the medium, so for $t' < 0$, it equals to zero. Note on right of the equal sign there is only the linear polarization term $P^L(z, t)$ in this case.

Fourier transform Eq.(2.5) and Eq.(2.6) combined with respect to t ($t \to \omega$) we obtain

$$(\frac{\partial^2}{\partial z^2} + \frac{\omega^2}{c^2})\widetilde{E}(z, \omega) = -\frac{\omega^2}{c^2}\chi^{(1)}(\omega)\widetilde{E}(z, \omega) \tag{2.7}$$

© 2018 Tous droits réservés.

lilliad.univ-lille.fr

Thèse de Junheng Shi, Université de Lille, 2018

where the linear susceptibility

$$\chi^{(1)}(\omega) = \int_0^{+\infty} \mathrm{d}t\ R^{(1)}(t)\mathrm{e}^{\mathrm{i}\omega t} \tag{2.8}$$

In this way we obtain the Helmholtz equation

$$\left(\frac{\partial^2}{\partial z^2} + k^2(\omega)\right)\widetilde{E}(z,\omega) = 0 \tag{2.9}$$

where the wavenumber

$$k^2(\omega) = \frac{\omega^2\epsilon(\omega)}{c^2} \tag{2.10}$$

$$\epsilon(\omega) = 1 + \chi^{(1)}(\omega) \tag{2.11}$$

note that the imaginary part of $\epsilon(\omega)$ is absorption coefficient which we do not take into consideration now.

After we obtain the Helmholtz equation, there are two steps to take. The First step is to separate the fast-varying exponential factor. Similar to the paraxial approximation, we presume that the frequency is narrowly distributed with its center at ω_0.

$$E(z,t) = \frac{1}{2}\left[\mathcal{E}(z,t)\mathrm{e}^{-\mathrm{i}\omega_0 t + \mathrm{i}k_0 z} + c.c\right] \tag{2.12}$$

where $\mathcal{E}(z,t)$ is the slowly varying envelope, $k_0 = k(\omega_0)$. For simplicity, we only consider the positive frequency.

We also need the slowly varying envelope in frequency domain:

$$\begin{aligned}\widetilde{E}(z,\omega) &= \int \frac{\mathrm{d}t}{\sqrt{2\pi}}\ E(z,t)\mathrm{e}^{\mathrm{i}\omega t} \\ &= \frac{1}{2}e^{\mathrm{i}k_0 z}\int \frac{\mathrm{d}t}{\sqrt{2\pi}}\ \mathcal{E}(z,t)\mathrm{e}^{\mathrm{i}\Omega t} \\ &= \frac{1}{2}\mathrm{e}^{\mathrm{i}k_0 z}\widetilde{\mathcal{E}}(z,\Omega)\end{aligned} \tag{2.13}$$

where $\Omega = \omega - \omega_0$.

Put Eq.(2.13) into Eq.(2.9) we obtain

$$\frac{\partial^2}{\partial z^2}\widetilde{\mathcal{E}}(z,\Omega) + 2\mathrm{i}k_0\frac{\partial}{\partial z}\widetilde{\mathcal{E}}(z,\Omega) + (k^2(\omega) - k_0^2)\widetilde{\mathcal{E}}(z,\Omega) = 0 \tag{2.14}$$

With the approximations that $k^2(\omega) - k_0^2 \approx 2k_0(k(\omega) - k_0)$ and $\left|\frac{\partial}{\partial z}\widetilde{\mathcal{E}}(z,\Omega)\right| \ll |k_0\widetilde{\mathcal{E}}(z,\Omega)|$, we neglect $\frac{\partial^2}{\partial z^2}\widetilde{\mathcal{E}}(z,\Omega)$ and obtain

$$\frac{\partial}{\partial z}\widetilde{\mathcal{E}}(z,\Omega) - \mathrm{i}(k(\omega) - k_0)\widetilde{\mathcal{E}}(z,\Omega) = 0 \tag{2.15}$$

© 2018 Tous droits réservés.

lilliad.univ-lille.fr

Thèse de Junheng Shi, Université de Lille, 2018

The second step is to expand $k(\omega)$ with respect to ω_0:

$$k(\omega) = k_0 + k_0'\Omega + \frac{1}{2}k_0''\Omega^2 + ... \tag{2.16}$$

where $k_0' = \frac{\partial k(\omega)}{\partial \omega}\Big|_{\omega=\omega_0}, k_0'' = \frac{\partial^2 k(\omega)}{\partial \omega^2}\Big|_{\omega=\omega_0}$. Note we only expand $k(\omega)$ to the second order here.

Put the expansion Eq.(2.16) into Eq.(2.15) we obtain

$$\frac{\partial}{\partial z}\widetilde{\mathcal{E}}(z,\Omega) - \mathrm{i}k_0'\Omega\,\widetilde{\mathcal{E}}(z,\Omega) - \mathrm{i}\frac{k_0''}{2}\Omega^2\,\widetilde{\mathcal{E}}(z,\Omega) = 0 \tag{2.17}$$

Using the inverse Fourier transform Eq.(2.17) ($\Omega \to t$) we obtain

$$\frac{\partial}{\partial z}\mathcal{E}(z,t) + k_0'\frac{\partial}{\partial t}\mathcal{E}(z,t) + \mathrm{i}\frac{k_0''}{2}\frac{\partial^2}{\partial t^2}\mathcal{E}(z,t) = 0 \tag{2.18}$$

To get rid of the second term, we switch to the traveling-wave coordinate:

$$\tau = (t - t_0) - k_0'(z - z_0) \tag{2.19}$$

$$\xi = z - z_0 \tag{2.20}$$

where t_0 and z_0 set the location of $\tau = 0$ within a waveform, mostly, at the center of a waveform.

Through the transformation of the coordinates:

$$\frac{\partial}{\partial z} = \frac{\partial}{\partial \tau}(-k_0') + \frac{\partial}{\partial \xi} \tag{2.21}$$

$$\frac{\partial}{\partial t} = \frac{\partial}{\partial \tau} \tag{2.22}$$

Eq.(2.18) becomes

$$\frac{\partial}{\partial \xi}\mathcal{E}(\xi,\tau) + \frac{\mathrm{i}k_0''}{2}\frac{\partial^2}{\partial \tau^2}\mathcal{E}(\xi,\tau) = 0 \tag{2.23}$$

From the coordinate transformation (2.19) it is easy to see that k_0' is the reciprocal of the group velocity. This is more evident when $k(\omega)$ is only expanded to the first order, we could obtain

$$\mathcal{E}(\xi,\tau) = \mathcal{E}(0,\tau) \tag{2.24}$$

under the traveling-wave coordinate, the waveform is not dependent on ξ because it is propagating with the group velocity inside the medium.

Since k_0' is regarded as the reciprocal of the group velocity, k_0'' could be regarded as the derivative of group velocity on ω, which is called GVD. Multiplying k_0'' with the propagation distance we obtain the total delay of group velocity, which is called Group Delay Dispersion (GDD), commonly denoted as D.

With these in mind, we Fourier transform Eq.(2.23) ($\tau \to \Omega$) once more and obtain

$$\frac{\partial}{\partial \xi}\widetilde{\mathcal{E}}(\xi,\Omega) - \frac{\mathrm{i}k_0''}{2}\Omega^2\widetilde{\mathcal{E}}(\xi,\tau) = 0 \tag{2.25}$$

© 2018 Tous droits réservés.

lilliad.univ-lille.fr

Thèse de Junheng Shi, Université de Lille, 2018

whose solution is

$$\widetilde{\mathcal{E}}(\xi,\Omega)=\widetilde{\mathcal{E}}(0,\Omega)\mathrm{e}^{\mathrm{i}\frac{D}{2}\Omega^2} \tag{2.26}$$

2.1.3 Space-Time Duality

By comparing Eq.(2.3) and Eq.(2.23) we discover that the spatial diffraction equation under the paraxial approximation shares similar mathematical form with the temporal dispersion equation under the quasi-monochromatic approximation. This similarity opens the gate for connecting the manipulation of spatial wavefront which is the surface of identical phase of a spatial wave and temporal waveform which is the shape of a wave in temporal domain. Wavefront is a distribution over spatial coordinates while waveform is a distribution over time. When the spatial wavefront and the temporal waveform all propagate along the z-axis, the two degrees of freedom in space x and y of the wavefront corresponds to the degree of freedom in time t of the waveform, in other words, the wavefront is analogous to the waveform while the angular spectrum is analogous to the spectrum. This is what is called the space-time duality.

Space-time duality does not originate from Fourier optics, but a technique named pulse compression which is commonly used in radar. In 1960, Klauder et al. proposed the concept of chirp radar[30], which could be used to compress at the receiver a long-duration signal emitted, solving the problem that increasing the duration of the signal could increase the SNR, but decrease the resolution. The basic idea behind pulse compression is to provide different frequency parts of the signal different group velocity compensations according to its frequency so all frequency parts could reach the receiver at the same time, thus obtaining a short-duration signal. It was such a simple yet useful idea. People soon seek its application for compressing light pulse. They tried many ways to achieve the dispersion, for example, the LiNbO2 phase modulator [19] which was used in the beginning, a pair of diffraction gratings [69] and a cell containing Rb vapor said to have group velocity dispersion approximately 1000 times larger than the nonresonant methods [24], until fiber came to use[25].

Nevertheless we know that Fresnel diffraction is not the only building block for wavefront manipulation in Fourier optics, the other one is lens which provides a quadratic phase modulation in real space. As we have found the temporal counterpart for Fresnel diffraction, now we have to find or construct the counterpart for spatial lens, so called time lens. We need this time lens to provide the waveform a quadratic phase modulation in time. These two building blocks enable us to characterize and manipulate waveform and spectrum of a light pulse–*Temporal Imaging*.

Spatial Imaging	Temporal Imaging
Diffraction: $\mathrm{e}^{-\mathrm{i}\frac{\xi}{2k}(k_x^2+k_y^2)}$	Dispersion: $\mathrm{e}^{\mathrm{i}\frac{D}{2}\Omega^2}$
Spatial Lens: $\mathrm{e}^{-\mathrm{i}\frac{k}{2\xi}(x^2+y^2)}$	Time Lens: $\mathrm{e}^{\mathrm{i}\frac{1}{2D}\tau^2}$

TABLE 2.1: Space-Time Duality

© 2018 Tous droits réservés.

lilliad.univ-lille.fr

Thèse de Junheng Shi, Université de Lille, 2018

2.2 Operator Algebra for Temporal Imaging

Before we look into how temporal imaging works, how dispersion and time lens can build basic temporal imaging systems such as Fraunhofer dispersion, single lens temporal imaging system etc, we develop a mathematic tool based on the operator algebra for Fourier optics first proposed by Nazarathy and Shamir in 1980 [54] and illustrated in detail by Goodman in his book *Introduction to Fourier Optics* [23].

The operator algebra does not only simplify, but also clarify the calculations in Fourier optics. As we know, calculations like Fresnel diffraction and Fourier transform include a lot of integrations. It's quite easy to be lost in these back-and-forth integrations, not easy to guess the functionality of the whole imaging system. Operator algebra on the other hand, concludes all calculations to three basic operators, each defined by its functionality, scaling, Fourier transform and multiplying by a quadratic phase. So our job is merely reducing the number of the operators describing a system to the least by exchanging the positions of the operators to cancel each other. Then the overall effect of the system is shown by the operators left.

As a matter of fact, operator algebra suits temporal imaging even better because temporal imaging is one-dimensional and basically only deals with coherent light. Also Gaussian shape is quite common in temporal light pulse. Gaussian shape could be regarded as a special case of quadratic phase multiplication operator by letting the coefficient be imaginary.

2.2.1 Definitions of Operators

First we have to define the operators. There are four in total, three of them are basic. An operator could act on a waveform or a spectrum, so here we use general notations such as $f(x)$ and $g(x)$ where x could be t or Ω. More often, they are denoted as f and g for convenience.

Scaling operator $\mathcal{V}$

The definition of scaling operator is

$$\mathcal{V}[s]g(x) = g(sx) \tag{2.27}$$

It serves the functionality of scaling a waveform or a spectrum without changing its shape. It has following properties:

$$\mathcal{V}[s_1]\mathcal{V}[s_2] = \mathcal{V}[s_2]\mathcal{V}[s_1] = \mathcal{V}[s_1 s_2] \tag{2.28}$$

$$\mathcal{V}^{-1}[s] = \mathcal{V}[\frac{1}{s}] \tag{2.29}$$

$$\mathcal{V}[s]fg = (\mathcal{V}[s]f)\mathcal{V}[s]g \tag{2.30}$$

© 2018 Tous droits réservés.

lilliad.univ-lille.fr

Thèse de Junheng Shi, Université de Lille, 2018

Fourier transform operator $\mathcal{F}$

As the name indicates, the functionality of this operator is to Fourier transform, hence its definition:

$$\mathcal{F}g(x) = \int \frac{\mathrm{d}x}{\sqrt{2\pi}} \mathrm{e}^{\mathrm{i}yx} g(x) \tag{2.31}$$

And its inverse operator

$$\begin{aligned} \mathcal{F}^{-1}g(x) &= \int \frac{\mathrm{d}x}{\sqrt{2\pi}}\, \mathrm{e}^{-\mathrm{i}yx} g(x) \\ &= \int \frac{\mathrm{d}x}{\sqrt{2\pi}}\, \mathrm{e}^{\mathrm{i}(-y)x} g(x) \\ &= \mathcal{V}[-1]\mathcal{F}g(x) \end{aligned} \tag{2.32}$$

which indicates the inverse Fourier transform operator could be decomposed into scaling operator and Fourier transform operator.

It also has the property that

$$\mathcal{F}(fg) = (\mathcal{F}f) * \mathcal{F}g \tag{2.33}$$

according to the convolution theorem.

Here the convolution is defined as

$$f(x) * g(x) = \int \frac{\mathrm{d}x'}{\sqrt{2\pi}} f(x - x') g(x') \tag{2.34}$$

Quadratic phase multiplication operator $\mathcal{Q}$

This operator is the essence of Fourier optics as well as in temporal imaging. As could be seen in Table 2.1, Fresnel diffraction or lens, its true nature is to multiply a quadratic phase in the corresponding domain. For this reason we define:

$$\mathcal{Q}[a]g(x) = \mathrm{e}^{\mathrm{i}\frac{a}{2}x^2} g(x) \tag{2.35}$$

And it has following properties:

$$\mathcal{Q}[a_1]\mathcal{Q}[a_2] = \mathcal{Q}[a_2]\mathcal{Q}[a_1] = \mathcal{Q}[a_1 + a_2] \tag{2.36}$$

$$\mathcal{Q}^{-1}[a] = \mathcal{Q}[-a] \tag{2.37}$$

$$\mathcal{Q}[a]fg = f\mathcal{Q}[a]g \tag{2.38}$$

Propagation operator $\mathcal{P}$

Except for these three basic operators, there is one more, in [54] it was named the Fresnel free-space propagation operator, to describe Fresnel diffraction in free space. In temporal imaging, light wave propagates in a dispersive medium instead. So it is named propagation operator.

Nevertheless this operator has another function. As we know, the effect of free space propagation, what we called Fresnel diffraction in real space, is just another

© 2018 Tous droits réservés.

lilliad.univ-lille.fr

Thèse de Junheng Shi, Université de Lille, 2018

quadratic phase multiplication in Fourier space. The effect of lens, what we considered quadratic phase multiplication in real space, could also be regarded as a Fresnel diffraction in Fourier space. So this operator is merely the quadratic phase multiplication operator in the conjugate domain, if we keep in mind the duality of real space and Fourier space.

In spatial Fourier optics, however, the two effects described above can not be united in one operator. The Fresnel free-space propagation operator can not be used to describe propagation in spatial lens in Fourier space. Fortunately for temporal imaging, there is no such limitation. As we shall see, propagation operator works for propagation in dispersive medium as well as in time lens. But first, they are defined separately:

For propagation in dispersive medium in temporal domain:

$$\mathcal{P}_1[D] = \mathcal{F}^{-1}\mathcal{Q}[D]\mathcal{F} \tag{2.39}$$

For propagation in time lens in frequency domain:

$$\mathcal{P}_2[D] = \mathcal{F}\mathcal{Q}[D]\mathcal{F}^{-1} \tag{2.40}$$

They are identical because

$$\begin{aligned} &\mathcal{P}_2[D] \\ =&\mathcal{F}\mathcal{Q}[D]\mathcal{F}^{-1} \\ =&\mathcal{F}\mathcal{Q}[D]\mathcal{V}[-1]\mathcal{F} \\ =&\mathcal{F}\mathcal{V}[-1]\mathcal{Q}[D]\mathcal{F} \\ =&\mathcal{F}^{-1}\mathcal{Q}[D]\mathcal{F} \\ =&\mathcal{P}_1[D] \end{aligned} \tag{2.41}$$

which indicates the duality of time and frequency.

The other way to decompose propagation operator is use analogous form as Fresnel diffraction. First we obtain the Fourier transform of quadratic phase $\exp\{\mathrm{i}\frac{D}{2}\Omega^2\}$:

$$\int \frac{\mathrm{d}\Omega}{\sqrt{2\pi}}\,\mathrm{e}^{-\mathrm{i}\Omega t}\mathrm{e}^{\mathrm{i}D\Omega^2/2} = \frac{\mathrm{e}^{\mathrm{i}\pi/4}}{\sqrt{D}}\mathrm{e}^{-\mathrm{i}\frac{t^2}{2D}} \tag{2.42}$$

then use the convolution theorem:

$$\begin{aligned} \mathcal{P}[D]f_1(t_1) =&\frac{\mathrm{e}^{\mathrm{i}\pi/4}}{\sqrt{D}}\int \frac{\mathrm{d}t_1}{\sqrt{2\pi}}\mathrm{e}^{-\mathrm{i}\frac{(t_2-t_1)^2}{2D}} f_1(t_1) \\ =&\frac{\mathrm{e}^{\mathrm{i}\pi/4}}{\sqrt{D}}e^{-\mathrm{i}\frac{t_2^2}{2D}}\int \frac{\mathrm{d}t_1}{\sqrt{2\pi}}\,\mathrm{e}^{\mathrm{i}\frac{t_2}{D}t_1}\{\mathrm{e}^{-\mathrm{i}\frac{t_1^2}{2D}}f_1(t_1)\} \\ =&\frac{\mathrm{e}^{\mathrm{i}\pi/4}}{\sqrt{D}}\mathcal{Q}\left[-\frac{1}{D}\right]\mathcal{V}\left[\frac{1}{D}\right]\mathcal{F}\mathcal{Q}\left[-\frac{1}{D}\right]f_1(t_1) \end{aligned} \tag{2.43}$$

Propagation operator has the property that

$$\mathcal{P}[D_1]\mathcal{P}[D_2] = \mathcal{P}[D_2]\mathcal{P}[D_1] = \mathcal{P}[D_1 + D_2] \tag{2.44}$$

© 2018 Tous droits réservés.

lilliad.univ-lille.fr

Thèse de Junheng Shi, Université de Lille, 2018

because

$$\begin{aligned}\mathcal{P}[D_1]\mathcal{P}[D_2] &= \mathcal{F}^{-1}\mathcal{Q}[D_1]\mathcal{F}\mathcal{F}^{-1}\mathcal{Q}[D_2]\mathcal{F} \\ &= \mathcal{F}^{-1}\mathcal{Q}[D_1]\mathcal{Q}[D_2]\mathcal{F} \\ &= \mathcal{F}^{-1}\mathcal{Q}[D_1+D_2]\mathcal{F} \\ &= \mathcal{P}[D_1+D_2]\end{aligned} \tag{2.45}$$

So its inverse operator is

$$\mathcal{P}^{-1}[D] = \mathcal{P}[-D] \tag{2.46}$$

2.2.2 Commutation Relations between the Operators

Since the basic idea of operator calculation is to commute operators so that we could cancel them as much as possible, we need the commutation relations for all operators as shown in Table 2.2. For convenience, $\mathcal{F}^{-1}$ is also included in the table.

	$\mathcal{V}$	$\mathcal{F}$	$\mathcal{F}^{-1}$	$\mathcal{Q}$	$\mathcal{P}$
$\mathcal{V}$	$\mathcal{V}[s_1]\mathcal{V}[s_2]$ $= \mathcal{V}[s_1 s_2]$	$\mathcal{V}[s]\mathcal{F}$ $= \frac{1}{\lvert s\rvert}\mathcal{F}\mathcal{V}\left[\frac{1}{s}\right]$	$\mathcal{V}[s]\mathcal{F}^{-1}$ $= \frac{1}{\lvert s\rvert}\mathcal{F}^{-1}\mathcal{V}\left[\frac{1}{s}\right]$	$\mathcal{V}[s]\mathcal{Q}[a]$ $= \mathcal{Q}[as^2]\mathcal{V}[s]$	$\mathcal{V}[s]\mathcal{P}[D]$ $= \mathcal{P}\left[\frac{D}{s^2}\right]\mathcal{V}[s]$
$\mathcal{F}$	$\mathcal{F}\mathcal{V}[s]$ $= \frac{1}{\lvert s\rvert}\mathcal{V}\left[\frac{1}{s}\right]\mathcal{F}$	$\mathcal{F}\mathcal{F}$ $= \mathcal{V}[-1]$	1	$\mathcal{F}\mathcal{Q}[D]$ $= \mathcal{P}[D]\mathcal{F}$	$\mathcal{F}\mathcal{P}[D]$ $= \mathcal{Q}[D]\mathcal{F}$
$\mathcal{F}^{-1}$	$\mathcal{F}^{-1}\mathcal{V}[s]$ $= \frac{1}{\lvert s\rvert}\mathcal{V}\left[\frac{1}{s}\right]\mathcal{F}^{-1}$	1	$\mathcal{F}^{-1}\mathcal{F}^{-1}$ $= \mathcal{V}[-1]$	$\mathcal{F}^{-1}\mathcal{Q}[D]$ $= \mathcal{P}[D]\mathcal{F}^{-1}$	$\mathcal{F}^{-1}\mathcal{P}[D]$ $= \mathcal{Q}[D]\mathcal{F}^{-1}$
$\mathcal{Q}$	$\mathcal{Q}[a]\mathcal{V}[s]$ $= \mathcal{V}[s]\mathcal{Q}\left[\frac{a}{s^2}\right]$	$\mathcal{Q}[D]\mathcal{F}$ $= \mathcal{F}\mathcal{P}[D]$	$\mathcal{Q}[D]\mathcal{F}^{-1}$ $= \mathcal{F}^{-1}\mathcal{P}[D]$	$\mathcal{Q}[a_1]\mathcal{Q}[a_2]$ $= \mathcal{Q}[a_1+a_2]$	$\mathcal{Q}[a]\mathcal{P}[b] =$ $\sqrt{1-ab}\mathcal{P}\left[\frac{b}{1-ab}\right]$ $\mathcal{Q}[a-a^2b]\mathcal{V}[1-ab]$
$\mathcal{P}$	$\mathcal{P}[D]\mathcal{V}[s]$ $= \mathcal{V}[s]\mathcal{P}[Ds^2]$	$\mathcal{P}[D]\mathcal{F}$ $= \mathcal{F}\mathcal{Q}[D]$	$\mathcal{P}[D]\mathcal{F}^{-1}$ $= \mathcal{F}^{-1}\mathcal{Q}[D]$	$\mathcal{P}[b]\mathcal{Q}[a] =$ $\sqrt{\frac{1}{1-ab}}\mathcal{Q}\left[\frac{a}{1-ab}\right]$ $\mathcal{V}\left[\frac{1}{1-ab}\right]\mathcal{P}\left[\frac{b}{1-ab}\right]$	$\mathcal{P}[D_1]\mathcal{P}[D_2]$ $= \mathcal{P}[D_1+D_2]$

TABLE 2.2: Commutation relations between operators

In the following there are proofs for some major commutation relations, so the readers could understand and familiarize themselves with rules for calculation.

Commutation relation between $\mathcal{V}$ and $\mathcal{F}$

This derived from the similarity theorem for Fourier transform:

$$\mathcal{F}\mathcal{V}[s] = \frac{1}{\lvert s\rvert}\mathcal{V}\left[\frac{1}{s}\right]\mathcal{F} \tag{2.47}$$

Commutation relation between $\mathcal{V}$ and $\mathcal{Q}$

$$\mathcal{V}[s]\mathcal{Q}[a] = \mathcal{Q}[as^2]\mathcal{V}[s] \tag{2.48}$$

© 2018 Tous droits réservés.

lilliad.univ-lille.fr

Thèse de Junheng Shi, Université de Lille, 2018

because

$$\begin{aligned}\mathcal{V}[s]\mathcal{Q}[a]g(x) =&\mathcal{V}[s]\left(\mathrm{e}^{\mathrm{i}\frac{a}{2}x^2}g(x)\right)\\ =&\mathrm{e}^{\mathrm{i}\frac{as^2}{2}x^2}g(sx)\end{aligned}$$

For the reverse situation, we have

$$\mathcal{Q}[a]\mathcal{V}[s] = \mathcal{V}[s]\mathcal{Q}\left[\frac{a}{s^2}\right] \tag{2.49}$$

because

$$\begin{aligned}\mathcal{Q}[a]\mathcal{V}[s]g(x) =&\mathrm{e}^{\mathrm{i}\frac{a}{2}x^2}g(sx)\\ =&\mathrm{e}^{\mathrm{i}\frac{1}{2}(a/s^2)(sx)^2}g(sx)\\ =&\mathcal{V}[s]\mathrm{e}^{\mathrm{i}\frac{1}{2}(a/s^2)x^2}g(x)\end{aligned}$$

Commutation relation between $\mathcal{V}$ and $\mathcal{P}$

The proof is

$$\begin{aligned}\mathcal{V}[s]\mathcal{P}[D] =&\mathcal{V}[s]\mathcal{F}^{-1}\mathcal{Q}[D]\mathcal{F}\\ =&\frac{1}{|s|}\mathcal{F}^{-1}\mathcal{V}\left[\frac{1}{s}\right]\mathcal{Q}[D]\mathcal{F}\\ =&\frac{1}{|s|}\mathcal{F}^{-1}\mathcal{Q}\left[\frac{D}{s^2}\right]\mathcal{V}\left[\frac{1}{s}\right]\mathcal{F}\\ =&\frac{1}{|s|}\mathcal{F}^{-1}\mathcal{Q}\left[\frac{D}{s^2}\right]|s|\mathcal{F}\mathcal{V}\left[s\right]\\ =&\mathcal{P}\left[\frac{D}{s^2}\right]\mathcal{V}[s]\end{aligned} \tag{2.50}$$

Commutation relation between $\mathcal{Q}$, $\mathcal{F}$ and $\mathcal{P}$

Unfortunately there is no direct commutation relations between any two among these three operators, and normally we don't commute $\mathcal{P}$ directly, we decompose it into the combination of three basic operators first.

It could be derived from Eq.(2.39) that:

$$\begin{aligned}&\mathcal{P}[D] = \mathcal{F}^{-1}\mathcal{Q}[D]\mathcal{F}\\ \Rightarrow&\mathcal{F}\mathcal{P}[D] = \mathcal{F}\mathcal{F}^{-1}\mathcal{Q}[D]\mathcal{F}\\ \Rightarrow&\mathcal{F}\mathcal{P}[D] = \mathcal{Q}[D]\mathcal{F}\end{aligned} \tag{2.51}$$

And from Eq.(2.40) that:

$$\begin{aligned}&\mathcal{P}[D] = \mathcal{F}\mathcal{Q}[D]\mathcal{F}^{-1}\\ \Rightarrow&\mathcal{P}[D]\mathcal{F} = \mathcal{F}\mathcal{Q}[D]\mathcal{F}^{-1}\mathcal{F}\\ \Rightarrow&\mathcal{P}[D]\mathcal{F} = \mathcal{F}\mathcal{Q}[D]\end{aligned} \tag{2.52}$$

© 2018 Tous droits réservés.

lilliad.univ-lille.fr

Thèse de Junheng Shi, Université de Lille, 2018

The commutation relation between $\mathcal{Q}$ and $\mathcal{P}$ (actually it would include a $\mathcal{V}$ on the right side of the equal sign) is not apparent. To obtain it we need to use the result of the single lens scaling system Eq. (2.58). Then by taking advantage of Eq. (2.46), the propagation operator on the left or right side of such combination as $\mathcal{PQP}$ could be canceled by adding an inverse propagation operator depending on what we want.

2.3 Classical Temporal Imaging Systems

After we learned about the operator algebra for temporal imaging, now we use it to investigate specific classical temporal imaging systems, Fraunhofer dispersion system, single-lens temporal imaging system and 2-f system. These three systems serve as building blocks for compound temporal imaging systems.

2.3.1 Fraunhofer Dispersion System

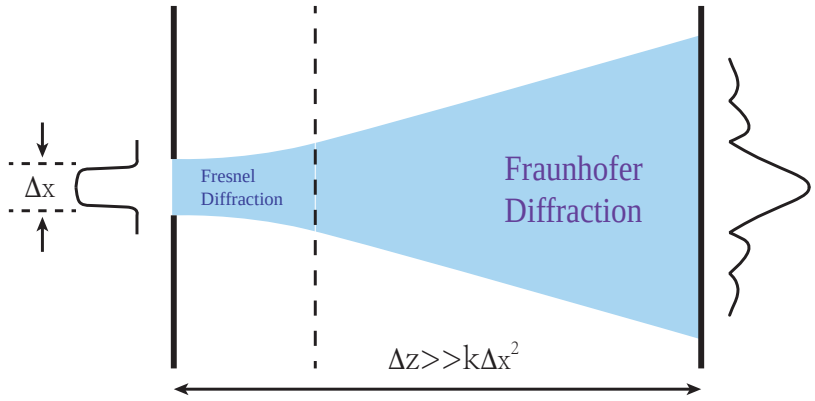

(A) One-dimensional Fraunhofer diffraction system.
Δz is the propagation distance, k is the wavenumber, Δx is the size of the aperture

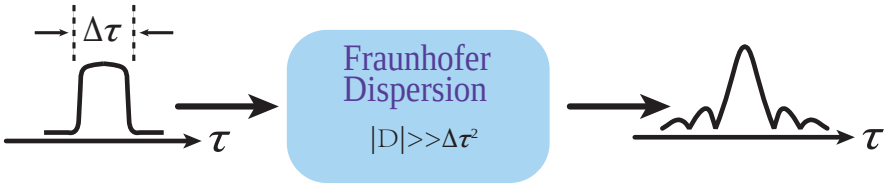

(B) Fraunhofer dispersion system.
D is the GDD introduced by the dispersive medium, $\Delta\tau$ is the temporal width of the input waveform.

FIGURE 2.1: Comparison between Fraunhofer diffraction and Fraunhofer dispersion.

Fraunhofer dispersion system could be the most simple temporal imaging system. It only requires a dispersive medium and is capable of doing Fourier transform.

Apparently the counterpart for Fraunhofer dispersion system is Fraunhofer diffraction system, or far-field diffraction. It is an approximation of the Fresnel diffraction

© 2018 Tous droits réservés.
lilliad.univ-lille.fr

Thèse de Junheng Shi, Université de Lille, 2018

under the condition that the propagation distance of the wavefront is much larger than the size of the transversal wavefront distribution squared and multiplied by the wavenumber while mostly the size of transversal wavefront distribution is determined by the aperture.

For temporal imaging, this condition means that the GDD introduced to the light wave after the propagation inside the dispersive medium is much larger than the width of the waveform squared. Because of that, the first operator $\mathcal{Q}\left[-\frac{1}{D}\right]$ in Eq.(2.43) could be neglected.

$$\begin{aligned}\mathcal{E}_{out}(\tau) &= \frac{e^{i\pi/4}}{\sqrt{D}}\mathcal{Q}\left[-\frac{1}{D}\right]\mathcal{V}\left[\frac{1}{D}\right]\mathcal{F}\mathcal{Q}\left[-\frac{1}{D}\right]\mathcal{E}_{in}(\tau') \\ &\approx \frac{e^{i\pi/4}}{\sqrt{D}}\mathcal{Q}\left[-\frac{1}{D}\right]\mathcal{V}\left[\frac{1}{D}\right]\mathcal{F}\mathcal{E}_{in}(\tau') \\ &= \frac{e^{i\pi/4}}{\sqrt{D}}e^{-i\frac{\tau^2}{2D}}\widetilde{\mathcal{E}}_{in}\left(\frac{\tau}{D}\right)\end{aligned} \tag{2.53}$$

As you could see, the output waveform of the Fraunhofer dispersion system is the Fourier transform of the input waveform.

2.3.2 Single-lens Temporal Imaging System

Different from Fraunhofer dispersion system, all other temporal imaging systems include a time lens which is analogous to spatial lens. The most typical one is the single-lens temporal imaging system consisting of two dispersive media and a time lens as shown in Figure 2.2b.

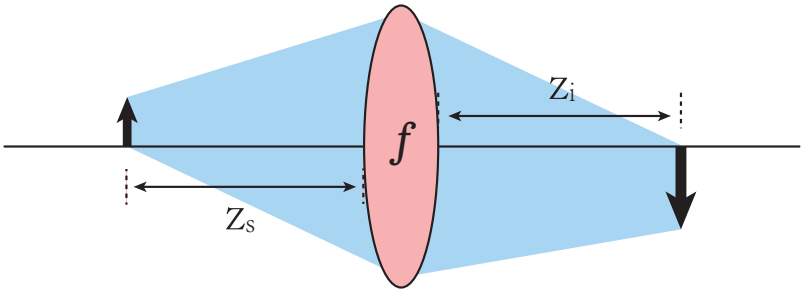

(A) Single-lens spatial imaging system.
z_s is the distance between the object and the lens, z_i is the distance between the lens and the image, f is the focal distance of the lens.

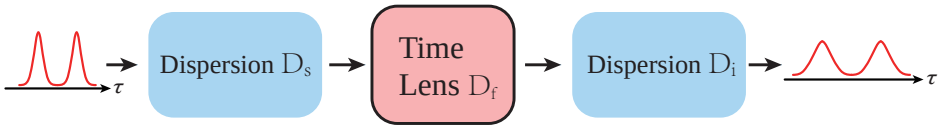

(B) Single-lens temporal imaging system.
D_s is the GDD of the first dispersive medium, D_i is the GDD of the second dispersive medium, D_f is the focal GDD of the time lens.

FIGURE 2.2: Comparison between the single-lens spatial and temporal imaging systems

© 2018 Tous droits réservés.

lilliad.univ-lille.fr

Thèse de Junheng Shi, Université de Lille, 2018

This is undoubtedly analogous to the single-lens spatial imaging system shown in Figure 2.2a, under the condition that

$$\frac{1}{z_s}+\frac{1}{z_i}=\frac{1}{f} \tag{2.54}$$

$$M=-\frac{z_i}{z_s} \tag{2.55}$$

the image is then a scaled and inverted version of the object with the scaling factor M.

To accomplish the same scaling effect for temporal imaging, we need the time lens to introduce a quadratic phase $\exp\{\mathrm{i}\frac{1}{D_f}\tau^2\}$, where D_f is called the focal GDD of time lens, analogous to the focal distance of spatial lens. As a result, if the condition

$$\frac{1}{D_s}+\frac{1}{D_i}=\frac{1}{D_f} \tag{2.56}$$

$$M=-\frac{D_i}{D_s} \tag{2.57}$$

is satisfied, we could calculate the total effect of such a system in temporal domain:

$$\begin{aligned}
\mathcal{T}_{temporal} =&\mathcal{P}[D_i]\mathcal{Q}\left[\frac{1}{D_f}\right]\mathcal{P}[D_s]\\
=&\sqrt{\frac{-1}{D_sD_i}}\mathcal{Q}\left[-\frac{1}{D_i}\right]\mathcal{V}\left[\frac{1}{D_i}\right]\mathcal{F}\mathcal{Q}\left[-\frac{1}{D_i}\right]\mathcal{Q}\left[\frac{1}{D_f}\right]\mathcal{Q}\left[-\frac{1}{D_s}\right]\mathcal{V}\left[\frac{1}{D_s}\right]\mathcal{F}\mathcal{Q}\left[-\frac{1}{D_s}\right]\\
=&\sqrt{\frac{-1}{D_sD_i}}\mathcal{Q}\left[-\frac{1}{D_i}\right]\mathcal{V}\left[\frac{1}{D_i}\right]\mathcal{F}\mathcal{Q}\left[\frac{1}{D_f}-\frac{1}{D_s}-\frac{1}{D_i}\right]\mathcal{V}\left[\frac{1}{D_s}\right]\mathcal{F}\mathcal{Q}\left[-\frac{1}{D_s}\right]\\
=&\sqrt{\frac{-1}{D_sD_i}}\mathcal{Q}\left[-\frac{1}{D_i}\right]\mathcal{V}\left[\frac{1}{D_i}\right]\mathcal{F}\mathcal{V}\left[\frac{1}{D_s}\right]\mathcal{F}\mathcal{Q}\left[-\frac{1}{D_s}\right]\\
=&\sqrt{\frac{-1}{D_sD_i}}\mathcal{Q}\left[-\frac{1}{D_i}\right]\mathcal{V}\left[\frac{1}{D_i}\right]|D_s|\mathcal{V}[D_s]\mathcal{F}\mathcal{F}\mathcal{Q}\left[-\frac{1}{D_s}\right]\\
=&\sqrt{-\frac{D_s^2}{D_sD_i}}\mathcal{Q}\left[-\frac{1}{D_i}\right]\mathcal{V}\left[-\frac{D_s}{D_i}\right]\mathcal{Q}\left[-\frac{1}{D_s}\right]\\
=&\frac{1}{\sqrt{M}}\mathcal{Q}\left[-\frac{1}{D_i}\right]\mathcal{V}\left[\frac{1}{M}\right]\mathcal{Q}\left[-\frac{1}{D_s}\right]\\
=&\frac{1}{\sqrt{M}}\mathcal{Q}\left[-\frac{1}{D_i}\right]\mathcal{Q}\left[-\frac{1}{M^2D_s}\right]\mathcal{V}\left[\frac{1}{M}\right]\\
=&\frac{1}{\sqrt{M}}\mathcal{Q}\left[\frac{1}{MD_f}\right]\mathcal{V}\left[\frac{1}{M}\right]
\end{aligned} \tag{2.58}$$

© 2018 Tous droits réservés.

lilliad.univ-lille.fr

Thèse de Junheng Shi, Université de Lille, 2018

The output waveform is

$$\begin{aligned}\mathcal{E}_{out}(\tau) =& \mathcal{T}_{temporal}\ \mathcal{E}_{in}(\tau') \\ =& \frac{1}{\sqrt{M}} \mathcal{Q}\left[\frac{1}{MD_f}\right] \mathcal{V}\left[\frac{1}{M}\right] \mathcal{E}_{in}(\tau) \\ =& \frac{1}{\sqrt{M}} e^{i\frac{\tau^2}{2MD_f}} \mathcal{E}_{in}\left(\frac{\tau}{M}\right)\end{aligned} \tag{2.59}$$

By adjusting the scaling factor M we are now able to control the output waveform as a magnification or compression of the input waveform.

There are three points to be further discussed.

First, in spatial imaging, since z_s and z_i are all positive, M is always negative, which means that the real image is always the reversed version of the object. In temporal imaging, however, such restriction does not exist. The GDD introduced by the dispersive medium could either be positive or negative, resulting in time inverting or non-inverting responses of the input waveform. The system with inverting response is named time reversal.

Second, except for the scaling effect that we desired, Eq.(2.59) shows that there is an additional phase term $\exp\{i\frac{1}{2MD_f}\tau^2\}$ which introduces unwanted aberration. It could also be seen as the effect of a time lens with focal GDD equals to MD_f. There are several measures to get rid of this residual phase such as adding another time lens [76]. Otherwise this temporal imaging system is only valid for magnification where this residual phase could be neglected. Compression could be achieved by combining two 2-f systems [17].

FIGURE 2.3: Spectral Imaging system.
D_s is the focal GDD of the first time lens, D_i is the focal GDD of the second time lens, D_f is the GDD of the dispersive medium.

Third, due to the equivalence of time and frequency, shown in Eq.(2.41), we could also build a spectral scaling system as in Figure 2.3 obtained by replacing dispersive medium with time lens and vice versa. Since we only care about what happened in the frequency domain, we use propagation operator $\mathcal{P}[\frac{1}{D}]$ instead of quadratic phase multiplication operator $\mathcal{Q}[\frac{1}{D}]$ to describe the effect of the time lens in this case.

Under the condition that

$$D_f = D_s + D_i \tag{2.60}$$

$$M' = -\frac{1/D_i}{1/D_s} \tag{2.61}$$

© 2018 Tous droits réservés.

lilliad.univ-lille.fr

Thèse de Junheng Shi, Université de Lille, 2018

we obtain

$$\begin{aligned}\mathcal{T}_{spectral} =&\mathcal{P}\left[\frac{1}{D_i}\right]\mathcal{Q}[D_f]\mathcal{P}\left[\frac{1}{D_s}\right]\\ =&\sqrt{-D_sD_i}\mathcal{Q}\left[-D_i\right]\mathcal{V}\left[D_i\right]\mathcal{F}\mathcal{Q}\left[-D_i\right]\mathcal{Q}\left[D_f\right]\mathcal{Q}\left[D_s\right]\mathcal{V}\left[D_s\right]\mathcal{F}\mathcal{Q}\left[-D_s\right]\\ =&\sqrt{-D_sD_i}\mathcal{Q}\left[-D_i\right]\mathcal{V}\left[D_i\right]\mathcal{F}\mathcal{V}\left[D_s\right]\mathcal{F}\mathcal{Q}\left[-D_s\right]\\ =&\sqrt{-D_sD_i}\mathcal{Q}\left[-D_i\right]\mathcal{V}\left[D_i\right]\frac{1}{|D_s|}\mathcal{V}\left[\frac{1}{D_s}\right]\mathcal{F}\mathcal{F}\mathcal{Q}\left[-D_s\right]\\ =&\frac{1}{\sqrt{M'}}\mathcal{Q}\left[-D_i\right]\mathcal{V}\left[\frac{1}{M'}\right]\mathcal{Q}\left[-D_s\right]\\ =&\frac{1}{\sqrt{M'}}\mathcal{Q}\left[-D_i\right]\mathcal{Q}\left[-\frac{D_s}{M'^2}\right]\mathcal{V}\left[\frac{1}{M'}\right]\\ =&\frac{1}{\sqrt{M'}}\mathcal{Q}\left[\frac{D_f}{M'}\right]\mathcal{V}\left[\frac{1}{M'}\right]\end{aligned} \tag{2.62}$$

The output spectrum is

$$\begin{aligned}\widetilde{\mathcal{E}}_{out}(\Omega) =&\mathcal{T}_{spectral}\widetilde{\mathcal{E}}_{in}(\Omega)\\ =&\frac{1}{\sqrt{M'}}\mathcal{Q}\left[\frac{D_f}{M'}\right]\mathcal{V}\left[\frac{1}{M'}\right]\widetilde{\mathcal{E}}_{in}(\Omega)\\ =&\frac{1}{\sqrt{M'}}\mathrm{e}^{\mathrm{j}\frac{D_f}{2M'}\Omega^2}\widetilde{\mathcal{E}}_{in}\left(\frac{\Omega}{M'}\right)\end{aligned} \tag{2.63}$$

similar to Eq.(2.59) that should only be used for spectral magnification.

2.3.3 Temporal 2-f system

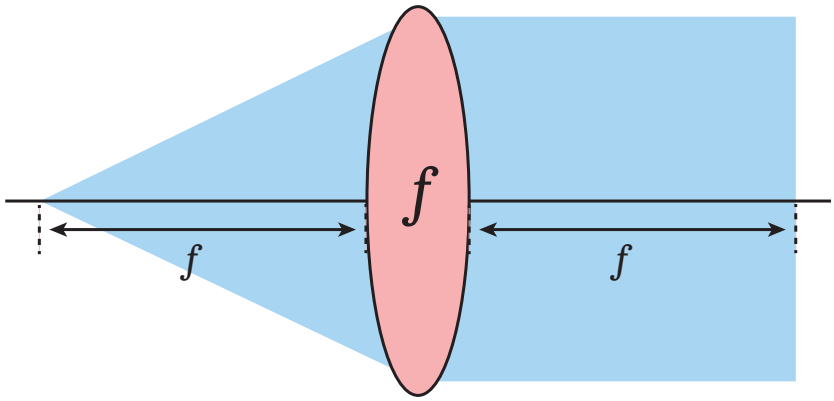

(A) Spatial 2-f system.

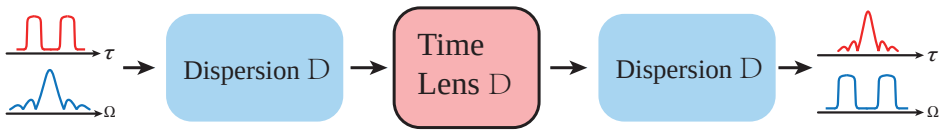

(B) Temporal 2-f system.

FIGURE 2.4: Comparison between spatial and temporal 2-f systems

© 2018 Tous droits réservés.

lilliad.univ-lille.fr

Thèse de Junheng Shi, Université de Lille, 2018

If D_s, D_f and D_i are all set to be equal in the above single-lens temporal imaging system, it becomes the temporal 2-f system, which serves the functionality of Fourier transform. Unlike the Fraunhofer dispersion system which only Fourier transform the waveform into spectrum, temporal 2-f system also Fourier transform the spectrum into the waveform.

Let's first calculate its effect in frequency domain:

$$\begin{aligned}\mathcal{T}_{spectral} =& \mathcal{Q}[D]\mathcal{P}\left[\frac{1}{D}\right]\mathcal{Q}[D]\\ =& e^{i\pi/4}\sqrt{D}\,\mathcal{Q}[D]\mathcal{Q}[-D]\mathcal{V}[D]\mathcal{F}\mathcal{Q}[-D]\mathcal{Q}[D]\\ =& e^{i\pi/4}\sqrt{D}\,\mathcal{V}[D]\mathcal{F}\\ =& e^{i\pi/4}\sqrt{D}\,\mathcal{V}[D]\mathcal{V}[-1]\mathcal{F}^{-1}\\ =& e^{i\pi/4}\sqrt{D}\,\mathcal{V}[-D]\mathcal{F}^{-1}\end{aligned} \tag{2.64}$$

So the output spectrum is

$$\begin{aligned}\widetilde{\mathcal{E}}_{out}(\Omega) =& \mathcal{T}_{spectral}\widetilde{\mathcal{E}}_{in}(\Omega')\\ =& e^{i\pi/4}\sqrt{D}\,\mathcal{V}[-D]\mathcal{F}^{-1}\widetilde{\mathcal{E}}_{in}(\Omega')\\ =& e^{i\pi/4}\sqrt{D}\mathcal{E}_{in}(-D\Omega)\end{aligned} \tag{2.65}$$

which carries the shape of the input waveform.

Then let's check its effect in temporal domain:

$$\begin{aligned}\mathcal{T}_{temporal} =& \mathcal{F}^{-1}\mathcal{T}_{spectral}\mathcal{F}\\ =& e^{i\pi/4}\sqrt{D}\,\mathcal{F}^{-1}\mathcal{V}[-D]\mathcal{F}^{-1}\mathcal{F}\\ =& e^{i\pi/4}\sqrt{D}\,\frac{1}{|D|}\mathcal{V}\left[-\frac{1}{D}\right]\mathcal{F}^{-1}\\ =& e^{i\pi/4}\,\frac{1}{\sqrt{D}}\mathcal{V}\left[-\frac{1}{D}\right]\mathcal{V}[-1]\mathcal{F}\\ =& e^{i\pi/4}\,\frac{1}{\sqrt{D}}\mathcal{V}\left[\frac{1}{D}\right]\mathcal{F}\end{aligned} \tag{2.66}$$

So the output waveform is

$$\begin{aligned}\mathcal{E}_{out}(\tau) =& \mathcal{T}_{temporal}\mathcal{E}_{in}(\tau')\\ =& \frac{e^{i\pi/4}}{\sqrt{D}}\mathcal{V}\left[\frac{1}{D}\right]\mathcal{F}\mathcal{E}_{in}(\tau')\\ =& \frac{e^{i\pi/4}}{\sqrt{D}}\widetilde{\mathcal{E}}_{in}\left(\frac{\tau}{D}\right)\end{aligned} \tag{2.67}$$

which carries the shape of the input spectrum.

Temporal 2-f system shows great prospect in ultrafast signal processing as it enables the single-shot measurement of ultrafast, arbitrary-shaped waveforms of events which are non-repetitive and may occur only once. The state-of-the-art silicon-chip-based ultrafast optical oscilloscope is reported to have subpicosecond resolution [16]. By adding a spectrometer, even higher resolution could be achieved, which enables the

© 2018 Tous droits réservés.

lilliad.univ-lille.fr

Thèse de Junheng Shi, Université de Lille, 2018

detection of optical events which requires single-shot measurement such as optical rogue waves [66].

There are three points to be further discussed.

First, although temporal 2-f system is able to Fourier transform both the waveform and the spectrum, they are not happening simultaneously. The spectrum is Fourier transformed after the time lens and the waveform Fourier transformed after the second dispersive medium. Therefore, if only the waveform or the spectrum needs Fourier transform, there is not need to construct the whole temporal 2-f system. For Fourier transform a spectrum, first a dispersive medium then a time lens is sufficient. For a waveform, first a time lens then a dispersive medium is sufficient. As a matter of fact, incomplete temporal 2-f system is similar to Fraunhofer dispersion system, so the unwanted residual phase is inevitable.

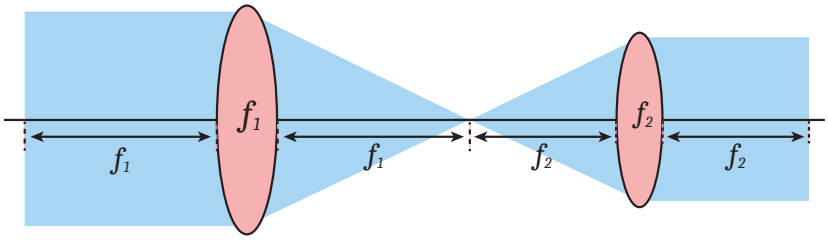

(A) Spacial 4-f system.
f_1 is the focal distance of the first spatial 2-f system, f_2 is the focal distance of the second spatial 2-f system.

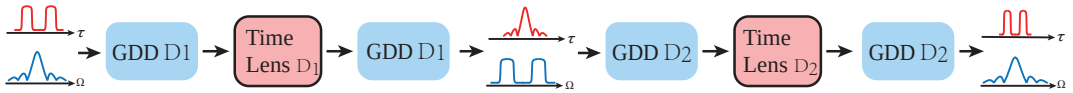

(B) Temporal 4-f system.
D_1 is the focal GDD of the first temporal 2-f system, D_2 is the focal GDD of the second temporal 2-f system

FIGURE 2.5: Comparison between spatial and temporal 4-f systems.

Second, two temporal 2-f systems could be combined to do scaling, especially waveform compression [17]. As shown in last subsection, single-lens temporal imaging system is not suitable for waveform compression because of the existence of the residual phase that introduces aberration. Analogous to the spatial 4-f system shown in Figure 2.5a, a temporal 4-f system as in Figure 2.5b is constructed by cascading two temporal 2-f systems with focal GDDs D_1 and D_2. Under the condition that

$$M = -\frac{D_2}{D_1} \tag{2.68}$$

© 2018 Tous droits réservés.

lilliad.univ-lille.fr

Thèse de Junheng Shi, Université de Lille, 2018

using Eq.(2.66), we obtain its effect:

$$\begin{aligned}\mathcal{T}_{temporal} =& \mathcal{T}_{2,temp}\mathcal{T}_{1,temp} \\ =& \sqrt{\frac{-1}{D_2 D_1}}\,\mathcal{V}\left[\frac{1}{D_2}\right]\mathcal{F}\mathcal{V}\left[\frac{1}{D_1}\right]\mathcal{F} \\ =& \sqrt{\frac{-1}{D_2 D_1}}\mathcal{V}\left[\frac{1}{D_2}\right]|D_1|\mathcal{V}[D_1]\mathcal{F}\mathcal{F} \\ =& \sqrt{\frac{-D_1^2}{D_2 D_1}}\mathcal{V}\left[-\frac{D_1}{D_2}\right] \\ =& \frac{1}{\sqrt{M}}\mathcal{V}\left[\frac{1}{M}\right]\end{aligned} \tag{2.69}$$

as a perfect scaling without any residual phase. Meanwhile, its spectrum is also perfectly scaled:

$$\begin{aligned}\mathcal{T}_{spectral} =& \mathcal{F}\mathcal{T}_{temporal}\mathcal{F}^{-1} \\ =& \frac{1}{\sqrt{M}}\mathcal{F}\mathcal{V}\left[\frac{1}{M}\right]\mathcal{F}^{-1} \\ =& \frac{1}{\sqrt{M}}\mathcal{F}\mathcal{F}^{-1}|M|\mathcal{V}\left[M\right] \\ =& \sqrt{M}\mathcal{V}\left[M\right]\end{aligned} \tag{2.70}$$

Third, the temporal 2-f system could be combined with Fraunhofer dispersion system to get ultralarge magnification. As could be seen in Figure 2.6, first the spectrum is Fourier transformed by the temporal 2-f system to resemble the shape of the input waveform. The following Fraunhofer dispersion transform this shape back to the waveform. Because the GDD of Fraunhofer dispersive medium D_2 is commonly very large, propagation inside the Fraunhofer dispersive medium will greatly stretch the waveform. Consequently the output waveform is the ultralarge magnification of the input waveform. In 2009, Salem et al. achieved highest temporal magnification reported , 520 times magnification, based on such system [60].

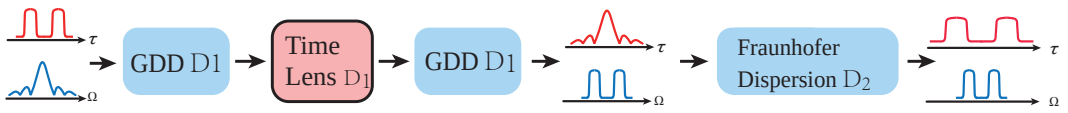

FIGURE 2.6: Temporal ultralarge magnification system. D_1 is the focal GDD of the temporal 2-f system, D_2 is the GDD of the Fraunhofer dispersion system.

© 2018 Tous droits réservés.

lilliad.univ-lille.fr

Thèse de Junheng Shi, Université de Lille, 2018

By combing Eq.(2.53) and Eq.(2.66), the effect of such system is

$$\begin{aligned}\mathcal{T}_{temporal} =& \mathcal{T}_{2,temp}\mathcal{T}_{1,temp}\\ =& \sqrt{\frac{-1}{D_2D_1}}\,\mathcal{Q}\left[-\frac{1}{D_2}\right]\mathcal{V}\left[\frac{1}{D_2}\right]\mathcal{F}\mathcal{V}\left[\frac{1}{D_1}\right]\mathcal{F}\\ =& \sqrt{\frac{-1}{D_2D_1}}\,\mathcal{Q}\left[-\frac{1}{D_2}\right]\mathcal{V}\left[\frac{1}{D_2}\right]|D_1|\mathcal{V}[D_1]\mathcal{F}\mathcal{F}\\ =& \sqrt{\frac{-D_1^2}{D_2D_1}}\mathcal{Q}\left[-\frac{1}{D_2}\right]\mathcal{V}\left[-\frac{D_1}{D_2}\right]\\ =& \frac{1}{\sqrt{M}}\mathcal{Q}\left[-\frac{1}{D_2}\right]\mathcal{V}\left[\frac{1}{M}\right]\end{aligned} \tag{2.71}$$

2.4 Summary of this chapter

In this chapter we revisit the classical temporal imaging starting from the space-time duality. We develop an operator algebra system with a set of definitions and rules and use it to understand various temporal imaging schemes including Fraunhofer dispersion, single-lens imaging system and 2-f system and their functionalities such as scaling and Fourier transform. We also discuss their advantages, drawbacks, limitations such as the extra phase shared by the Frauhofer dispersion and single-lens imaging system. This phase could be seen as an effect of an extra time lens. We explore the combinations of these temporal imaging systems to serve larger variety of applications such as spectral imaging, 4-f imaging system and etc.

© 2018 Tous droits réservés.

lilliad.univ-lille.fr

© 2018 Tous droits réservés.

lilliad.univ-lille.fr

Thèse de Junheng Shi, Université de Lille, 2018

Chapter 3

Quantum Temporal Imaging with Squeezed Light

For classical temporal imaging, the intensity of the signal field is high that quantum fluctuations could be neglected. But such omission is no longer valid if the signal field for temporal imaging is switched from classical light to nonclassical light, which is called *Quantum Temporal Imaging*. The influence of quantum fluctuations inside the temporal imaging process must be considered now. It might deteriorate the quantum property of the signal field. Such investigation is meaningful because the application of temporal imaging on quantum light would be quite promising. For example, when building a quantum network where quantum light would be produced, manipulated and detected. For a large network we expect the coherence time of all quantum lights in it to be identical to each other and to the response time of the detector. Temporal imaging could play the part of manipulation to make this come true. Certain attempts have been made for the single or entangled photons, including temporal shaping [7, 49, 57], optical waveform conversion [29], spectral compression [35], matching the characteristic time [76] etc.

Here we try to understand under what condition the quantum property such broadband squeezing would be preserved or destroyed in temporal imaging. Before that we need to investigate the temporal imaging system especially the time lens quantumly.

3.1 Quantum Treatment of Four-wave Mixing Processes

To investigate FWM time lens, we start with the quantum treatment of the FWM processes. There are two configurations: one consists in four waves propagating in the same directions. It is called Copropagating Four-Wave Mixing (CFWM). The other one requires the four waves to be divided into two groups, the two waves in every group are propagating in the opposite directions to each other, which is called Counter-Propagating Four-Wave Mixing (CPFWM).

3.1.1 Quantum Treatment of Copropagating Four-wave Mixing

A nonlinear polarization term is added to Eq. (2.5) that it becomes

$$\left[\frac{\partial^2}{\partial z^2} - \frac{1}{c^2}\frac{\partial^2}{\partial t^2}\right]\hat{\mathbf{E}}(z,t) = \mu_0 \frac{\partial^2}{\partial t^2}\left[\hat{\mathbf{P}}^L(z,t) + \hat{\mathbf{P}}^{NL}(z,t)\right] \tag{3.1}$$

© 2018 Tous droits réservés.

lilliad.univ-lille.fr

Thèse de Junheng Shi, Université de Lille, 2018

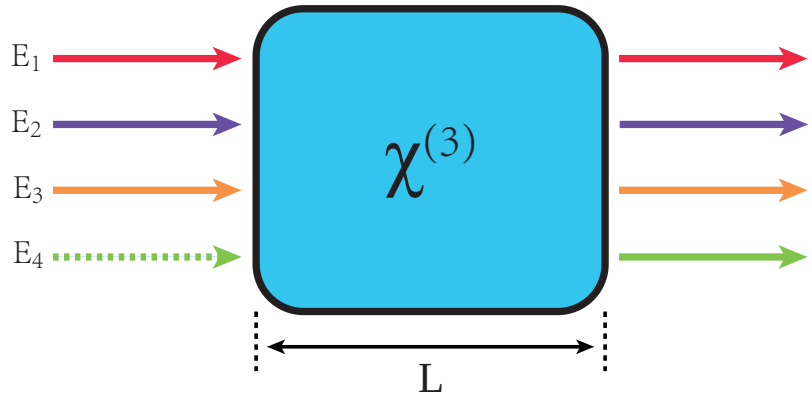

FIGURE 3.1: Configuration of copropagating four-wave mixing.

For FWM the nonlinear polarization is the third order polarization

$$\begin{aligned}&\hat{\mathbf{P}}^{NL}(z,t) = \hat{\mathbf{P}}^{(3)}(z,t)\\ =&\epsilon_0 \int_0^{+\infty} \mathrm{d}t_1 \int_0^{+\infty} \mathrm{d}t_2 \int_0^{+\infty} \mathrm{d}t_3\, R^{(3)}(t_1,t_2,t_3)\hat{\mathbf{E}}(z,t-t_1)\hat{\mathbf{E}}(z,t-t_2)\hat{\mathbf{E}}(z,t-t_3)\end{aligned} \tag{3.2}$$

where $R^{(3)}(t_1,t_2,t_3)$ is the third order response function. It equals to zero if any of t_1, t_2 and t_3 is negative.

The copropagating FWM configuration is shown in Figure 3.1, so the field operator $\hat{\mathbf{E}}(z,t)$ is a mixture of four fields linearly polarized in the same direction, $\hat{E}_1(z,t)$, $\hat{E}_2(z,t)$, $\hat{E}_3(z,t)$ and $\hat{E}_4(z,t)$, with their corresponding carrier frequencies ω_1, ω_2, ω_3, ω_4 which satisfy the energy conservation relation as shown in Figure 3.2. Among them two are the pump fields, one is the signal field and one is the idler field. But for now we don't specify which is which. The full field is:

$$\hat{\mathbf{E}}(z,t) = \sum_j \hat{E}_j(z,t) \tag{3.3}$$

where $j \in \{1,2,3,4\}$.

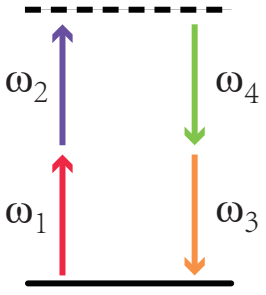

FIGURE 3.2: Energy conservation relation of copropagating four-wave mixing. The lengths of the vectors are irrelevant to the frequencies they denote.

© 2018 Tous droits réservés.

lilliad.univ-lille.fr

Thèse de Junheng Shi, Université de Lille, 2018

For each field we have

$$\hat{E}_j(z,t) = \frac{1}{2}[\hat{E}_j^{(+)}(z,t) + \hat{E}_j^{(-)}(z,t)] \tag{3.4}$$

where $\hat{E}_j^{(+)}(z,t)$ is the positive frequency part of the electric field operators.

Combine Eq. (3.1), Eq. (3.2), Eq. (3.3) and Eq. (3.4) we obtain

$$\begin{aligned}
&\frac{\partial^2}{\partial z^2}\hat{E}_j^{(+)}(z,t) - \frac{1}{c^2}\frac{\partial^2}{\partial t^2}\hat{E}_j^{(+)}(z,t) - \frac{1}{c^2}\frac{\partial^2}{\partial t^2}\int_0^{+\infty} \mathrm{d}t'\, R^{(1)}(t')\hat{E}_j^{(+)}(z,t-t') \\
&= \sum_{k,l,m}\frac{1}{4c^2}\frac{\partial^2}{\partial t^2}\int_0^{+\infty}\mathrm{d}t_1\int_0^{+\infty}\mathrm{d}t_2\int_0^{+\infty}\mathrm{d}t_3\, R^{(2)}(t_1,t_2,t_3) \\
&\quad\times[\hat{E}_k^{(+)}(z,t-t_1) + \hat{E}_k^{(-)}(z,t-t_1)] \\
&\quad\times[\hat{E}_l^{(+)}(z,t-t_2) + \hat{E}_l^{(-)}(z,t-t_2)] \\
&\quad\times[\hat{E}_m^{(+)}(z,t-t_3) + \hat{E}_m^{(-)}(z,t-t_3)]
\end{aligned} \tag{3.5}$$

where $k,l,m \in \{1,2,3,4\}$, for simplicity we only consider the positive frequency component for $\mathbf{E}_j(z,t)$.

Using the Fourier transform that

$$\hat{E}_j(z,t) = \frac{1}{2}\int\frac{\mathrm{d}\omega'}{\sqrt{2\pi}}\mathrm{e}^{-\mathrm{i}\omega_j' t}\,[\hat{E}_j^{(+)}(z,\omega_j') + \hat{E}_j^{(-)}(z,-\omega_j')] \tag{3.6}$$

and transform Eq. (3.5) into frequency domain

$$\begin{aligned}
&\frac{\partial^2}{\partial z^2}\hat{E}_j^{(+)}(z,\omega_j') + \frac{\omega_j'^2}{c^2}\hat{E}_j^{(+)}(z,\omega_j') + \frac{\omega_j'^2}{c^2}\chi^{(1)}(\omega_j')\hat{E}_j^{(+)}(z,\omega_j') \\
&= -\sum_{k,l,m}\frac{\omega_j'^2}{4c^2}\int\frac{\mathrm{d}\omega_k'}{\sqrt{2\pi}}[\hat{E}_k^{(+)}(z,\omega_k') + \hat{E}_k^{(-)}(z,-\omega_k')] \\
&\quad\times\int\frac{\mathrm{d}\omega_l'}{\sqrt{2\pi}}[\hat{E}_k^{(+)}(z,\omega_l') + \hat{E}_k^{(-)}(z,-\omega_l')] \\
&\quad\times\int\frac{\mathrm{d}\omega_m'}{\sqrt{2\pi}}[\hat{E}_k^{(+)}(z,\omega_m') + \hat{E}_k^{(-)}(z,-\omega_m')] \\
&\quad\times\chi^{(3)}(\omega_k'+\omega_l'+\omega_m';\omega_k',\omega_l',\omega_m')\int\mathrm{d}t\,\mathrm{e}^{\mathrm{i}(\omega_j'-\omega_k'-\omega_l'-\omega_m')t} \\
&= -\sum_{k,l,m}\frac{\omega_j'^2}{4c^2}\int\frac{\mathrm{d}\omega_k'}{\sqrt{2\pi}}[\hat{E}_k^{(+)}(z,\omega_k') + \hat{E}_k^{(-)}(z,-\omega_k')] \\
&\quad\times\int\frac{\mathrm{d}\omega_l'}{\sqrt{2\pi}}[\hat{E}_k^{(+)}(z,\omega_l') + \hat{E}_k^{(-)}(z,-\omega_l')] \\
&\quad\times\int\frac{\mathrm{d}\omega_m'}{\sqrt{2\pi}}[\hat{E}_k^{(+)}(z,\omega_m') + \hat{E}_k^{(-)}(z,-\omega_m')] \\
&\quad\times\chi^{(3)}(\omega_k'+\omega_l'+\omega_m';\omega_k',\omega_l',\omega_m')\,\sqrt{2\pi}\delta(\omega_j'-\omega_k'-\omega_l'-\omega_m')
\end{aligned} \tag{3.7}$$

© 2018 Tous droits réservés.

lilliad.univ-lille.fr

Thèse de Junheng Shi, Université de Lille, 2018

ω'_k	ω'_l	ω'_m
ω'_1	ω'_2	$-\omega'_3$
ω'_1	$-\omega'_3$	ω'_2
ω'_2	ω'_1	$-\omega'_3$
ω'_2	$-\omega'_3$	ω'_1
$-\omega'_3$	ω'_1	ω'_2
$-\omega'_3$	ω'_2	ω'_1

TABLE 3.1: All combinations in the FWM category.

ω'_k	ω'_l	ω'_m	ω'_k	ω'_l	ω'_m	ω'_k	ω'_l	ω'_m
ω'_1	$-\omega'_1$	ω'_4	ω'_2	$-\omega'_2$	ω'_4	ω'_3	$-\omega'_3$	ω'_4
ω'_1	ω'_4	$-\omega'_1$	ω'_2	ω'_4	$-\omega'_2$	ω'_3	ω'_4	$-\omega'_3$
$-\omega'_1$	ω'_1	ω'_4	$-\omega'_2$	ω'_2	ω'_4	$-\omega'_3$	ω'_3	ω'_4
$-\omega'_1$	ω'_4	ω'_1	$-\omega'_2$	ω'_4	ω'_2	$-\omega'_3$	ω'_4	ω'_3
ω'_4	ω'_1	$-\omega'_1$	ω'_4	ω'_2	$-\omega'_2$	ω'_4	ω'_3	$-\omega'_3$
ω'_4	$-\omega'_1$	ω'_1	ω'_4	$-\omega'_2$	ω'_2	ω'_4	$-\omega'_3$	ω'_3

TABLE 3.2: All combinations in the XPM category.

where the third order susceptibility equals to

$$\begin{aligned}&\chi^{(3)}(\omega'_k+\omega'_l+\omega'_m;\omega'_k,\omega'_l,\omega'_m)\\&=\int_0^{+\infty}\mathrm{d}t_1\int_0^{+\infty}\mathrm{d}t_2\int_0^{+\infty}\mathrm{d}t_3\,R^{(3)}(t_1,t_2,t_3)\mathrm{e}^{\mathrm{i}(\omega'_k t_1+\omega'_l t_2+\omega'_m t_3)}\end{aligned}\tag{3.8}$$

In principal for each ω'_j there are twenty-seven different combinations of ω'_k, ω'_l and ω'_l, divided in three categories: FWM, Cross-Phase Modulation (XPM) and Self-Phase Modulation (SPM).

Take $\omega'_j = \omega'_4$ as an example. Six are in the FWM category as shown in Table 3.1. Eighteen are in the category of Cross-Phase Modulation (XPM) as shown in Table 3.2. Three are in the category of Self-Phase Modulation (SPM) as shown in Table 3.3

For simplicity here we only consider FWM category , which reduces Eq. (3.7) to

$$\begin{aligned}&\frac{\partial^2}{\partial z^2}\hat{E}_4^{(+)}(z,\omega'_4)+k^2(\omega'_4)\hat{E}_4^{(+)}(z,\omega'_4)\\&=-\frac{3\omega'^2_4\chi^{(3)}}{2c^2}\int\frac{\mathrm{d}\omega'_2}{\sqrt{2\pi}}\int\frac{\mathrm{d}\omega'_3}{\sqrt{2\pi}}\hat{E}_1^{(+)}(z,\omega'_4+\omega'_3-\omega'_2)\hat{E}_2^{(+)}(z,\omega'_2)\hat{E}_3^{(-)}(z,-\omega'_3)\end{aligned}\tag{3.9}$$

It should be noted because of the intrinsic permutation symmetry of the nonlinear tensor that the third-order susceptibilities for all six combinations are equivalent and is denoted as $\chi^{(3)}$.

ω'_k	ω'_l	ω'_m
ω'_4	$-\omega'_4$	ω'_4
ω'_4	ω'_4	$-\omega'_4$
$-\omega'_4$	ω'_4	ω'_4

TABLE 3.3: All combinations in the SPM category.

© 2018 Tous droits réservés.

lilliad.univ-lille.fr

Thèse de Junheng Shi, Université de Lille, 2018

Under the quasi-monochromatic approximation, we decompose the positive frequency field operators into slowly varying envelopes represented by annihilation operators

$$\hat{E}_j^{(+)}(z,t) = \mathcal{E}_j e^{-i\omega_j t + ik_j z} \int \frac{d\Omega_j}{\sqrt{2\pi}} e^{i(k(\omega_j+\Omega_j)-k_j)z} \hat{a}_j(z,\Omega_j) e^{-i\Omega_j t} \tag{3.10}$$

where $k_j = k(\omega_j)$ and $\mathcal{E}_j = \sqrt{\frac{\hbar\omega_j^2}{2\epsilon_0 c^2 k_j}}$ and $\Omega_j = \omega_j' - \omega_j$ is the deviation from the carrier frequency.

It is easy to find that

$$\hat{E}_j^{(+)}(z,\omega_j') = \mathcal{E}_j e^{ik(\omega_j+\Omega_j)z} \hat{a}_j(z,\Omega_j) \tag{3.11}$$

Note for the negative frequency component, we have $\Omega_j = (-\omega_j') - (-\omega_j)$:

$$\hat{E}_j^{(-)}(z,-\omega_j') = \mathcal{E}_j e^{-ik(\omega_j+\Omega_j)z} \hat{a}_j^\dagger(z,\Omega_j) \tag{3.12}$$

By using Eq. (3.11) and Eq. (3.12), Eq. (3.9) could be reduced to

$$\begin{aligned} &\frac{\partial^2}{\partial z^2}\hat{a}_4(z,\Omega_4) + 2ik(\omega_4+\Omega_4)\frac{\partial}{\partial z}\hat{a}_4(z,\Omega_4) \\ =& -\frac{3(\omega_4+\Omega_4)^2\chi^{(3)}}{2c^2}\frac{\mathcal{E}_1\mathcal{E}_2\mathcal{E}_3}{\mathcal{E}_4}\int\frac{d\Omega_2}{\sqrt{2\pi}}\int\frac{d\Omega_3}{\sqrt{2\pi}} \\ &\times \hat{a}_1(z,\Omega_4+\Omega_3-\Omega_2)\hat{a}_2(z,\Omega_2)\hat{a}_3^\dagger(z,\Omega_3)e^{-i\Delta(\Omega_4,\Omega_3,\Omega_2)z} \end{aligned} \tag{3.13}$$

where the phase mismatch is

$$\Delta(\Omega_4,\Omega_3,\Omega_2) = k(\omega_4+\Omega_4)+k(\omega_3+\Omega_3)-k(\omega_2+\Omega_2)-k(\omega_1+\Omega_4+\Omega_3-\Omega_2) \tag{3.14}$$

Under the quasi-monochromatic approximation we adopt two approximations. The first is due to the property of the slowly varying envelope

$$\left|\langle\frac{\partial}{\partial z}\hat{a}_j(z,\Omega_j)\rangle\right| \ll |k(\omega_j+\Omega_j)\langle\hat{a}_j(z,\Omega_j)\rangle| \tag{3.15}$$

that $\frac{\partial^2}{\partial z^2}\hat{a}_4(z,\Omega_4)$ is neglected

The second one is because of the deviation is very small compared to the carrier frequency

$$\Omega_j \ll \omega_j \tag{3.16}$$

that

$$\frac{(\omega_j+\Omega_j)^2}{k(\omega_j+\Omega_j)} \approx \frac{\omega_j^2}{k_j} \tag{3.17}$$

© 2018 Tous droits réservés.

lilliad.univ-lille.fr

Thèse de Junheng Shi, Université de Lille, 2018

With these approximations, Eq. (3.13) becomes

$$\begin{aligned}\frac{\partial}{\partial z}\hat{a}_4(z,\Omega_4) = \mathrm{i}g\int\frac{\mathrm{d}\Omega_2}{\sqrt{2\pi}}\int\frac{\mathrm{d}\Omega_3}{\sqrt{2\pi}} \\ \times\,\hat{a}_1(z,\Omega_4+\Omega_3-\Omega_2)\hat{a}_2(z,\Omega_2)\hat{a}_3^\dagger(z,\Omega_3)\mathrm{e}^{-\mathrm{i}\Delta(\Omega_4,\Omega_3,\Omega_2)z}\end{aligned} \tag{3.18}$$

where the nonlinear coupling constant $g = \chi^{(3)}\frac{3\epsilon_0^2}{\hbar^2}\mathcal{E}_1\mathcal{E}_2\mathcal{E}_3\mathcal{E}_4$, proportional to the third order susceptibility.

By applying this method to $\omega_j' = \omega_1'$, $\omega_j' = \omega_2'$ and $\omega_j' = \omega_3'$ we finally obtain the coupled equations for FWM process

$$\frac{\partial}{\partial z}\hat{a}_1(z,\Omega) = \mathrm{i}g\int\frac{\mathrm{d}\Omega'}{\sqrt{2\pi}}\int\frac{\mathrm{d}\Omega''}{\sqrt{2\pi}}\hat{a}_2^\dagger(z,\Omega'+\Omega''-\Omega)\hat{a}_3(z,\Omega')\hat{a}_4(z,\Omega'')\mathrm{e}^{\mathrm{i}\Delta(\Omega'',\Omega',\Omega''+\Omega'-\Omega)z} \tag{3.19a}$$

$$\frac{\partial}{\partial z}\hat{a}_2(z,\Omega) = \mathrm{i}g\int\frac{\mathrm{d}\Omega'}{\sqrt{2\pi}}\int\frac{\mathrm{d}\Omega''}{\sqrt{2\pi}}\hat{a}_1^\dagger(z,\Omega'+\Omega''-\Omega)\hat{a}_3(z,\Omega')\hat{a}_4(z,\Omega'')\mathrm{e}^{\mathrm{i}\Delta(\Omega'',\Omega',\Omega)z} \tag{3.19b}$$

$$\frac{\partial}{\partial z}\hat{a}_3(z,\Omega) = \mathrm{i}g\int\frac{\mathrm{d}\Omega'}{\sqrt{2\pi}}\int\frac{\mathrm{d}\Omega''}{\sqrt{2\pi}}\hat{a}_1(z,\Omega''+\Omega-\Omega')\hat{a}_2(z,\Omega')\hat{a}_4^\dagger(z,\Omega'')\mathrm{e}^{-\mathrm{i}\Delta(\Omega'',\Omega,\Omega')z} \tag{3.19c}$$

$$\frac{\partial}{\partial z}\hat{a}_4(z,\Omega) = \mathrm{i}g\int\frac{\mathrm{d}\Omega'}{\sqrt{2\pi}}\int\frac{\mathrm{d}\Omega''}{\sqrt{2\pi}}\hat{a}_1(z,\Omega+\Omega''-\Omega')\hat{a}_2(z,\Omega')\hat{a}_3^\dagger(z,\Omega'')\mathrm{e}^{-\mathrm{i}\Delta(\Omega,\Omega'',\Omega')z} \tag{3.19d}$$

The reason why we do not specify which of the four waves are the pumps, the signal and idler is because there are actually two kinds of configurations which follow different energy conservation relations. One of the two configurations conjugates the phase of the signal wave to that of the idler wave, so it is named Phase-Conjugating (PC). The other one, however, does not conjugate the phase of the signal wave, hence is named Phase-Preserving (PP). They shall be investigated in detail in the following subsections.

Before we continue, there is an important approximation to emphasize. The phase mismatch term Eq. (3.14) is usually expanded with respect to Ω_4, Ω_3 and Ω_2

$$\begin{aligned}\Delta(\Omega_4,\Omega_3,\Omega_2) =& \Delta_0 + k_4'\Omega_4 + k_3'\Omega_3 - k_2'\Omega_2 - k_1'(\Omega_4+\Omega_3-\Omega_2) \\ &+ \frac{1}{2}k_4''\Omega_4^2 + \frac{1}{2}k_3''\Omega_3^2 - \frac{1}{2}k_2''\Omega_2^2 - \frac{1}{2}k_1''(\Omega_4+\Omega_3-\Omega_2)^2 + \ldots\end{aligned} \tag{3.20}$$

where $k_j^{(n)} = \frac{\partial^n}{\partial\Omega_j^n}k(\omega_j+\Omega_j)$ and

$$\Delta_0 = k_4 + k_3 - k_2 - k_1 \tag{3.21}$$

The expansion terms of no less than the first order bring aberrations affecting the resolution and field of view of a temporal imaging system which is the main topic of our next chapter. Here we only presume that

$$\Delta(\Omega_4,\Omega_3,\Omega_2) \approx \Delta_0 \tag{3.22}$$

© 2018 Tous droits réservés.

lilliad.univ-lille.fr

Thèse de Junheng Shi, Université de Lille, 2018

Phase-conjugating copropagating four-wave mixing

For this configuration, we let $\mathbf{E}_1(z,t)$ and $\mathbf{E}_2(z,t)$ be the two pump fields, $\mathbf{E}_3(z,t)$ be the signal field and $\mathbf{E}_4(z,t)$ be the idler field. The energy conservation relation for their carrier frequencies is shown in Figure 3.3.

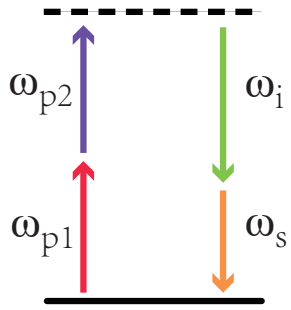

FIGURE 3.3: Energy conservation relation of phase-conjugating co-propagating four-wave mixing.

We presume the pump waves are classical and undepleted, $\alpha_{p1}(\Omega_1)$ and $\alpha_{p2}(\Omega_2)$, as a result equations (3.19) are reduced to two equations

$$\frac{\partial}{\partial z}\hat{a}_s(z,\Omega) = \mathrm{i}g\int\frac{\mathrm{d}\Omega'}{\sqrt{2\pi}}\int\frac{\mathrm{d}\Omega''}{\sqrt{2\pi}}\alpha_{p1}(\Omega''+\Omega-\Omega')\alpha_{p2}(\Omega')\hat{a}_i^\dagger(z,\Omega'')\mathrm{e}^{-\mathrm{i}\Delta_0 z} \tag{3.23a}$$

$$\frac{\partial}{\partial z}\hat{a}_i(z,\Omega) = \mathrm{i}g\int\frac{\mathrm{d}\Omega'}{\sqrt{2\pi}}\int\frac{\mathrm{d}\Omega''}{\sqrt{2\pi}}\alpha_{p1}(\Omega+\Omega''-\Omega')\alpha_{p2}(\Omega')\hat{a}_s^\dagger(z,\Omega'')\mathrm{e}^{-\mathrm{i}\Delta_0 z} \tag{3.23b}$$

It still looks unsolvable in frequency domain, so we transform it back to temporal domain, take Eq. (3.23a) as an example

$$\begin{aligned}
\frac{\partial}{\partial z}\hat{a}_s(z,\tau) &= \int\frac{\mathrm{d}\Omega}{\sqrt{2\pi}}\mathrm{e}^{-\mathrm{i}\Omega\tau}\frac{\partial}{\partial z}\hat{a}_s(z,\Omega)\\
&= \int\frac{\mathrm{d}\Omega}{\sqrt{2\pi}}\mathrm{e}^{-\mathrm{i}\Omega\tau}\,\mathrm{i}g\int\frac{\mathrm{d}\Omega'}{\sqrt{2\pi}}\int\frac{\mathrm{d}\Omega''}{\sqrt{2\pi}}\int\frac{\mathrm{d}\tau'}{\sqrt{2\pi}}\mathrm{e}^{\mathrm{i}(\Omega''+\Omega-\Omega')\tau'}\alpha_{p1}(\tau')\\
&\quad\times\int\frac{\mathrm{d}\tau''}{\sqrt{2\pi}}\mathrm{e}^{\mathrm{i}\Omega'\tau''}\alpha_{p2}(\tau'')\int\frac{\mathrm{d}\tau'''}{\sqrt{2\pi}}\mathrm{e}^{\mathrm{i}\Omega''\tau'''}\hat{a}_i^\dagger(z,-\tau''')\mathrm{e}^{-\mathrm{i}\Delta_0 z}\\
&= \mathrm{i}g\,\mathrm{e}^{-\mathrm{i}\Delta_0 z}\int\frac{\mathrm{d}\tau'}{\sqrt{2\pi}}\int\frac{\mathrm{d}\tau''}{\sqrt{2\pi}}\int\frac{\mathrm{d}\tau'''}{\sqrt{2\pi}}\alpha_{p1}(\tau')\alpha_{p2}(\tau'')\hat{a}_i^\dagger(z,-\tau''')\\
&\quad\times\int\frac{\mathrm{d}\Omega}{\sqrt{2\pi}}\mathrm{e}^{-\mathrm{i}\Omega(\tau-\tau')}\int\frac{\mathrm{d}\Omega'}{\sqrt{2\pi}}\mathrm{e}^{-\mathrm{i}\Omega'(\tau'-\tau'')}\int\frac{\mathrm{d}\Omega''}{\sqrt{2\pi}}\mathrm{e}^{-\mathrm{i}\Omega''(-\tau'''-\tau')}\\
&= \mathrm{i}g\,\mathrm{e}^{-\mathrm{i}\Delta_0 z}\alpha_{p1}(\tau)\alpha_{p2}(\tau)\hat{a}_i^\dagger(z,\tau)
\end{aligned} \tag{3.24}$$

By Fourier transforming Eq. (3.23b) in the same way, we obtain the coupled equations in temporal domain

$$\frac{\partial}{\partial z}\hat{a}_s(z,\tau) = \mathrm{i}g\,\mathrm{e}^{-\mathrm{i}\Delta_0 z}\alpha_{p1}(\tau)\alpha_{p2}(\tau)\hat{a}_i^\dagger(z,\tau) \tag{3.25a}$$

$$\frac{\partial}{\partial z}\hat{a}_i(z,\tau) = \mathrm{i}g\,\mathrm{e}^{-\mathrm{i}\Delta_0 z}\alpha_{p1}(\tau)\alpha_{p2}(\tau)\hat{a}_s^\dagger(z,\tau) \tag{3.25b}$$

© 2018 Tous droits réservés.

lilliad.univ-lille.fr

Thèse de Junheng Shi, Université de Lille, 2018

The two pump waves could be written as

$$\alpha_{p1}(\tau) = A_{p1}(\tau)e^{i\phi_{p1}(\tau)} \tag{3.26a}$$
$$\alpha_{p2}(\tau) = A_{p2}(\tau)e^{i\phi_{p2}(\tau)} \tag{3.26b}$$

where $A_{p1}(\tau)$ and $A_{p2}(\tau)$ are the real modules, $\phi_{p1}(\tau)$ and $\phi_{p2}(\tau)$ are the real phases.

The solution to equations (3.25) describe the evolutions of the annihilation and creation operators of the signal and idler waves inside the nonlinear medium:

$$\begin{aligned}\hat{a}_s(z,\tau) = &\left[\cosh(\gamma z) + \frac{i\Delta_0}{2\gamma}\sinh(\gamma z)\right]\hat{a}_s(0,\tau)e^{-i\Delta_0 z/2} \\ &+ \frac{ig\alpha_{p1}(\tau)\alpha_{p2}(\tau)}{\gamma}\sinh(\gamma z)\hat{a}_i^\dagger(0,\tau)e^{-i\Delta_0 z/2}\end{aligned} \tag{3.27a}$$

$$\begin{aligned}\hat{a}_i(z,\tau) = &\left[\cosh(\gamma z) + \frac{i\Delta_0}{2\gamma}\sinh(\gamma z)\right]\hat{a}_i(0,\tau)e^{-i\Delta_0 z/2} \\ &+ \frac{ig\alpha_{p1}(\tau)\alpha_{p2}(\tau)}{\gamma}\sinh(\gamma z)\hat{a}_s^\dagger(0,\tau)e^{-i\Delta_0 z/2}\end{aligned} \tag{3.27b}$$

where $\gamma = \sqrt{g^2 A_{p1}^2(\tau)A_{p2}^2(\tau) - \Delta_0^2/4}$

For a nonlinear medium of length L we obtain the relations of the annihilation and creation operators of the signal and idler waves at the input of the nonlinear medium, i.e. $z = 0$, and its output at $z = L$:

$$\hat{a}_s(L,\tau) = u(\tau)\hat{a}_s(0,\tau) + ie^{i\phi_p(\tau)}v(\tau)\hat{a}_i^\dagger(0,\tau) \tag{3.28a}$$
$$\hat{a}_i(L,\tau) = ie^{i\phi_p(\tau)}v(\tau)\hat{a}_s^\dagger(0,\tau) + u(\tau)\hat{a}_i(0,\tau) \tag{3.28b}$$

where $\phi_p(\tau) = \phi_{p1}(\tau) + \phi_{p2}(\tau)$.

The coefficients $u(\tau)$ and $v(\tau)$ are related to the nonlinear coupling constant, the amplitudes of the two pump waves and the length of the nonlinear medium:

$$u(\tau) = \left[\cosh(\gamma L) + \frac{i\Delta_0}{2\gamma}\sinh(\gamma L)\right]e^{-i\Delta_0 L/2} \tag{3.29}$$
$$v(\tau) = \frac{gA_{p1}(\tau)A_{p2}(\tau)}{\gamma}\sinh(\gamma L)e^{-i\Delta_0 L/2} \tag{3.30}$$

It is easy to see that these coefficients satisfy the relation $|u(\tau)|^2 - |v(\tau)|^2 = 1$ which shows the true nature of the PCFWM as a parametrically amplification process. This process parametrically amplifies the signal and the idler waves at the output of the nonlinear medium by the phase-insensitive parametric gain $G = |v(\tau)|^2$.

When the perfect phase-matching is achieved, i.e. $\Delta_0 = 0$, the coefficients could be simplified to

$$u(\tau) = \cosh[gA_{p1}(\tau)A_{p2}(\tau)L] \tag{3.31}$$
$$v(\tau) = \sinh[gA_{p1}(\tau)A_{p2}(\tau)L] \tag{3.32}$$

© 2018 Tous droits réservés.

lilliad.univ-lille.fr

Thèse de Junheng Shi, Université de Lille, 2018

Phase-preserving copropagating four-wave mixing

Now we switch the second pump wave and the signal wave. $\mathbf{E}_1(z,t)$ and $\mathbf{E}_3(z,t)$ are the two pump fields and $\mathbf{E}_2(z,t)$ become the signal field. The energy conservation relation for their carrier frequencies is shown in Figure 3.4. This configuration is also known as Bragg-scattering. Since the distance between the carrier frequencies of one pump wave and the signal wave is identical to the distance between the carrier frequencies of the other pump wave and the idler wave, it is commonly used for quantum state translation and frequency translation[40, 48, 52].

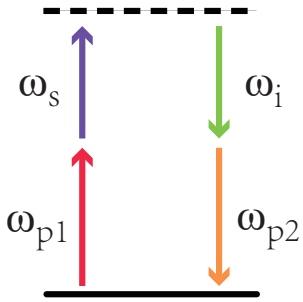

FIGURE 3.4: Energy conservation relation of phase-preserving co-propagating four-wave mixing.

With the same classical and undepleted pump approximation, equations (3.19) are also reduced to two coupled equations of signal and idler waves:

$$\frac{\partial}{\partial z}\hat{a}_s(z,\Omega) = ig\int\frac{d\Omega'}{\sqrt{2\pi}}\int\frac{d\Omega''}{\sqrt{2\pi}}\alpha^*_{p1}(\Omega''+\Omega-\Omega')\alpha_{p2}(\Omega')\hat{a}_i(z,\Omega'')e^{i\Delta_0 z} \tag{3.33a}$$

$$\frac{\partial}{\partial z}\hat{a}_i(z,\Omega) = ig\int\frac{d\Omega'}{\sqrt{2\pi}}\int\frac{d\Omega''}{\sqrt{2\pi}}\alpha_{p1}(\Omega+\Omega''-\Omega')\alpha^*_{p2}(\Omega'')\hat{a}_s(z,\Omega')e^{-i\Delta_0 z} \tag{3.33b}$$

Using the method shown in Eq. (3.24), we Fourier transform equations (3.33) into temporal domain:

$$\frac{\partial}{\partial z}\hat{a}_s(z,\tau) = ig\,e^{i\Delta_0 z}\alpha^*_{p1}(\tau)\alpha_{p2}(\tau)\hat{a}_i(z,\tau) \tag{3.34a}$$

$$\frac{\partial}{\partial z}\hat{a}_i(z,\tau) = ig\,e^{-i\Delta_0 z}\alpha_{p1}(\tau)\alpha^*_{p2}(\tau)\hat{a}_s(z,\tau) \tag{3.34b}$$

© 2018 Tous droits réservés.

lilliad.univ-lille.fr

Thèse de Junheng Shi, Université de Lille, 2018

Its solution describe the evolution of the annihilation and creation operators of the signal and idler waves inside the nonlinear medium:

$$\hat{a}_s(z,\tau) = \left[\cos(\gamma z) - \frac{i\Delta_0}{2\gamma}\sin(\gamma z)\right]\hat{a}_s(0,\tau)e^{i\Delta_0 z/2} + \frac{ig\alpha^*_{p1}(\tau)\alpha_{p2}(\tau)}{\gamma}\sin(\gamma z)\hat{a}_i(0,\tau)e^{i\Delta_0 z/2} \tag{3.35a}$$

$$\hat{a}_i(z,\tau) = \left[\cos(\gamma z) + \frac{i\Delta_0}{2\gamma}\sin(\gamma z)\right]\hat{a}_i(0,\tau)e^{-i\Delta_0 z/2} + \frac{ig\alpha_{p1}(\tau)\alpha^*_{p2}(\tau)}{\gamma}\sin(\gamma z)\hat{a}_s(0,\tau)e^{-i\Delta_0 z/2} \tag{3.35b}$$

where $\gamma = \sqrt{g^2 A^2_{p1}(\tau)A^2_{p2}(\tau) + \Delta_0^2/4}$.

Equations (3.35) could be used to obtain the relations of the annihilation operators of the signal and idler waves at the input of the nonlinear medium and its output:

$$\hat{a}_s(L,\tau) = c^*(\tau)\hat{a}_s(0,\tau) + ie^{-i\phi_p(\tau)}s(\tau)\hat{a}_i(0,\tau) \tag{3.36a}$$

$$\hat{a}_i(L,\tau) = ie^{i\phi_p(\tau)}s(\tau)\hat{a}_s(0,\tau) + c(\tau)\hat{a}_i(0,\tau) \tag{3.36b}$$

where $\phi_p(\tau) = \phi_{p1}(\tau) - \phi_{p2}(\tau)$.

The coefficients $c(\tau)$ and $s(\tau)$ depend on the nonlinear coupling constant, the amplitudes of the two pump waves and the length of the nonlinear medium:

$$c(\tau) = \left[\cos(\gamma L) + \frac{i\Delta_0}{2\gamma}\sin(\gamma L)\right]e^{i\Delta_0 L/2} \tag{3.37}$$

$$s(\tau) = \frac{gA_{p1}(\tau)A_{p2}(\tau)}{\gamma}\sinh(\gamma L)e^{-i\Delta_0 L/2} \tag{3.38}$$

These coefficients satisfy the relation of $|c(\tau)|^2 + |s(\tau)|^2 = 1$ which is equivalent to a beam splitter that they could be understood as the reflection and transmission coefficients. As a result we could define the transmission efficiency $\eta = |s(\tau)|^2$ which is also commonly referred to as conversion efficiency.

When perfect phase-matching is achieved, these coefficients could be simplified as

$$c(\tau) = \cos[gA_{p1}(\tau)A_{p2}(\tau)L] \tag{3.39}$$

$$s(\tau) = \sin[gA_{p1}(\tau)A_{p2}(\tau)L] \tag{3.40}$$

3.1.2 Quantum Treatment of Counter-Propagating Four-Wave Mixing

The configuration of CPFWM [2, 3, 8, 10, 68] is shown in Figure 3.5. Four waves including two pump waves, a signal wave and an idler wave are divided into two pairs. For each pair the two waves propagates in the opposite directions to each other. But these pairs are not necessarily parallel to each other, there is a small angle between them which is neglected for simplicity. The energy conservation relation for the carrier frequencies of these four waves is shown in Figure 3.6.

© 2018 Tous droits réservés.

lilliad.univ-lille.fr

Thèse de Junheng Shi, Université de Lille, 2018

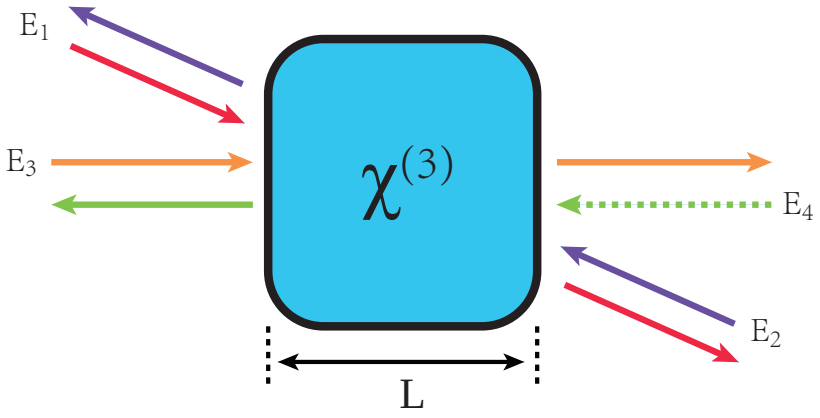

FIGURE 3.5: Configuration of counter-propagating four-wave mixing.

The derivation for positive frequency operators of CPFWM is similar to that for CFWM from Eq. (3.1) to Eq. (3.9) until when the positive frequency field operators are decomposed into slowly varying envelopes represented by annihilation operators. Because of the counter-propagating geometry, the decompositions of the four waves now become

$$\hat{E}_1^{(+)}(z,t) = \mathcal{E}_1 e^{-i\omega_1 t + ik_1 z} \int \frac{d\Omega_1}{\sqrt{2\pi}} e^{i(k(\omega_1+\Omega_1)-k_1)z} \hat{a}_1(z,\Omega_1) e^{-i\Omega_1 t} \tag{3.41a}$$

$$\hat{E}_2^{(+)}(z,t) = \mathcal{E}_2 e^{-i\omega_2 t - ik_2 z} \int \frac{d\Omega_2}{\sqrt{2\pi}} e^{-i(k(\omega_2+\Omega_2)-k_2)z} \hat{a}_2(z,\Omega_2) e^{-i\Omega_2 t} \tag{3.41b}$$

$$\hat{E}_3^{(+)}(z,t) = \mathcal{E}_3 e^{-i\omega_3 t + ik_3 z} \int \frac{d\Omega_3}{\sqrt{2\pi}} e^{i(k(\omega_3+\Omega_3)-k_3)z} \hat{a}_3(z,\Omega_3) e^{-i\Omega_3 t} \tag{3.41c}$$

$$\hat{E}_4^{(+)}(z,t) = \mathcal{E}_4 e^{-i\omega_4 t - ik_4 z} \int \frac{d\Omega_4}{\sqrt{2\pi}} e^{-i(k(\omega_4+\Omega_4)-k_4)z} \hat{a}_j(z,\Omega_4) e^{-i\Omega_4 t} \tag{3.41d}$$

Their differences with Eq.(3.10) are the wavenumbers of the two counter-propagating waves $E_2^{(+)}$ and $E_4^{(+)}$ now carry an opposite sign.

For positive frequency field operators in frequency domain:

$$\hat{E}_1(z,\omega_1') = \mathcal{E}_1 e^{ik(\omega_1+\Omega_1)z} \hat{a}_1(z,\Omega_j) \tag{3.42a}$$

$$\hat{E}_2(z,\omega_2') = \mathcal{E}_2 e^{-ik(\omega_2+\Omega_2)z} \hat{a}_2(z,\Omega_2) \tag{3.42b}$$

$$\hat{E}_3(z,\omega_3') = \mathcal{E}_3 e^{ik(\omega_3+\Omega_3)z} \hat{a}_3(z,\Omega_3) \tag{3.42c}$$

$$\hat{E}_4(z,\omega_4') = \mathcal{E}_4 e^{-ik(\omega_4+\Omega_4)z} \hat{a}_4(z,\Omega_4) \tag{3.42d}$$

© 2018 Tous droits réservés.

lilliad.univ-lille.fr

Thèse de Junheng Shi, Université de Lille, 2018

We still take ω_4' as an example and put Eq. (3.42d) into Eq. (3.9):

$$\begin{aligned}&\frac{\partial^2}{\partial z^2}\hat{a}_4(z,\Omega_4) - 2ik(\omega_4+\Omega_4)\frac{\partial}{\partial z}\hat{a}_4(z,\Omega_4)\\ =&-\frac{3(\omega_4+\Omega_4)^2\chi^{(3)}}{2c^2}\frac{\mathcal{E}_1\mathcal{E}_2\mathcal{E}_3}{\mathcal{E}_4}\int\frac{\mathrm{d}\Omega_2}{\sqrt{2\pi}}\int\frac{\mathrm{d}\Omega_3}{\sqrt{2\pi}}\\ &\times\hat{a}_1(z,\Omega_4+\Omega_3-\Omega_2)\hat{a}_2(z,\Omega_2)\hat{a}_3^\dagger(z,\Omega_3)\mathrm{e}^{-\mathrm{i}\Delta(\Omega_4,\Omega_3,\Omega_2)z}\end{aligned} \tag{3.43}$$

where the phase mismatch is

$$\Delta(\Omega_4,\Omega_3,\Omega_2) = -k(\omega_4+\Omega_4)+k(\omega_3+\Omega_3)+k(\omega_2+\Omega_2)-k(\omega_1+\Omega_4+\Omega_3-\Omega_2) \tag{3.44}$$

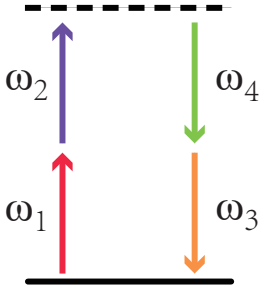

FIGURE 3.6: Energy conservation relation of counter-propagating four-wave mixing. The lengths of the vectors are irrelevant to the frequencies they denote.

Using the quasi-monochromatic approximations as Eq. (3.15) and Eq. (3.17).

$$\frac{\partial}{\partial z}\hat{a}_1(z,\Omega) = \mathrm{i}g\int\frac{\mathrm{d}\Omega'}{\sqrt{2\pi}}\int\frac{\mathrm{d}\Omega''}{\sqrt{2\pi}}\hat{a}_2^\dagger(z,\Omega'+\Omega''-\Omega)\hat{a}_3(z,\Omega')\hat{a}_4(z,\Omega'')\mathrm{e}^{\mathrm{i}\Delta(\Omega'',\Omega',\Omega''+\Omega'-\Omega)z} \tag{3.45a}$$

$$\frac{\partial}{\partial z}\hat{a}_2(z,\Omega) = -\mathrm{i}g\int\frac{\mathrm{d}\Omega'}{\sqrt{2\pi}}\int\frac{\mathrm{d}\Omega''}{\sqrt{2\pi}}\hat{a}_1^\dagger(z,\Omega'+\Omega''-\Omega)\hat{a}_3(z,\Omega')\hat{a}_4(z,\Omega'')\mathrm{e}^{\mathrm{i}\Delta(\Omega'',\Omega',\Omega)z} \tag{3.45b}$$

$$\frac{\partial}{\partial z}\hat{a}_3(z,\Omega) = \mathrm{i}g\int\frac{\mathrm{d}\Omega'}{\sqrt{2\pi}}\int\frac{\mathrm{d}\Omega''}{\sqrt{2\pi}}\hat{a}_1(z,\Omega''+\Omega-\Omega')\hat{a}_2(z,\Omega')\hat{a}_4^\dagger(z,\Omega'')\mathrm{e}^{-\mathrm{i}\Delta(\Omega'',\Omega,\Omega')z} \tag{3.45c}$$

$$\frac{\partial}{\partial z}\hat{a}_4(z,\Omega) = -\mathrm{i}g\int\frac{\mathrm{d}\Omega'}{\sqrt{2\pi}}\int\frac{\mathrm{d}\Omega''}{\sqrt{2\pi}}\hat{a}_1(z,\Omega+\Omega''-\Omega')\hat{a}_2(z,\Omega')\hat{a}_3^\dagger(z,\Omega'')\mathrm{e}^{-\mathrm{i}\Delta(\Omega,\Omega'',\Omega')z} \tag{3.45d}$$

© 2018 Tous droits réservés.

lilliad.univ-lille.fr

Thèse de Junheng Shi, Université de Lille, 2018

Phase-preserving counter-propagating four-wave mixing

Now we get down to the specific configuration where $\mathbf{E}_2(z,t)$ and $\mathbf{E}_3(z,t)$ are the two pump fields, $\mathbf{E}_1(z,t)$ is the signal field and $\mathbf{E}_4(z,t)$ is the idler field. With the classical and undepleted pump wave approximation, we reduce equations (3.45) to two coupled equations:

$$\frac{\partial}{\partial z}\hat{a}_s(z,\Omega) = \mathrm{i}g\int\frac{\mathrm{d}\Omega'}{\sqrt{2\pi}}\int\frac{\mathrm{d}\Omega''}{\sqrt{2\pi}}\alpha^*_{p1}(\Omega''+\Omega-\Omega')\alpha_{p2}(\Omega')\hat{a}_i(z,\Omega'')\mathrm{e}^{\mathrm{i}\Delta_0 z} \tag{3.46a}$$

$$\frac{\partial}{\partial z}\hat{a}_i(z,\Omega) = -\mathrm{i}g\int\frac{\mathrm{d}\Omega'}{\sqrt{2\pi}}\int\frac{\mathrm{d}\Omega''}{\sqrt{2\pi}}\alpha_{p1}(\Omega+\Omega''-\Omega')\alpha^*_{p2}(\Omega'')\hat{a}_s(z,\Omega')\mathrm{e}^{-\mathrm{i}\Delta_0 z} \tag{3.46b}$$

where the phase mismatch is approximated to the zero order:

$$\Delta_0 = -k_4 + k_3 + k_2 - k_1 \tag{3.47}$$

To solve equations (3.46) we transform them into frequency domain:

$$\frac{\partial}{\partial z}\hat{a}_s(z,\tau) = \mathrm{i}g\,\mathrm{e}^{\mathrm{i}\Delta_0 z}\alpha^*_{p1}(\tau)\alpha_{p2}(\tau)\hat{a}_i(z,\tau) \tag{3.48a}$$

$$\frac{\partial}{\partial z}\hat{a}_i(z,\tau) = -\mathrm{i}g\,\mathrm{e}^{-\mathrm{i}\Delta_0 z}\alpha_{p1}(\tau)\alpha^*_{p2}(\tau)\hat{a}_s(z,\tau) \tag{3.48b}$$

Note that due to the counter-propagating geometry, the input position of the annihilation operator of the idler wave is no longer $z=0$, but $z=L$. Consequently $\hat{a}_i(L,t)$ is the input idler wave and $\hat{a}_i(0,\tau)$ is the output idler wave.

In the case of perfect phase-matching, i.e. $\Delta_0 = 0$, we obtain the relation of the input and output signal and idler waves:

$$\hat{a}_s(L,\tau) = c(\tau)\hat{a}_s(0,\tau) + \mathrm{i}\mathrm{e}^{-\mathrm{i}\phi_p}s(\tau)\hat{a}_i(L,\tau) \tag{3.49a}$$

$$\hat{a}_i(0,\tau) = \mathrm{i}\mathrm{e}^{\mathrm{i}\phi_p}s(\tau)\hat{a}_s(L,\tau) + c(\tau)\hat{a}_i(0,\tau) \tag{3.49b}$$

The coefficients $c(\tau)$ and $s(\tau)$ are in the form of hyperbolic functions:

$$c(\tau) = \frac{1}{\cosh(gA_{p1}(\tau)A_{p2}(\tau)L)} \tag{3.50}$$

$$s(\tau) = \tanh(gA_{p1}(\tau)A_{p2}(\tau)L) \tag{3.51}$$

Yet they satisfy the relation of $|c(\tau)|^2 + |s(\tau)|^2 = 1$ which means they also could be understood as the reflection and transmission coefficients of a beam splitter.

© 2018 Tous droits réservés.

lilliad.univ-lille.fr

Thèse de Junheng Shi, Université de Lille, 2018

3.2 Multimode Squeezed States

3.2.1 Single-Mode Coherent State and Squeezed State

Coherent state

In quantum optics, the electromagnetic field is quantized based on the equivalence between a mode of electromagnetic field and a mechanical harmonic oscillator. For $\mathbf{k}, s$ mode of the electromagnetic field, the canonical variables $q_{\mathbf{k}s}(t)$ and $p_{\mathbf{k}s}(t)$ for describing the classical field are now quantized to a pair of canonically conjugate operators $\hat{q}_{\mathbf{k}s}(t)$ and $\hat{p}_{\mathbf{k}s}(t)$ which could be defined by the annihilation and creation operators of $\mathbf{k}, s$ mode:

$$\hat{q}_{\mathbf{k}s}(t) = \sqrt{\frac{\hbar}{2\omega}}[\hat{a}_{\mathbf{k}s}(t) + \hat{a}^{\dagger}_{\mathbf{k}s}(t)] \tag{3.52a}$$

$$\hat{p}_{\mathbf{k}s}(t) = \mathrm{i}\sqrt{\frac{\hbar\omega}{2}}[\hat{a}^{\dagger}_{\mathbf{k}s}(t) - \hat{a}_{\mathbf{k}s}(t)] \tag{3.52b}$$

where $\mathbf{k}$ is the wave vector of the electromagnetic field, s is the direction of the polarization. For each $\mathbf{k}$ there are two independent polarization directions.

Due to the canonical commutation relation between the annihilation operator and the creation operator, these two Hermitian operators $q_{\mathbf{k}s}(t)$ and $\hat{p}_{\mathbf{k}s}(t)$ also have the nonzero commutator $\mathrm{i}\hbar$ which leads to an uncertainty relation between them and also suggests that the wavefunction corresponds to the classical field must have minimum uncertainty. The state vector corresponding to such a wave packet with minimum uncertainty is called coherent state. It is corresponding to a classical field in quantum treatment. This concept was first introduced by Shrödinger [62] and elaborated later by Glauber [21].

For this subsection, we only deal with single-mode state.

The most basic coherent state is the vacuum state $|0\rangle$, a coherent state $|\alpha\rangle$ could be obtained by applying the displacement operator $\hat{D}(\alpha)$ to the vacuum state:

$$|\alpha\rangle = \hat{D}(\alpha)|0\rangle \tag{3.53}$$

where the displacement operator is in the form of:

$$\hat{D}(\alpha) = \mathrm{e}^{|\alpha|^2/2}\mathrm{e}^{-\alpha^*\hat{a}}\mathrm{e}^{\alpha\hat{a}^{\dagger}} \tag{3.54}$$

To show the minimum uncertainty property we discussed above, we introduce a pair of canonically conjugate operators which are essentially dimensionless $q_{\mathbf{k}s}(t)$ and $\hat{p}_{\mathbf{k}s}(t)$:

$$\hat{X}_1 = \frac{1}{2}[\hat{a} + \hat{a}^{\dagger}] \tag{3.55a}$$

$$\hat{X}_2 = \frac{1}{2\mathrm{i}}[\hat{a} - \hat{a}^{\dagger}] \tag{3.55b}$$

Of course they are Hermitian operators corresponding to a pair of quadrature amplitudes of the field.

© 2018 Tous droits réservés.

lilliad.univ-lille.fr

Thèse de Junheng Shi, Université de Lille, 2018

Their commutation relation

$$[\hat{X}_1, \hat{X}_2] = \frac{i}{2} \tag{3.56}$$

determines the minimum uncertainty

$$\langle(\Delta\hat{X}_1)^2\rangle\langle(\Delta\hat{X}_2)^2\rangle \geq \frac{1}{4}\left|\langle[\hat{X}_1, \hat{X}_2]\rangle\right|^2 = \frac{1}{16} \tag{3.57}$$

where the variance is defined as

$$\begin{aligned}\langle(\Delta\hat{X}_1)^2\rangle &= \langle(\hat{X}_1 - \langle\hat{X}_1\rangle)^2\rangle \\ &= \langle\hat{X}_1^2\rangle - \langle\hat{X}_1\rangle^2\end{aligned} \tag{3.58}$$

Since coherent state is the eigenstate of annihilation operator, it's obvious that these two amplitudes corresponds to the real and imaginary parts of the α:

$$\langle\alpha|\hat{X}_1|\alpha\rangle = Re\,\alpha \tag{3.59a}$$

$$\langle\alpha|\hat{X}_2|\alpha\rangle = Im\,\alpha \tag{3.59b}$$

and the variances of both amplitudes are

$$\langle\alpha|(\Delta\hat{X}_1)^2|\alpha\rangle = \langle\alpha|(\Delta\hat{X}_2)^2|\alpha\rangle = \frac{1}{4} \tag{3.60}$$

So the minimum uncertainty is achieved with the variances of both quadratures of the field equal to each other. Its uncertainty region is then a circle in phase space as shown in Figure 3.7.

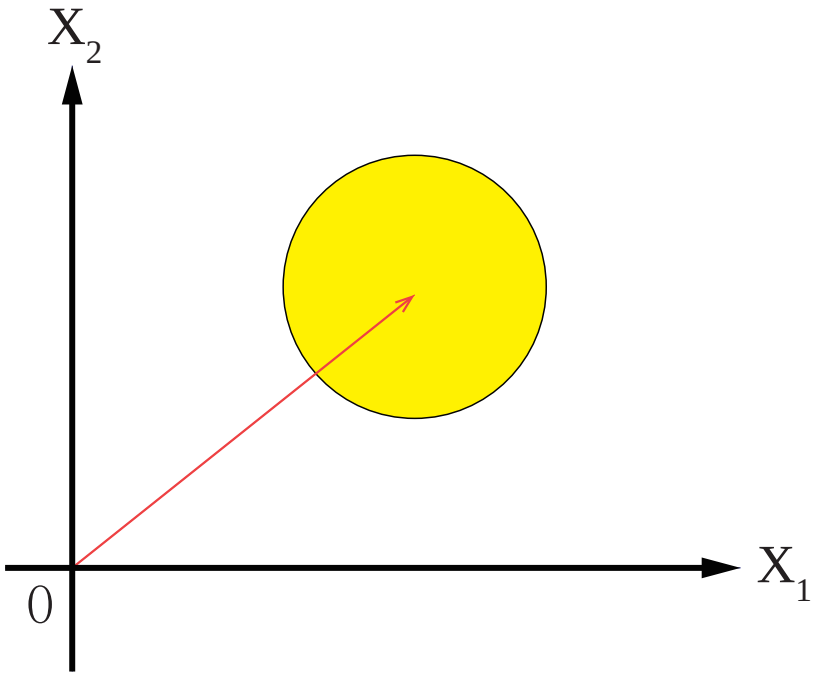

FIGURE 3.7: Uncertainty region of a coherent state.

© 2018 Tous droits réservés.

lilliad.univ-lille.fr

Thèse de Junheng Shi, Université de Lille, 2018

Squeezed state

Since coherent state represents classical field in quantum domain, now it's time for us to meet some nonclassical members of the light, one of them is the squeezed state.

Squeezed state is a state that the minimum uncertainty Eq. (3.57) still holds yet the variances of quadrature amplitudes no longer equal to each other. The variance of one quadrature is reduced below $\frac{1}{4}$ as if the uncertainty region corresponding to that quadrature is squeezed. For this reason it is called squeezed state.

A squeezed state is obtained:

$$|\alpha, z\rangle = \hat{S}(z)\hat{D}(\alpha)|0\rangle \tag{3.61}$$

by using the squeezing operator:

$$\hat{S}(z) = \exp\left\{-\frac{1}{2}(z\hat{a}^{\dagger 2} - z^*\hat{a}^2)\right\} \tag{3.62}$$

where $z = r\,\mathrm{e}^{2\mathrm{i}\phi}$

To show clearly the squeezing effect, a new pair of quadratures is introduced by rotating the original quadrature amplitudes by an angle ϕ:

$$\hat{Y}_1 = \frac{1}{2}\left[\hat{a}\mathrm{e}^{-\mathrm{i}\phi} + \hat{a}^\dagger \mathrm{e}^{\mathrm{i}\phi}\right] \tag{3.63a}$$

$$\hat{Y}_2 = \frac{1}{2i}\left[\hat{a}\mathrm{e}^{-\mathrm{i}\phi} - \hat{a}^\dagger \mathrm{e}^{\mathrm{i}\phi}\right] \tag{3.63b}$$

With the help from

$$\hat{S}^\dagger(z)\hat{a}\hat{S}(z) = \hat{a}\cosh r - \hat{a}^\dagger \mathrm{e}^{2\mathrm{i}\phi}\sinh r \tag{3.64a}$$

$$\hat{S}^\dagger(z)\hat{a}^\dagger\hat{S}(z) = \hat{a}^\dagger\cosh r - \hat{a}\mathrm{e}^{-2\mathrm{i}\phi}\sinh r \tag{3.64b}$$

We could obtain

$$\hat{S}^\dagger(z)\hat{Y}_1\hat{S}(z) = \hat{Y}_1\mathrm{e}^{r} \tag{3.65a}$$

$$\hat{S}^\dagger(z)\hat{Y}_2\hat{S}(z) = \hat{Y}_2\mathrm{e}^{-r} \tag{3.65b}$$

and then their variances

$$\langle\alpha, z|(\Delta\hat{Y}_1)^2|\alpha, z\rangle = \frac{1}{4}\mathrm{e}^{-2r} \tag{3.66a}$$

$$\langle\alpha, z|(\Delta\hat{Y}_2)^2|\alpha, z\rangle = \frac{1}{4}\mathrm{e}^{2r} \tag{3.66b}$$

While the minimum uncertainty which is the multiplication of the variances of both quadrature components still holds:

$$\langle\alpha, z|(\Delta\hat{Y}_1)^2|\alpha, z\rangle\langle\alpha, z|(\Delta\hat{Y}_1)^2|\alpha, z\rangle = \frac{1}{16} \tag{3.67}$$

the variance of one quadrature amplitude is squeezed, shown in Eq. (3.66a), at the price of the amplification of the variance of the other quadrature amplitude, shown in Eq. (3.66b). This effect is illustrated in Figure 3.8. For this reason, r is called the

© 2018 Tous droits réservés.

lilliad.univ-lille.fr

Thèse de Junheng Shi, Université de Lille, 2018

squeezing parameter as a measure of how much is uncertainty of one quadrature component being squeezed.

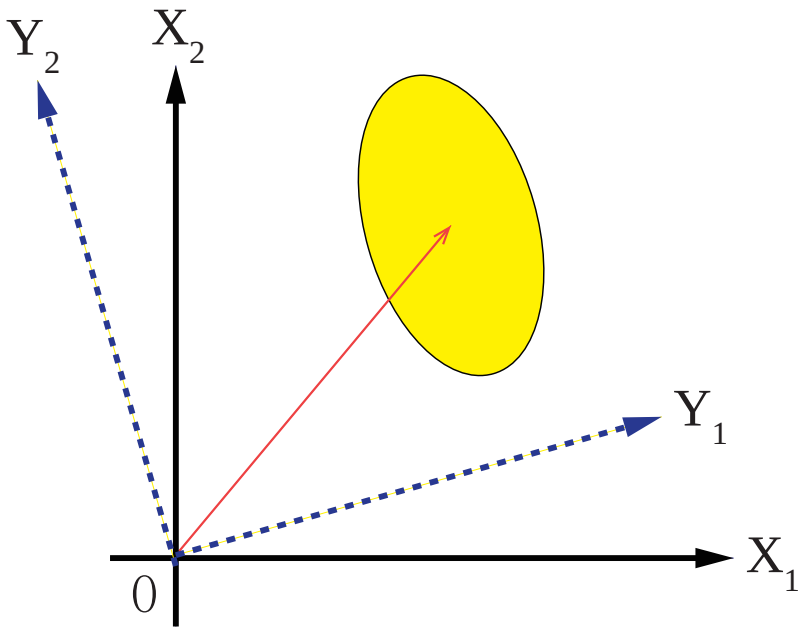

FIGURE 3.8: Uncertainty region of a squeezed state.

Since we have $\hat{S}^{-1}(z) = \hat{S}^{\dagger}(z)$, we could see the squeezing operator as a unitary operator for Bogoliubov transformation such as equations (3.64) where the transformed annihilation operator is the linear combination of the annihilation and creation operators.

3.2.2 Multimode Squeezing

Temporal fluctuation of light

Before we proceed to investigate multimode squeezing, it is important to understand the shot-noise limit of the photocurrent noise spectrum caused by the quantum fluctuation of light in time.

Since most detections of the electromagnetic field, e.g. a photodetector, is achieved by photoelectric effect which requires the absorption of photons. This process is described by the positive frequency part of the field operator $\hat{E}^{(+)}(z,t)$. Any spatial effect in the transverse area of the light beam is neglected since we are only concerned with temporal fluctuations of light.

According to quantum mechanics, the probability of finding a electromagnetic field to be in a quantum state $|\psi_f\rangle$ after the detection is $|\langle\psi_f|\hat{E}^{(+)}(z,t)|\psi_i\rangle|^2$, given its initial quantum state is a pure state $|\psi_i\rangle$. So the probability of photodetection irrespective of the final state of the field is to sum over the detection probabilities of all

© 2018 Tous droits réservés.

lilliad.univ-lille.fr

Thèse de Junheng Shi, Université de Lille, 2018

final states:

$$\begin{aligned} P &= \sum_{|\psi_f\rangle} |\langle\psi_f|\hat{E}^{(+)}(z,t)|\psi_i\rangle|^2 \\ &= \sum_{|\psi_f\rangle} \langle\psi_i|\hat{E}^{(-)}(z,t)|\psi_f\rangle\langle\psi_f|\hat{E}^{(+)}(z,t)|\psi_i\rangle \\ &= \langle\psi_i|\hat{E}^{(-)}(z,t)\hat{E}^{(+)}(z,t)|\psi_i\rangle \end{aligned} \tag{3.68}$$

According to [33], for a quasimonochromatic plane wave traveling in positive z direction:

$$\hat{E}^{(+)}(z,t) = \sqrt{\frac{\hbar\omega_0}{2\epsilon_0 cS}}\, \mathrm{e}^{\mathrm{i}(k_0 z - \omega_0 t)}\hat{a}(t) \tag{3.69}$$

where ω_0 is its carrier frequency, k_0 is its wavenumber, S is the intersection area of photodetector and the wave. The annihilation and creation operators satisfy the commutation relations:

$$[\hat{a}(t), \hat{a}\dagger(t')] = \delta(t - t') \tag{3.70}$$

$$[\hat{a}(t), \hat{a}(t')] = 0 \tag{3.71}$$

Since $\hat{E}^{(-)}(z,t)\hat{E}^{(+)}(z,t) = \dfrac{\hbar\omega_0}{2\epsilon_0 cS}\hat{a}^\dagger(t)\hat{a}(t)$, it's natural to define the photo flux operator

$$\hat{I}(t) = \hat{a}^\dagger(t)\hat{a}(t) \tag{3.72}$$

and the photocurrent operator

$$\hat{i}(t) = \eta_d \hat{I}(t) \tag{3.73}$$

where η_d is the detection efficiency of the photodetector. For simplicity, we presume it to be one.

Temporal fluctuation of light is then described by the deviation of photocurrent operator from its mean value:

$$\delta\hat{i}(t) = \hat{i}(t) - \langle\hat{i}(t)\rangle \tag{3.74}$$

Then we obtain the autocorrelation function of the photocurrent fluctuation:

$$\begin{aligned} &\langle\delta\hat{i}(t)\delta\hat{i}(t+\tau)\rangle \\ =&\langle(\hat{a}^\dagger(t)\hat{a}(t) - \langle\hat{I}(t)\rangle)(\hat{a}^\dagger(t+\tau)\hat{a}(t+\tau) - \langle\hat{I}(t+\tau)\rangle)\rangle \\ =&\langle\hat{a}^\dagger(t)\hat{a}(t)\hat{a}^\dagger(t+\tau)\hat{a}(t+\tau)\rangle - \langle\hat{I}(t)\rangle\langle\hat{I}(t+\tau)\rangle \\ =&G^{(2)}(t;t+\tau) + \langle\hat{a}^\dagger(t)\hat{a}(t+\tau)\rangle\delta(\tau) - \langle\hat{I}(t)\rangle\langle\hat{I}(t+\tau)\rangle \end{aligned} \tag{3.75}$$

where the second order correlation function is defined as

$$G^{(2)}(t;t+\tau) = \langle\hat{a}^\dagger(t)\hat{a}^\dagger(t+\tau)\hat{a}(t+\tau)\hat{a}(t)\rangle \tag{3.76}$$

Presume the light intensity is stationary in time so the second order correlation function only depends on the time difference $G^{(2)}(t;t+\tau) = G^{(2)}(\tau)$.

© 2018 Tous droits réservés.

lilliad.univ-lille.fr

Thèse de Junheng Shi, Université de Lille, 2018

Also we define the average intensity as:

$$\langle \hat{I}(t) \rangle = \langle \hat{I}(t+\tau) \rangle = \sqrt{G^{(2)}(\infty)} \tag{3.77}$$

denoted as $\langle I \rangle$ because the intensities become totally uncorrelated when they are separated sufficiently far in time.

Then the autocorrelation function could be written as

$$\langle \delta\hat{i}(t)\delta\hat{i}(t+\tau) \rangle = \langle I \rangle \delta(\tau) + G^{(2)}(\tau) - \langle I \rangle^2 \tag{3.78}$$

The normalized second order correlation function is

$$g^{(2)}(\tau) = \frac{G^{(2)}(\tau)}{\langle I \rangle^2} \tag{3.79}$$

For classical fields, we always have

$$g^{(2)}(\tau) \geq 1 \tag{3.80}$$

which means $G^{(2)}(\tau) - \langle I \rangle^2$ is no less than zero.

The photocurrent noise spectrum $(\delta i)^2_\Omega$ is defined as the Fourier transform of the autocorrelation function:

$$\begin{aligned} (\delta i)^2_\Omega &= \int \mathrm{d}\tau \mathrm{e}^{\mathrm{i}\Omega\tau} \langle \delta\hat{i}(t)\delta\hat{i}(t+\tau) \rangle \\ &= \int \mathrm{d}\tau \mathrm{e}^{\mathrm{i}\Omega\tau} [\langle I \rangle \delta(\tau) + G^{(2)}(\tau) - \langle I \rangle^2] \\ &= \langle I \rangle + \widetilde{G}^{(2)}(\Omega) - \langle I \rangle^2 \delta(\Omega) \\ &\geq \langle I \rangle \end{aligned} \tag{3.81}$$

where

$$\widetilde{G}^{(2)}(\Omega) = \int \mathrm{d}\tau \mathrm{e}^{\mathrm{i}\Omega\tau} G^{(2)}(\tau) \tag{3.82}$$

Therefore for classical electromagnetic fields, the noise spectrum always has a lowest limit $\langle I \rangle$. This is called shot-noise limit.

Generation of multimode squeezed light

To help understanding multimode squeezing, we could have a look at an actual example to generate multimode squeezed light. For the convenience of illustration, here our derivations for the CFWM: equations (3.19) is used.

If we presume that $\hat{a}_3$ is the signal wave, $\hat{a}_4$ is the idler wave, $\hat{a}_1$ and $\hat{a}_2$ are the identical undepleted, monochromatic pump wave which means for Eq. (3.19c) and Eq. (3.19d) we have:

$$\hat{a}_1(z, \Omega'' + \Omega - \Omega') \approx \alpha_p \sqrt{2\pi} \delta(\Omega'' + \Omega - \Omega') \tag{3.83a}$$

$$\hat{a}_2(z, \Omega') \approx \alpha_p \sqrt{2\pi} \delta(\Omega') \tag{3.83b}$$

© 2018 Tous droits réservés.

lilliad.univ-lille.fr

Thèse de Junheng Shi, Université de Lille, 2018

Using this approximation we could reduce equations (3.19) to:

$$\frac{\partial}{\partial z}\hat{a}_s(z,\Omega) = \mathrm{i}g\alpha_p^2\hat{a}_i^\dagger(z,-\Omega)\mathrm{e}^{-\mathrm{i}\Delta(\Omega)z} \tag{3.84a}$$

$$\frac{\partial}{\partial z}\hat{a}_i(z,\Omega) = \mathrm{i}g\alpha_p^2\hat{a}_s^\dagger(z,-\Omega)\mathrm{e}^{-\mathrm{i}\Delta(\Omega)z} \tag{3.84b}$$

where

$$\Delta(\Omega) = k(\omega_s+\Omega) + k(\omega_i-\Omega) - 2k_p \tag{3.85}$$

The solutions to the coupled equations (3.84) are

$$\hat{a}_s(l,\Omega) = U(\Omega)\hat{a}_s(0,\Omega) + V(\Omega)\hat{a}_i^\dagger(0,-\Omega) \tag{3.86a}$$

$$\hat{a}_i(l,\Omega) = U(\Omega)\hat{a}_i(0,\Omega) + V(\Omega)\hat{a}_s^\dagger(0,-\Omega) \tag{3.86b}$$

These coefficients are

$$U(\Omega) = \left[\cosh(\Gamma(\Omega)l) + \frac{\mathrm{i}\Delta(\Omega)}{2\Gamma(\Omega)}\sinh(\Gamma(\Omega)l)\right]\mathrm{e}^{-\mathrm{i}\Delta(\Omega)l/2} \tag{3.87a}$$

$$V(\Omega) = \frac{\mathrm{i}g\alpha_p^2}{\Gamma(\Omega)}\sinh(\Gamma(\Omega)l)\mathrm{e}^{-\mathrm{i}\Delta(\Omega)l/2} \tag{3.87b}$$

where $\Gamma(\Omega) = \sqrt{g^2|\alpha_p|^4 - \Delta(\Omega)^2/4}$

Then if we use a 50/50 beam splitter to mix the signal wave and idler wave:

$$\hat{a}_{in}(0,\Omega) = \frac{1}{\sqrt{2}}[\hat{a}_s(0,\Omega) + \hat{a}_i(0,\Omega)] \tag{3.88a}$$

$$\hat{a}_{in}(l,\Omega) = \frac{1}{\sqrt{2}}[\hat{a}_s(l,\Omega) + \hat{a}_i(l,\Omega)] \tag{3.88b}$$

The subscript of $\hat{a}_{in}$ is to indicate that this is the input of a temporal imaging system.

Therefore the mixed wave satisfy the Bogoliubov transformation:

$$\hat{a}_{in}(l,\Omega) = U(\Omega)\hat{a}_{in}(0,\Omega) + V(\Omega)\hat{a}_{in}^\dagger(0,-\Omega) \tag{3.89}$$

since from (3.87) we have the relation $|U(\Omega)|^2 - |V(\Omega)|^2 = 1$.

As would be seen in next subsection, such transformation indicates the presence of multimode squeezing, and in this particular case, the compression of shot-noise.

In the following sections, however, we use a temporally broadband squeezed state of light produced by a traveling-wave Optical Parametric Amplifier (OPA) as shown in Figure 3.9 [33]. A monochromatic plane wave α_p with its frequency $\omega_p = 2\omega_0$ and its wavenumber k_p pass through a second-order nonlinear crystal with length equals to L. The direction of the pump wave is normal to the surface of the nonlinear crystal. The signal wave and the idler are produced thanks to the parametric down conversion. The frequencies of the two waves are $\omega_0 + \Omega$ and $\omega_0 - \Omega$, their wave vectors are $\mathbf{k}(\mathbf{q},\Omega)$ and $\mathbf{k}(-\mathbf{q},-\Omega)$ where $\mathbf{q}$ is the transverse component. For simplicity, we presume $\mathbf{q}$ to be zero since it's not of our concern in this case. As a result, we still get the Bogolubov transformation relation from the input ($\zeta = 0$) to the output ($\zeta = l$) of the OPA as Eq.(3.89). Nevertheless, the complex coefficients $U(\Omega)$ and $V(\Omega)$ have

© 2018 Tous droits réservés.

lilliad.univ-lille.fr

Thèse de Junheng Shi, Université de Lille, 2018

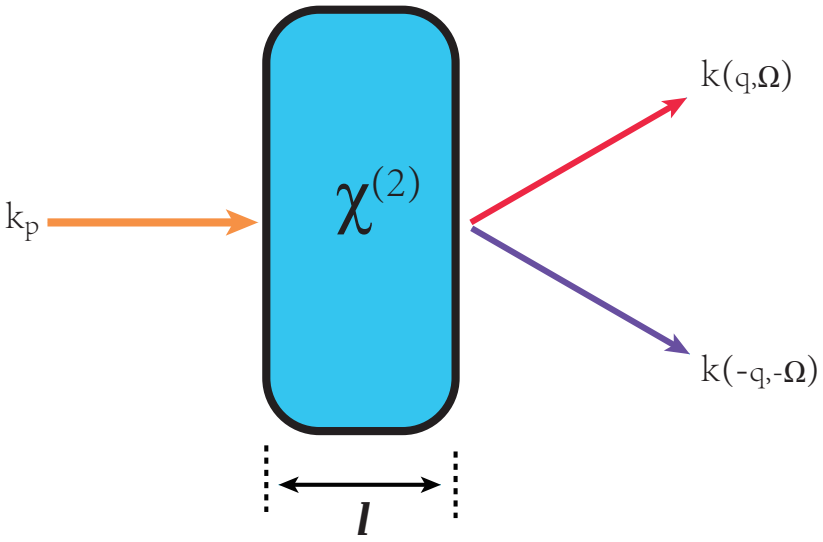

FIGURE 3.9: An optical parametric amplifier in a second-order nonlinear crystal.

changed, they become

$$U(\Omega) = \left[\cosh(\Gamma l) + \frac{i\Delta(\Omega)}{2\Gamma}\sinh(\Gamma l)\right] e^{-i\Delta(\Omega)l/2} \tag{3.90a}$$

$$V(\Omega) = \frac{\sigma}{\Gamma}\sinh(\Gamma l) e^{-i\Delta(\Omega)l/2} \tag{3.90b}$$

The phase mismatch term becomes

$$\Delta(\Omega) = k(\Omega) + k(-\Omega) - k_p \tag{3.91}$$

where $\Gamma = \sqrt{|\sigma|^2 - \Delta(\Omega)^2/4}$ and $\sigma = g\alpha_p$. g is proportional to the second-order susceptibility $\chi^{(2)}$. It's not hard to see that $|U(\Omega)|^2 - |V(\Omega)|^2 = 1$ still holds.

3.2.3 Squeezing Spectrum of Squeezed Vacuum

To obtain the noise spectrum of a squeezed state, one has to resort to a technique called balanced homodyne detection first introduced by Yuen[75] and developed by Mandel and Wolf [37]. Its configuration could be seen in Figure 3.10, a signal wave is mixed with a very strong local oscillator $\beta = |\beta|e^{i\phi_\beta}$ in a 50/50 beam splitter. The outputs of the beam splitter are measured by two photodetectors separately. The difference current from two balanced photodetectors is the output.

The signal wave is a squeezed vacuum state:

$$\hat{a}_{in}(l,\Omega) = U(\Omega)\hat{a}_{in}(0,\Omega) + V(\Omega)\hat{a}^\dagger_{in}(0,-\Omega) \tag{3.92}$$

© 2018 Tous droits réservés.

lilliad.univ-lille.fr

Thèse de Junheng Shi, Université de Lille, 2018

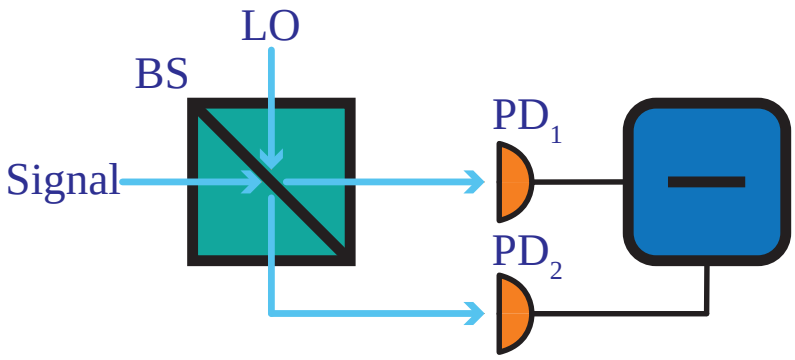

FIGURE 3.10: Configuration of balanced homodyne detection. BS is the beam splitter, LO is the local oscillator, PD is the photodetector

With the signal wave and the local oscillator taken as inputs, we obtain the two outputs from the beam splitter

$$\hat{b}_1(\tau) = \frac{1}{\sqrt{2}}[\beta + \hat{a}_{in}(l,\tau)] \tag{3.93a}$$

$$\hat{b}_2(\tau) = \frac{1}{\sqrt{2}}[\beta - \hat{a}_{in}(l,\tau)] \tag{3.93b}$$

Their difference current of these two photodetectors is

$$\begin{aligned}\hat{I}(\tau) =& \hat{b}_1^\dagger(\tau)\hat{b}_1(\tau) - \hat{b}_2^\dagger(\tau)\hat{b}_2(\tau) \\ =& \frac{1}{2}\Big[\big(\beta^* + \hat{a}_{in}^\dagger(l,\tau)\big)\big(\beta + \hat{a}_{in}(l,\tau)\big) - \big(\beta^* - \hat{a}_{in}^\dagger(l,\tau)\big)\big(\beta - \hat{a}_{in}(l,\tau)\big)\Big] \\ =& \beta^*\hat{a}_{in}(l,\tau) + \beta\hat{a}_{in}^\dagger(l,\tau)\end{aligned} \tag{3.94}$$

The variance of the difference current is then

$$\begin{aligned}\langle \Delta\hat{I}(\tau)\Delta\hat{I}(\tau+t)\rangle =& \langle[\hat{I}(\tau) - \langle\hat{I}(\tau)\rangle][\hat{I}(\tau+t) - \langle\hat{I}(\tau+t)\rangle] \\ =& \langle\hat{I}(\tau)\hat{I}(\tau+t)\rangle - \langle\hat{I}(\tau)\rangle\langle\hat{I}(\tau+t)\rangle\end{aligned} \tag{3.95}$$

Since we deal with squeezed vacuum, we have

$$\langle\hat{I}(\tau)\rangle = 0 \tag{3.96}$$

© 2018 Tous droits réservés.

lilliad.univ-lille.fr

Thèse de Junheng Shi, Université de Lille, 2018

Consequently what we need to calculate is the autocorrelation function of this difference current:

$$\begin{aligned}
&\langle \hat{I}(\tau)\hat{I}(\tau+t)\rangle \\
=&\langle \Big[\beta^*\hat{a}_{in}(l,\tau)+\beta\hat{a}_{in}^\dagger(l,\tau)\Big]\Big[\beta^*\hat{a}_{in}(l,\tau+t)+\beta\hat{a}_{in}^\dagger(l,\tau+t)\Big]\rangle \\
=&\beta\beta^*\langle \hat{a}_{in}^\dagger(l,\tau)\hat{a}_{in}(l,\tau+t)\rangle \\
&+\beta^*\beta\langle \hat{a}_{in}(l,\tau)\hat{a}_{in}^\dagger(l,\tau+t)\rangle \\
&+\beta^*\beta^*\langle \hat{a}_{in}(l,\tau)\hat{a}_{in}(l,\tau+t)\rangle \\
&+\beta\beta\langle \hat{a}_{in}^\dagger(l,\tau)\hat{a}_{in}^\dagger(l,\tau+t)\rangle
\end{aligned} \tag{3.97}$$

Before we proceed to calculate the noise spectrum which is the Fourier transform of the autocorrelation function, we need to calculate

$$\begin{aligned}
&\langle \hat{a}_{in}^\dagger(l,\tau)\hat{a}_{in}(l,\tau+t)\rangle \\
=&\langle \int\frac{\mathrm{d}\Omega_1}{\sqrt{2\pi}}\mathrm{e}^{-\mathrm{i}\Omega_1\tau}\hat{a}_{in}^\dagger(l,-\Omega_1)\int\frac{\mathrm{d}\Omega_2}{\sqrt{2\pi}}\mathrm{e}^{-\mathrm{i}\Omega_2(\tau+t)}\hat{a}_{in}(l,\Omega_2)\rangle \\
=&\int\frac{\mathrm{d}\Omega_1}{\sqrt{2\pi}}\int\frac{\mathrm{d}\Omega_2}{\sqrt{2\pi}}\mathrm{e}^{-\mathrm{i}\Omega_2 t}\mathrm{e}^{-\mathrm{i}(\Omega_2+\Omega_1)\tau} \\
&\times\langle \hat{a}_{in}^\dagger(l,-\Omega_1)\hat{a}_{in}(l,\Omega_2)\rangle \\
=&\int\frac{\mathrm{d}\Omega_1}{\sqrt{2\pi}}\int\frac{\mathrm{d}\Omega_2}{\sqrt{2\pi}}\mathrm{e}^{-\mathrm{i}\Omega_2 t}\mathrm{e}^{-\mathrm{i}(\Omega_2+\Omega_1)\tau} \\
&\times\langle 0|\Big[U^*(-\Omega_1)\hat{a}_{in}^\dagger(0,-\Omega_1)+V^*(-\Omega_1)\hat{a}_{in}(0,\Omega_1)\Big]\Big[U(\Omega_2)\hat{a}_{in}(0,\Omega_2)+V(\Omega_2)\hat{a}_{in}^\dagger(0,-\Omega_2)\Big]|0\rangle \\
=&\int\frac{\mathrm{d}\Omega_1}{\sqrt{2\pi}}\int\frac{\mathrm{d}\Omega_2}{\sqrt{2\pi}}\mathrm{e}^{-\mathrm{i}\Omega_2 t}\mathrm{e}^{-\mathrm{i}(\Omega_2+\Omega_1)\tau}V^*(-\Omega_1)V(\Omega_2)\delta(\Omega_1+\Omega_2) \\
=&\frac{1}{\sqrt{2\pi}}\int\frac{\mathrm{d}\Omega_2}{\sqrt{2\pi}}\mathrm{e}^{-\mathrm{i}\Omega_2 t}|V(\Omega_2)|^2
\end{aligned} \tag{3.98}$$

$$\begin{aligned}
&\langle \hat{a}_{in}(l,\tau)\hat{a}_{in}^\dagger(l,\tau+t)\rangle \\
=&\langle \int\frac{\mathrm{d}\Omega_1}{\sqrt{2\pi}}\mathrm{e}^{-\mathrm{i}\Omega_1\tau}\hat{a}_{in}(l,\Omega_1)\int\frac{\mathrm{d}\Omega_2}{\sqrt{2\pi}}\mathrm{e}^{-\mathrm{i}\Omega_2(\tau+t)}\hat{a}_{in}^\dagger(l,-\Omega_2)\rangle \\
=&\int\frac{\mathrm{d}\Omega_1}{\sqrt{2\pi}}\int\frac{\mathrm{d}\Omega_2}{\sqrt{2\pi}}\mathrm{e}^{-\mathrm{i}\Omega_2 t}\mathrm{e}^{-\mathrm{i}(\Omega_2+\Omega_1)\tau} \\
&\times\langle \hat{a}_{in}(l,\Omega_1)\hat{a}_{in}^\dagger(l,-\Omega_2)\rangle \\
=&\int\frac{\mathrm{d}\Omega_1}{\sqrt{2\pi}}\int\frac{\mathrm{d}\Omega_2}{\sqrt{2\pi}}\mathrm{e}^{-\mathrm{i}\Omega_2 t}\mathrm{e}^{-\mathrm{i}(\Omega_2+\Omega_1)\tau} \\
&\times\langle 0|\Big[U(\Omega_1)\hat{a}_{in}(0,\Omega_1)+V(\Omega_1)\hat{a}_{in}^\dagger(0,-\Omega_1)\Big]\Big[U^*(-\Omega_2)\hat{a}_{in}^\dagger(0,-\Omega_2)+V^*(-\Omega_2)\hat{a}_{in}(0,\Omega_2)\Big]|0\rangle \\
=&\int\frac{\mathrm{d}\Omega_1}{\sqrt{2\pi}}\int\frac{\mathrm{d}\Omega_2}{\sqrt{2\pi}}\mathrm{e}^{-\mathrm{i}\Omega_2 t}\mathrm{e}^{-\mathrm{i}(\Omega_2+\Omega_1)\tau}U(\Omega_1)U^*(-\Omega_2)\delta(\Omega_1+\Omega_2) \\
=&\frac{1}{\sqrt{2\pi}}\int\frac{\mathrm{d}\Omega_2}{\sqrt{2\pi}}\mathrm{e}^{-\mathrm{i}\Omega_2 t}|U(-\Omega_2)|^2
\end{aligned} \tag{3.99}$$

© 2018 Tous droits réservés.

lilliad.univ-lille.fr

Thèse de Junheng Shi, Université de Lille, 2018

$$
\begin{aligned}
&\langle \hat{a}_{in}(l,\tau)\hat{a}_{in}(l,\tau+t)\rangle \\
=&\langle \int \frac{\mathrm{d}\Omega_1}{\sqrt{2\pi}} \mathrm{e}^{-\mathrm{i}\Omega_1\tau}\hat{a}_{in}(l,\Omega_1) \int \frac{\mathrm{d}\Omega_2}{\sqrt{2\pi}} \mathrm{e}^{-\mathrm{i}\Omega_2(\tau+t)}\hat{a}_{in}(l,\Omega_2)\rangle \\
=&\int \frac{\mathrm{d}\Omega_1}{\sqrt{2\pi}} \int \frac{\mathrm{d}\Omega_2}{\sqrt{2\pi}} \mathrm{e}^{-\mathrm{i}\Omega_2 t}\mathrm{e}^{-\mathrm{i}(\Omega_2+\Omega_1)\tau} \\
&\times \langle \hat{a}_{in}(l,\Omega_1)\hat{a}_{in}(l,\Omega_2)\rangle \\
=&\int \frac{\mathrm{d}\Omega_1}{\sqrt{2\pi}} \int \frac{\mathrm{d}\Omega_2}{\sqrt{2\pi}} \mathrm{e}^{-\mathrm{i}\Omega_2 t}\mathrm{e}^{-\mathrm{i}(\Omega_2+\Omega_1)\tau} \\
&\times \langle 0| \Big[U(\Omega_1)\hat{a}_{in}(0,\Omega_1) + V(\Omega_1)\hat{a}^\dagger_{in}(0,-\Omega_1)\Big] \Big[U(\Omega_2)\hat{a}_{in}(0,\Omega_2) + V(\Omega_2)\hat{a}^\dagger_{in}(0,-\Omega_2)\Big] |0\rangle \\
=&\int \frac{\mathrm{d}\Omega_1}{\sqrt{2\pi}} \int \frac{\mathrm{d}\Omega_2}{\sqrt{2\pi}} \mathrm{e}^{-\mathrm{i}\Omega_2 t}\mathrm{e}^{-\mathrm{i}(\Omega_2+\Omega_1)\tau} U(\Omega_1)V(\Omega_2)\delta(\Omega_1+\Omega_2) \\
=&\frac{1}{\sqrt{2\pi}} \int \frac{\mathrm{d}\Omega_2}{\sqrt{2\pi}} \mathrm{e}^{-\mathrm{i}\Omega_2 t} U(-\Omega_2)V(\Omega_2)
\end{aligned}
\tag{3.100}
$$

$$
\begin{aligned}
&\langle \hat{a}^\dagger_{in}(l,\tau)\hat{a}^\dagger_{in}(l,\tau+t)\rangle \\
=&\langle \int \frac{\mathrm{d}\Omega_1}{\sqrt{2\pi}} \mathrm{e}^{-\mathrm{i}\Omega_1\tau}\hat{a}^\dagger_{in}(l,-\Omega_1) \int \frac{\mathrm{d}\Omega_2}{\sqrt{2\pi}} \mathrm{e}^{-\mathrm{i}\Omega_2(\tau+t)}\hat{a}^\dagger_{in}(l,-\Omega_2)\rangle \\
=&\int \frac{\mathrm{d}\Omega_1}{\sqrt{2\pi}} \int \frac{\mathrm{d}\Omega_2}{\sqrt{2\pi}} \mathrm{e}^{-\mathrm{i}\Omega_2 t}\mathrm{e}^{-\mathrm{i}(\Omega_2+\Omega_1)\tau} \\
&\times \langle \hat{a}^\dagger_{in}(l,-\Omega_1)\hat{a}^\dagger_{in}(l,-\Omega_2)\rangle \\
=&\int \frac{\mathrm{d}\Omega_1}{\sqrt{2\pi}} \int \frac{\mathrm{d}\Omega_2}{\sqrt{2\pi}} \mathrm{e}^{-\mathrm{i}\Omega_2 t}\mathrm{e}^{-\mathrm{i}(\Omega_2+\Omega_1)\tau} \\
&\times \langle 0| \Big[U^*(-\Omega_1)\hat{a}^\dagger_{in}(0,-\Omega_1) + V^*(-\Omega_1)\hat{a}_{in}(0,\Omega_1)\Big] \Big[U^*(-\Omega_2)\hat{a}^\dagger_{in}(0,-\Omega_2) + V^*(-\Omega_2)\hat{a}_{in}(0,\Omega_2)\Big] |0\rangle \\
=&\int \frac{\mathrm{d}\Omega_1}{\sqrt{2\pi}} \int \frac{\mathrm{d}\Omega_2}{\sqrt{2\pi}} \mathrm{e}^{-\mathrm{i}\Omega_2 t}\mathrm{e}^{-\mathrm{i}(\Omega_2+\Omega_1)\tau} V^*(-\Omega_1)U^*(-\Omega_2)\delta(\Omega_1+\Omega_2) \\
=&\frac{1}{\sqrt{2\pi}} \int \frac{\mathrm{d}\Omega_2}{\sqrt{2\pi}} \mathrm{e}^{-\mathrm{i}\Omega_2 t} U^*(-\Omega_2)V^*(\Omega_2)
\end{aligned}
\tag{3.101}
$$

© 2018 Tous droits réservés.

lilliad.univ-lille.fr

Thèse de Junheng Shi, Université de Lille, 2018

With the results of these calculations, we obtain the noise spectrum

$$\begin{aligned}
(\delta i)^2_\Omega =& \int \frac{\mathrm{d}t}{\sqrt{2\pi}} \mathrm{e}^{\mathrm{i}\Omega t} \langle \hat{I}(\tau)\hat{I}(\tau+t)\rangle \\
=& \int \frac{\mathrm{d}t}{\sqrt{2\pi}} \mathrm{e}^{\mathrm{i}\Omega t} |\beta|^2 \Big[\langle \hat{a}^\dagger_{in}(l,\tau)\hat{a}_{in}(l,\tau+t)\rangle \\
&+ \langle \hat{a}_{in}(l,\tau)\hat{a}^\dagger_{in}(l,\tau+t)\rangle \\
&+ \mathrm{e}^{-2\mathrm{i}\phi_\beta} \langle \hat{a}_{in}(l,\tau)\hat{a}_{in}(l,\tau+t)\rangle \\
&+ \mathrm{e}^{2\mathrm{i}\phi_\beta} \langle \hat{a}^\dagger_{in}(l,\tau)\hat{a}^\dagger_{in}(l,\tau+t)\rangle \Big] \\
=& \frac{|\beta|^2}{\sqrt{2\pi}} \int \frac{\mathrm{d}t}{\sqrt{2\pi}} \mathrm{e}^{\mathrm{i}\Omega t} \int \frac{\mathrm{d}\Omega_2}{\sqrt{2\pi}} \mathrm{e}^{-\mathrm{i}\Omega_2 t} \Big[|V(\Omega_2)|^2 + |U(-\Omega_2)|^2 \\
&+ \mathrm{e}^{-2\mathrm{i}\phi_\beta} U(-\Omega_2)V(\Omega_2) + \mathrm{e}^{2\mathrm{i}\phi_\beta} U^*(-\Omega_2)V^*(\Omega_2) \Big] \\
=& |\beta|^2 \int \frac{\mathrm{d}\Omega_2}{\sqrt{2\pi}} \delta(\Omega-\Omega_2) \Big[|V(\Omega_2)|^2 + |U(-\Omega_2)|^2 \\
&+ \mathrm{e}^{-2\mathrm{i}\phi_\beta} U(-\Omega_2)V(\Omega_2) + \mathrm{e}^{2\mathrm{i}\phi_\beta} U^*(-\Omega_2)V^*(\Omega_2) \Big] \\
=& \frac{|\beta|^2}{\sqrt{2\pi}} \Big[|V(\Omega)|^2 + |U(-\Omega)|^2 \\
&+ \mathrm{e}^{-2\mathrm{i}\phi_\beta} U(-\Omega)V(\Omega) + \mathrm{e}^{2\mathrm{i}\phi_\beta} U^*(-\Omega)V^*(\Omega) \Big]
\end{aligned} \tag{3.102}$$

If we separate the phase out of the the coefficients

$$U(-\Omega)V(\Omega) = |U(-\Omega)V(\Omega)|\mathrm{e}^{2\mathrm{i}\psi(\Omega)} \tag{3.103}$$

and let

$$\theta(\Omega) = \psi(\Omega) - \phi_\beta \tag{3.104}$$

Then the noise spectrum in Eq. (3.102) could be written as

$$\begin{aligned}
&(\delta i)^2_\Omega \\
=& \frac{|\beta|^2}{\sqrt{2\pi}} \Big[|V(\Omega)|^2 + |U(-\Omega)|^2 \\
&+ \mathrm{e}^{2\mathrm{i}\theta(\Omega)} |U(-\Omega)||V(\Omega)| + \mathrm{e}^{-2\mathrm{i}\theta(\Omega)} |U(-\Omega)||V(\Omega)| \Big] \\
=& \frac{|\beta|^2}{\sqrt{2\pi}} \Bigg[\Big[\cos^2(\theta(\Omega)) + \sin^2(\theta(\Omega)) \Big] \Big[|V(\Omega)|^2 + |U(-\Omega)|^2 \Big] \\
&+ 2\Big[\cos^2(\theta(\Omega)) - \sin^2(\theta(\Omega)) \Big] |U(-\Omega)||V(\Omega)| \Bigg] \\
=& \frac{|\beta|^2}{\sqrt{2\pi}} \Bigg[\cos^2(\theta(\Omega)) \Big[|U(-\Omega)| + |V(\Omega)| \Big]^2 \\
&+ \sin^2(\theta(\Omega)) \Big[|U(-\Omega)| - |V(\Omega)| \Big]^2 \Bigg]
\end{aligned} \tag{3.105}$$

Since $|U(-\Omega)| = |U(\Omega)|$, and with the squeezing properties that $|U(\Omega)| \pm |V(\Omega)| =$

© 2018 Tous droits réservés.

lilliad.univ-lille.fr

Thèse de Junheng Shi, Université de Lille, 2018

$e^{\pm r(\Omega)}$ where $r(\Omega)$ is the squeezing parameter. Normalizing the noise spectrum with $|\beta|^2/\sqrt{2\pi}$, we obtain the squeezing spectrum as

$$S_{in}(\Omega) = \cos^2(\theta(\Omega))e^{2r(\Omega)} + \sin^2(\theta(\Omega))e^{-2r(\Omega)} \tag{3.106}$$

The maximized squeezing is achieved by letting $\theta(0) = \pi/2$ by adjusting the phase of the local oscillator. And the maximum squeezing parameter is defined as

$$r_m = r(0) \tag{3.107}$$

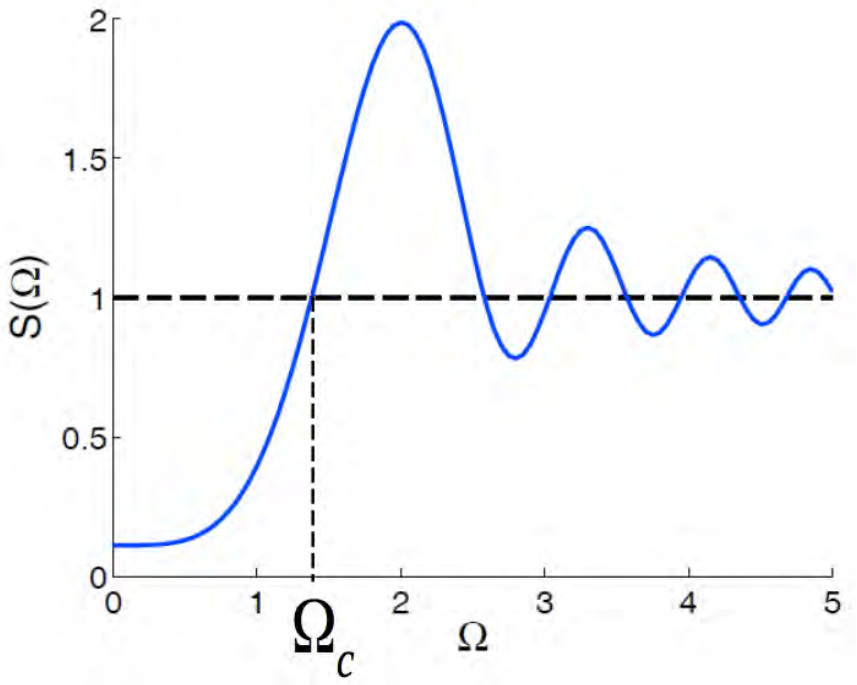

FIGURE 3.11: Squeezing spectrum of broadband squeezed light. The maximum squeezing parameter $e^{r_m} = 3$. The ordinates are graduated in shot-noise units.

The squeezing Spectrum is shown in Figure 3.11. The presence of broadband squeezing is indicated by the fact that for $\Omega < \Omega_c$, the squeezing spectrum is below shot noise, in other words, the noise has been suppressed.

We could actually approximately evaluate the value of Ω_c in this particular case. According to equations (3.103) and (3.104), we could use the definitions of $U(\Omega)$ and $V(\Omega)$ from equations (3.90) to obtain

$$\psi(\Omega) = -\frac{l}{4}(\Delta(\Omega) + \Delta(-\Omega)) \tag{3.108}$$

According to the definition of $\Delta(\Omega)$ in Eq. (3.91), we could finally obtain $\theta(\Omega)$ as

$$\theta(\Omega) = -\frac{1}{2}[k(\Omega) + k(-\Omega) - k_p]l - \phi_\beta \tag{3.109}$$

© 2018 Tous droits réservés.

lilliad.univ-lille.fr

Thèse de Junheng Shi, Université de Lille, 2018

Expand it with respect to Ω to the second order (since the first-order terms would cancel each other) we obtain

$$\psi(\Omega) \approx \psi(0) - \frac{\Omega^2}{\Omega_c^2} \tag{3.110}$$

where $\Omega_c = (k''l/2)^{-1/2}$

3.3 Four-Wave Mixing Time Lens with Squeezed Light

In the second chapter we concluded that the required functionality for a time lens is to multiply the input waveform with a quadratic phase in time. And from Eq. (3.28b) and (3.36b) we could see that such functionality could be provided by the FWM process if we let the phase of the pump wave be the quadratic phase we wanted.

A pump wave with such phase is produced by passing an ultrashort pulse with femtosecond plusewidth through a dispersive medium with large group velocity dispersion. If the initial pump wave is

$$A_{p,in}(\tau) = A_p \mathrm{e}^{-\frac{\tau^2}{2\sigma^2}} \tag{3.111}$$

where σ is its temporal pulsewidth.

This field is assumed to be Fourier-limited that its bandwidth:

$$\delta\omega_p = \frac{1}{\sigma} \tag{3.112}$$

The GDD of this dispersive medium equals to D, then the amplitude of the pump wave after the dispersion becomes

$$A_{p,out}(\tau) = A_p \exp\left\{-\frac{\tau^2/2}{\sigma^2/(\frac{\sigma^2}{D})^2 + \sigma^2}\right\} \approx A_p \exp\left\{-\frac{\tau^2}{2(D/\sigma)^2}\right\} \tag{3.113}$$

and its phase becomes

$$\phi_p(\tau) = \frac{1}{1 + (\sigma^2/D)^2}\frac{\tau^2}{2D} \approx \frac{\tau^2}{2D} \tag{3.114}$$

Approximations made in (3.113) and (3.114) are under the assumption that $\sigma^2 \ll D$, in other words, this is the case of Fraunhofer dispersion which we discussed in section 2.3.1. Through this method, we not only obtain the quadratic pump phase as we wanted (3.114), but also transform the typical long bandwidth of femtosecond pulse into long temporal duration which could be considered as the aperture of a time lens. Two birds killed with one stone.

The pump wave could also be written as

$$A_{p,out} = A_p \exp\left\{-\frac{\tau^2}{2(D\delta\omega_p)^2}\right\} \tag{3.115}$$

© 2018 Tous droits réservés.

lilliad.univ-lille.fr

Thèse de Junheng Shi, Université de Lille, 2018

3.3.1 Phase-Conjugating Four-Wave Mixing Time Lens with Squeezed Light

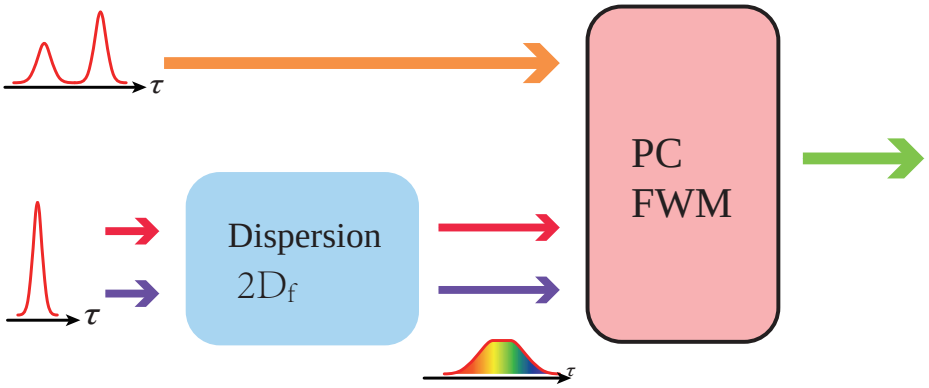

FIGURE 3.12: Configuration of phase-conjugating four-wave mixing time lens.

The configuration of PCFWM time lens is shown in Figure 3.12. Two pump waves with their carrier frequencies as ω_{p1} and ω_{p2}, produced by passing femtosecond pulses through a dispersive medium whose GDD equals to $2D_f$, converted a signal wave with carrier frequency ω_s into a idler wave with carrier frequency ω_i in a nonlinear medium where PCFWM takes place. According to our derivations in section 3.1.1, if we presume a perfect phase-matching condition of this FWM process, from Eq. (3.28b) we have the transformation relation between the input signal and the output idler:

$$\hat{a}_{out}(\tau) = \mathrm{i}e^{\mathrm{i}\phi_p(\tau)} v(\tau)\hat{a}^{\dagger}_{s,in}(\tau) + u(\tau)\hat{a}_{i,in}(\tau) \tag{3.116}$$

where

$$u(\tau) = \cosh[gA_p^2(\tau)L] \tag{3.117a}$$

$$v(\tau) = \sinh[gA_p^2(\tau)L] \tag{3.117b}$$

Because of the parametric amplification relation between $u(\tau)$ and $v(\tau)$, we define the parametric gain parameter $G(\tau) = |v(\tau)|^2$.

The amplitude and the total phase of the pump waves are

$$A_p(\tau) = A_p \exp\left\{-\frac{\tau^2}{2(2D_f\delta\omega_p)^2}\right\} \tag{3.118}$$

$$\phi_p(\tau) = \frac{\tau^2}{2(2D_f)} \times 2 = \frac{\tau^2}{2D_f} \tag{3.119}$$

As could be seen in Eq. (3.116), the signal wave is not the only input, the input idler should also be taken into consideration.

If we are only dealing with classical light that we replace the annihilation operator with α, since the input idler wave is a vacuum, that it would not affect the output wave:

$$\alpha_{out}(\tau) = \mathrm{i}v(\tau)\mathcal{Q}\left[\frac{1}{D_f}\right]\alpha^*_{s,in}(\tau) \tag{3.120}$$

© 2018 Tous droits réservés.

lilliad.univ-lille.fr

Thèse de Junheng Shi, Université de Lille, 2018

From the quantum perspective, however, situations have changed. In order to show that, we need to evaluate the effect of PCFWM time lens on broadband squeezed light. We use the squeezed vacuum produced in section 3.2.2. Hence the notation of $\hat{a}_{s,in}(\tau)$ is changed to $\hat{a}_{in}(l,\tau)$.

The method of evaluating the squeezing spectrum is what was illustrated in section 3.2.3 - balanced homodyne detection. This time, we use the pump wave adding an additional phase ϕ_β as the local oscillator so we could cancel out the quadratic phase introduced by the pump wave in Eq. (3.116).

As shown in Figure 3.10, the output idler from the time lens is mixed with the local oscillator, resulting in the difference current of the two photodetectors:

$$\hat{I}(\tau) = \beta^*(\tau)\hat{a}_{out}(\tau) + \beta(\tau)\hat{a}^\dagger_{out}(\tau) \tag{3.121}$$

and its autocorrelation function

$$\begin{aligned}
&\langle \hat{I}(\tau)\hat{I}(\tau+t)\rangle \\
=&\beta(\tau)\beta^*(\tau+t)\langle \hat{a}^\dagger_{out}(\tau)\hat{a}_{out}(\tau+t)\rangle \\
&+\beta^*(\tau)\beta(\tau+t)\langle \hat{a}_{out}(\tau)\hat{a}^\dagger_{out}(\tau+t)\rangle \\
&+\beta^*(\tau)\beta^*(\tau+t)\langle \hat{a}_{out}(\tau)\hat{a}_{out}(\tau+t)\rangle \\
&+\beta(\tau)\beta(\tau+t)\langle \hat{a}^\dagger_{out}(\tau)\hat{a}^\dagger_{out}(\tau+t)\rangle
\end{aligned} \tag{3.122}$$

We have to calculate each term first

$$\begin{aligned}
&\langle \hat{a}^\dagger_{out}(\tau)\hat{a}_{out}(\tau+t)\rangle \\
=&\langle [v(\tau)\hat{a}_{in}(l,\tau) + u(\tau)\hat{a}^\dagger_{i,in}(\tau)][v(\tau+t)\hat{a}^\dagger_{in}(l,\tau+t) + u(\tau+t)\hat{a}_{i,in}(\tau+t)]\rangle \\
=&v(\tau)v(\tau+t)\langle \hat{a}_{in}(l,\tau)\hat{a}^\dagger_{in}(l,\tau+t)\rangle + u(\tau)u(\tau+t)\langle 0|\hat{a}^\dagger_{i,in}(\tau)\hat{a}_{i,in}(\tau+t)|0\rangle_i \\
=&v(\tau)v(\tau+t)\langle \hat{a}_{in}(l,\tau)\hat{a}^\dagger_{in}(l,\tau+t)\rangle \\
=&\ ... \\
=&v(\tau)v(\tau+t)\frac{1}{\sqrt{2\pi}}\int \frac{d\Omega_2}{\sqrt{2\pi}} e^{-i\Omega_2 t}|U(-\Omega_2)|^2
\end{aligned} \tag{3.123}$$

$$\begin{aligned}
&\langle \hat{a}_{out}(\tau)\hat{a}^\dagger_{out}(\tau+t)\rangle \\
=&\langle [v(\tau)\hat{a}^\dagger_{in}(l,\tau) + u(\tau)\hat{a}_{i,in}(\tau)][v(\tau+t)\hat{a}_{in}(l,\tau+t) + u(\tau+t)\hat{a}^\dagger_{i,in}(\tau+t)]\rangle \\
=&v(\tau)v(\tau+t)\langle \hat{a}^\dagger_{in}(l,\tau)\hat{a}_{in}(l,\tau+t)\rangle + u(\tau)u(\tau+t)\langle 0|\hat{a}_{i,in}(\tau)\hat{a}^\dagger_{i,in}(\tau+t)|0\rangle_i \\
=&u(\tau)u(\tau+t)\delta(t) + v(\tau)v(\tau+t)\langle \hat{a}^\dagger_{in}(l,\tau)\hat{a}_{in}(l,\tau+t)\rangle \\
=&\ ... \\
=&u(\tau)u(\tau+t)\delta(t) + v(\tau)v(\tau+t)\frac{1}{\sqrt{2\pi}}\int \frac{d\Omega_2}{\sqrt{2\pi}} e^{-i\Omega_2 t}|V(\Omega_2)|^2
\end{aligned} \tag{3.124}$$

© 2018 Tous droits réservés.

lilliad.univ-lille.fr

Thèse de Junheng Shi, Université de Lille, 2018

$$
\begin{aligned}
&\langle \hat{a}_{out}(\tau)\hat{a}_{out}(\tau+t)\rangle \\
=&\langle [v(\tau)\hat{a}^{\dagger}_{in}(l,\tau)+u(\tau)\hat{a}_{i,in}(\tau)][v(\tau+t)\hat{a}^{\dagger}_{in}(l,\tau+t)+u(\tau+t)\hat{a}_{i,in}(\tau+t)]\rangle \\
=&v(\tau)v(\tau+t)\langle \hat{a}^{\dagger}_{in}(l,\tau)\hat{a}^{\dagger}_{in}(l,\tau+t)\rangle + u(\tau)u(\tau+t)\langle 0|\hat{a}_{i,in}(\tau)\hat{a}_{i,in}(\tau+t)|0\rangle_i \\
=&v(\tau)v(\tau+t)\langle \hat{a}^{\dagger}_{in}(l,\tau)\hat{a}^{\dagger}_{in}(l,\tau+t)\rangle \\
=&\ldots \\
=&v(\tau)v(\tau+t)\frac{1}{\sqrt{2\pi}}\int \frac{\mathrm{d}\Omega_2}{\sqrt{2\pi}}\mathrm{e}^{-\mathrm{i}\Omega_2 t}U^*(-\Omega_2)V^*(\Omega_2)
\end{aligned}
\tag{3.125}
$$

$$
\begin{aligned}
&\langle \hat{a}^{\dagger}_{out}(\tau)\hat{a}^{\dagger}_{out}(\tau+t)\rangle \\
=&\langle [v(\tau)\hat{a}_{in}(l,\tau)+u(\tau)\hat{a}^{\dagger}_{i,in}(\tau)][v(\tau+t)\hat{a}^{\dagger}_{in}(l,\tau+t)+u(\tau+t)\hat{a}^{\dagger}_{i,in}(\tau+t)]\rangle \\
=&v(\tau)v(\tau+t)\langle \hat{a}_{in}(l,\tau)\hat{a}_{in}(l,\tau+t)\rangle + u(\tau)u(\tau+t)\langle 0|\hat{a}^{\dagger}_{i,in}(\tau)\hat{a}^{\dagger}_{i,in}(\tau+t)|0\rangle_i \\
=&v(\tau)v(\tau+t)\langle \hat{a}_{in}(l,\tau)\hat{a}_{in}(l,\tau+t)\rangle \\
=&\ldots \\
=&v(\tau)v(\tau+t)\frac{1}{\sqrt{2\pi}}\int \frac{\mathrm{d}\Omega_2}{\sqrt{2\pi}}\mathrm{e}^{-\mathrm{i}\Omega_2 t}U(-\Omega_2)V(\Omega_2)
\end{aligned}
\tag{3.126}
$$

The additional phase $\mathrm{e}^{\mathrm{i}\pi/2}$ in front of $v(\tau)$ is absorbed into the phase of local oscillator so it now becomes $\phi_\beta - \pi/2$. The neglected parts in the calculations could be found in equations (3.98), (3.99), (3.100) and (3.101).

Since $|\beta(\tau)|$, $u(\tau)$ and $v(\tau)$ are all functions of $A_p(\tau)$ whose temporal duration is considerably long compared to $\frac{1}{\Omega}$ for typical Ω. They could be regarded as stationary with respect to t:

$$|\beta(\tau)\beta(\tau+t)| \approx |\beta(\tau)|^2 \tag{3.127}$$
$$v(\tau)v(\tau+t) \approx G(\tau) \tag{3.128}$$
$$u(\tau)u(\tau+t) \approx 1+G(\tau) \tag{3.129}$$

© 2018 Tous droits réservés.

lilliad.univ-lille.fr

Thèse de Junheng Shi, Université de Lille, 2018

The noise spectrum become

$$\begin{aligned}
(\delta i)^2_\Omega =& \int \frac{\mathrm{d}t}{\sqrt{2\pi}} \mathrm{e}^{\mathrm{i}\Omega t} \langle \hat{I}(\tau)\hat{I}(\tau+t)\rangle \\
=& \int \frac{\mathrm{d}t}{\sqrt{2\pi}} \mathrm{e}^{\mathrm{i}\Omega t} |\beta(\tau)|^2 \\
& \times \Big[\langle \hat{a}^\dagger_{out}(\tau)\hat{a}_{out}(\tau+t)\rangle \\
& + \langle \hat{a}_{out}(\tau)\hat{a}^\dagger_{out}(\tau+t)\rangle \\
& + \mathrm{e}^{-2\mathrm{i}\phi_\beta} \langle \hat{a}_{out}(\tau)\hat{a}_{out}(\tau+t)\rangle \\
& + \mathrm{e}^{2\mathrm{i}\phi_\beta} \langle \hat{a}^\dagger_{out}(\tau)\hat{a}^\dagger_{out}(\tau+t)\rangle \Big] \\
=& |\beta(\tau)|^2 \Bigg\{ \int \frac{\mathrm{d}t}{\sqrt{2\pi}} \mathrm{e}^{\mathrm{i}\Omega t} [1+G(\tau)]\delta(t) \\
& + \frac{G(\tau)}{\sqrt{2\pi}} \int \frac{\mathrm{d}t}{\sqrt{2\pi}} \mathrm{e}^{\mathrm{i}\Omega t} \int \frac{\mathrm{d}\Omega_2}{\sqrt{2\pi}} \mathrm{e}^{-\mathrm{i}\Omega_2 t} \Big[|V(\Omega_2)|^2 + |U(-\Omega_2)|^2 \\
& + \mathrm{e}^{-2\mathrm{i}\phi_\beta} U^*(-\Omega_2)V^*(\Omega_2) + \mathrm{e}^{2\mathrm{i}\phi_\beta} U(-\Omega_2)V(\Omega_2) \Big] \Bigg\} \\
=& \frac{|\beta(\tau)|^2}{\sqrt{2\pi}} \Big\{ 1 + G(\tau) + G(\tau) \Big[\cos^2(\theta'(\Omega)) \mathrm{e}^{2r(\Omega)} + \sin^2(\theta'(\Omega)) \mathrm{e}^{-2r(\Omega)} \Big] \Big\}
\end{aligned} \tag{3.130}$$

After normalization we obtain the squeezing spectrum as

$$S_{out}(\Omega) = 1 + G(\tau) + G(\tau) \Big[\cos^2(\theta'(\Omega)) \mathrm{e}^{2r(\Omega)} + \sin^2(\theta'(\Omega)) \mathrm{e}^{-2r(\Omega)} \Big] \tag{3.131}$$

where other parameters remain unchanged except

$$\theta'(\Omega) = \psi(\Omega) - \phi'_\beta \tag{3.132}$$

where $\phi'_\beta(\tau) = -\phi_\beta(\tau) + \pi/2$. The sign of the phase of the local oscillator is reversed because of the phase-conjugating nature of the time lens being used.

If we also take the scaling effect of the whole temporal imaging system into consideration, the squeezing spectrum becomes

$$S_{out}(\Omega) = 1 + G + G \Big[\cos^2(\theta'(\widetilde{\Omega})) \mathrm{e}^{2r(\widetilde{\Omega})} + \sin^2(\theta'(\widetilde{\Omega})) \mathrm{e}^{-2r(\widetilde{\Omega})} \Big] \tag{3.133}$$

where $\widetilde{\Omega} = M\Omega$ and M is the magnification factor. $G(\tau)$ is approximated as constant because $A_p(\tau)$ barely varies during the temporal imaging process.

As could be seen in Figure 3.13. The squeezing spectrum is no longer below the shot-noise, even within the range of $\Omega < \widetilde{\Omega}_c$, and instead of approaching shot-noise when Ω increases, it now approaches $1 + 2G$. The broadband squeezing is completely destroyed. This is due to the fact that the phase-conjugating nonlinear processes is always accompanied with parametric amplification which deteriorates any squeezing property the input signal happens to have.

© 2018 Tous droits réservés.

lilliad.univ-lille.fr

Thèse de Junheng Shi, Université de Lille, 2018

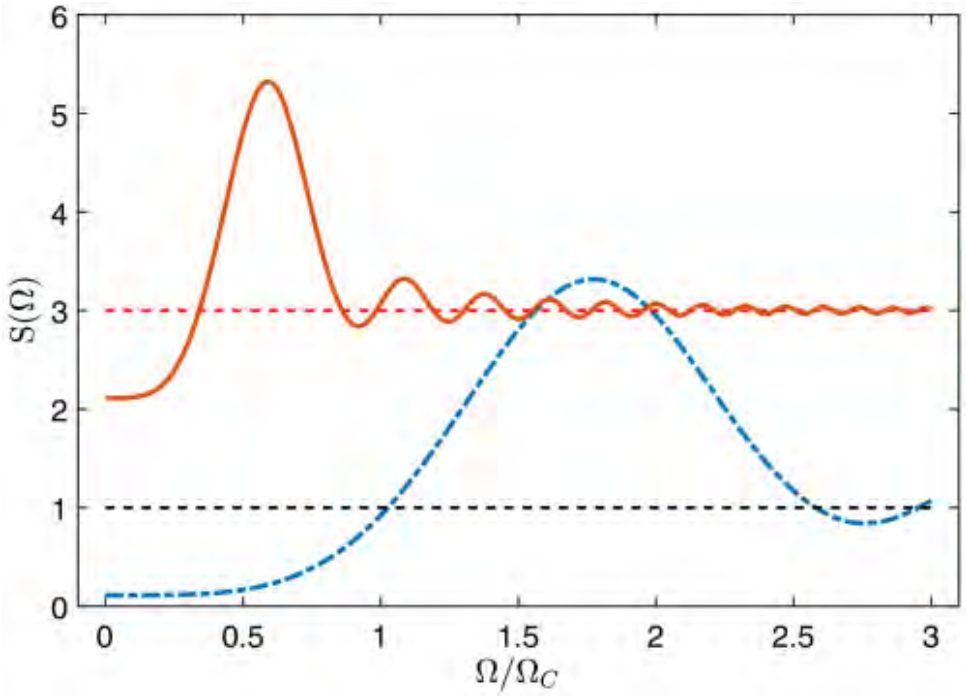

FIGURE 3.13: Squeezing spectrum of broadband squeezed light (dashed-dotted) and after a phase-conjugating time lens based temporal imaging system with magnification factor $M = -3$ (solid). The parametric gain $G = 1$ and the maximum squeezing parameter $e^{r_m} = 3$. The ordinates are graduated in shot-noise units. Copyright 2017 Optical Society of America, reprinted with permission, from Junheng *et al.*, Optics Letters, 2017, 42(16): 3121-3124.

© 2018 Tous droits réservés.

lilliad.univ-lille.fr

Thèse de Junheng Shi, Université de Lille, 2018

Therefore, despite the popularity of PCFWM time lens based temporal imaging system in classical temporal imaging [59], it is not appropriate for the quantum temporal imaging. We have to seek other possibilities in nonlinear process based time lens to find an alternative solution suitable for quantum temporal imaging.

3.3.2 Phase-Preserving Four-Wave Mixing Time Lens with Squeezed Light

Luckily PCFWM is not the only FWM process we get. Another kind of FWM, of which the input phase is not conjugated, but preserved. Such FWM process is also named Bragg-scattering in literature [12, 28, 34, 38, 39, 41–47, 50, 51] and it has been investigated in section 3.1.1. The configuration of PPFWM time lens is shown in Figure 3.14. Two pump waves with their carrier frequencies ω_{p1} and ω_{p2}, produced by separately passing two femtosecond pulses through two different dispersive media. One dispersive medium is with positive group velocity dispersion, its GDD equals to $2D_f$. The other one is with negative group velocity dispersion, its GDD equals to $-2D_f$. The reason behind such arrangement is that the total phase in PPFWM is not the sum of the two pump phases, but their difference. Also, the two pumps need to have equal temporal widths. That's why they are chirped with $2D_f$ and $-2D_f$, not other configurations, for an example, one is chirped with D_f and the other one is not chirped. Then the two pump pulses are mixed with the input signal wave inside a nonlinear medium where FWM takes place. And a idler wave is produced.

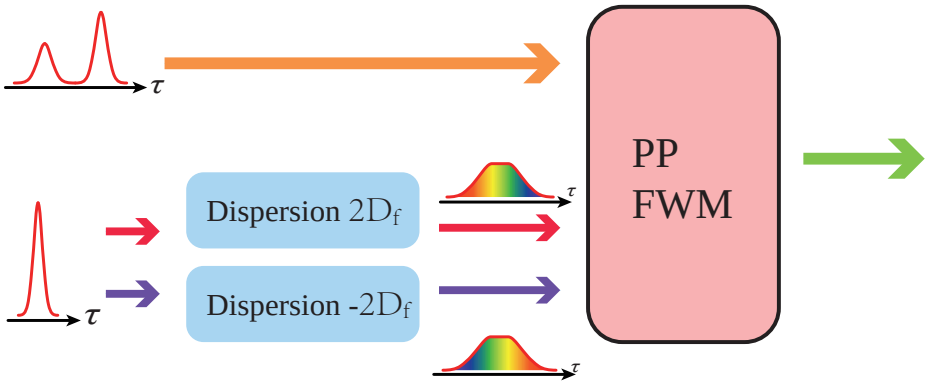

FIGURE 3.14: Configuration of phase-preserving four-wave mixing time lens.

According to Eq. (3.36b) and with an assumption that the perfect phase matching condition is satisfied. We obtain the transformation relation between the input signal and the output idler:

$$\hat{a}_{out}(\tau) = \mathrm{i}e^{\mathrm{i}\phi_p(\tau)} s(\tau)\hat{a}_{s,in}(\tau) + c(\tau)\hat{a}_{i,in}(\tau) \tag{3.134}$$

where

$$c(\tau) = \cos[gA_p^2(\tau)L] \tag{3.135a}$$

$$s(\tau) = \sin[gA_p^2(\tau)L] \tag{3.135b}$$

Due to the beam splitter relation between $c(\tau)$ and $s(\tau)$, we define the conversion efficiency $\eta(\tau) = |s(\tau)|^2$.

© 2018 Tous droits réservés.

lilliad.univ-lille.fr

Thèse de Junheng Shi, Université de Lille, 2018

The amplitude and the total phase of the pump waves are

$$A_p(\tau) = A_p \exp\left\{-\frac{\tau^2}{2(2D_f\delta\omega_p)^2}\right\} \tag{3.136}$$

$$\phi_p(\tau) = \frac{\tau^2}{2(2D_f)} - \frac{\tau^2}{2(-2D_f)} = \frac{\tau^2}{2D_f} \tag{3.137}$$

Just like in PCFWM, the idler input needs to be considered and the phase of the input signal is now preserved. For classical temporal imaging, the input idler could be neglected as long as it's vacuum:

$$\alpha_{out}(\tau) = \mathrm{i}s(\tau)\mathcal{Q}\left[\frac{1}{D_f}\right]\alpha_{s,in}(\tau) \tag{3.138}$$

Of course this is not enough, we need to investigate its effect on broadband squeezed light produced by OPA in section 3.2.2. For the convenience of following calculation, the notation of $\hat{a}_{s,in}(\tau)$ is changed to $\hat{a}_{in}(l,\tau)$.

Here again we consider the balanced homodyne detection technique with the pump wave used as the local oscillator. As shown in Figure 3.10, the output idler from the time lens is mixed with the local oscillator inside the beam splitter, we obtain the same autocorrelation function of the difference current from the two photodetectors as in Eq. (3.122). Nevertheless, the calculation for each term has changed:

$$\begin{aligned}
&\langle\hat{a}^\dagger_{out}(\tau)\hat{a}_{out}(\tau+t)\rangle\\
=&\langle[s(\tau)\hat{a}^\dagger_{in}(l,\tau)+c(\tau)\hat{a}^\dagger_{i,in}(\tau)][s(\tau+t)\hat{a}_{in}(l,\tau+t)+c(\tau+t)\hat{a}_{i,in}(\tau+t)]\rangle\\
=&s(\tau)s(\tau+t)\langle\hat{a}^\dagger_{in}(l,\tau)\hat{a}_{in}(l,\tau+t)\rangle + c(\tau)c(\tau+t)\langle 0|\hat{a}^\dagger_{i,in}(\tau)\hat{a}_{i,in}(\tau+t)|0\rangle_i\\
=&s(\tau)s(\tau+t)\langle\hat{a}^\dagger_{in}(l,\tau)\hat{a}_{in}(l,\tau+t)\rangle\\
=&\ldots\\
=&s(\tau)s(\tau+t)\frac{1}{\sqrt{2\pi}}\int\frac{\mathrm{d}\Omega_2}{\sqrt{2\pi}}\mathrm{e}^{-\mathrm{i}\Omega_2 t}|V(\Omega_2)|^2
\end{aligned} \tag{3.139}$$

$$\begin{aligned}
&\langle\hat{a}_{out}(\tau)\hat{a}^\dagger_{out}(\tau+t)\rangle\\
=&\langle[s(\tau)\hat{a}_{in}(l,\tau)+c(\tau)\hat{a}_{i,in}(\tau)][s(\tau+t)\hat{a}^\dagger_{in}(l,\tau+t)+c(\tau+t)\hat{a}^\dagger_{i,in}(\tau+t)]\rangle\\
=&s(\tau)s(\tau+t)\langle\hat{a}_{in}(l,\tau)\hat{a}^\dagger_{in}(l,\tau+t)\rangle + c(\tau)c(\tau+t)\langle 0|\hat{a}_{i,in}(\tau)\hat{a}^\dagger_{i,in}(\tau+t)|0\rangle_i\\
=&c(\tau)c(\tau+t)\delta(t) + s(\tau)s(\tau+t)\langle\hat{a}_{in}(l,\tau)\hat{a}^\dagger_{in}(l,\tau+t)\rangle\\
=&\ldots\\
=&c(\tau)c(\tau+t)\delta(t) + s(\tau)s(\tau+t)\frac{1}{\sqrt{2\pi}}\int\frac{\mathrm{d}\Omega_2}{\sqrt{2\pi}}\mathrm{e}^{-\mathrm{i}\Omega_2 t}|U(-\Omega_2)|^2
\end{aligned} \tag{3.140}$$

© 2018 Tous droits réservés.

lilliad.univ-lille.fr

Thèse de Junheng Shi, Université de Lille, 2018

$$
\begin{aligned}
&\langle \hat{a}_{out}(\tau)\hat{a}_{out}(\tau+t)\rangle \\
=&\langle [s(\tau)\hat{a}_{in}(l,\tau)+c(\tau)\hat{a}_{i,in}(\tau)][s(\tau+t)\hat{a}_{in}(l,\tau+t)+c(\tau+t)\hat{a}_{i,in}(\tau+t)]\rangle \\
=&s(\tau)s(\tau+t)\langle \hat{a}_{in}(l,\tau)\hat{a}_{in}(l,\tau+t)\rangle + c(\tau)c(\tau+t)\langle 0|\hat{a}_{i,in}(\tau)\hat{a}_{i,in}(\tau+t)|0\rangle_i \\
=&s(\tau)s(\tau+t)\langle \hat{a}_{in}(l,\tau)\hat{a}_{in}(l,\tau+t)\rangle \\
=&\ ... \\
=&s(\tau)s(\tau+t)\frac{1}{\sqrt{2\pi}}\int \frac{\mathrm{d}\Omega_2}{\sqrt{2\pi}}\mathrm{e}^{-\mathrm{i}\Omega_2 t}U(-\Omega_2)V(\Omega_2)
\end{aligned}
\tag{3.141}
$$

$$
\begin{aligned}
&\langle \hat{a}^{\dagger}_{out}(\tau)\hat{a}^{\dagger}_{out}(\tau+t)\rangle \\
=&\langle [s(\tau)\hat{a}^{\dagger}_{in}(l,\tau)+c(\tau)\hat{a}^{\dagger}_{i,in}(\tau)][s(\tau+t)\hat{a}^{\dagger}_{in}(l,\tau+t)+c(\tau+t)\hat{a}^{\dagger}_{i,in}(\tau+t)]\rangle \\
=&s(\tau)s(\tau+t)\langle \hat{a}^{\dagger}_{in}(l,\tau)\hat{a}^{\dagger}_{in}(l,\tau+t)\rangle + c(\tau)c(\tau+t)\langle 0|\hat{a}^{\dagger}_{i,in}(\tau)\hat{a}^{\dagger}_{i,in}(\tau+t)|0\rangle_i \\
=&s(\tau)s(\tau+t)\langle \hat{a}^{\dagger}_{in}(l,\tau)\hat{a}^{\dagger}_{in}(l,\tau+t)\rangle \\
=&\ ... \\
=&s(\tau)s(\tau+t)\frac{1}{\sqrt{2\pi}}\int \frac{\mathrm{d}\Omega_2}{\sqrt{2\pi}}\mathrm{e}^{-\mathrm{i}\Omega_2 t}U^*(-\Omega_2)V^*(\Omega_2)
\end{aligned}
\tag{3.142}
$$

The additional phase $\mathrm{e}^{\mathrm{i}\pi/2}$ in front of $v(\tau)$ is absorbed into the phase of local oscillator so it now becomes $\phi_\beta - \pi/2$. The neglected parts in the calculations could be found in equations (3.98), (3.99), (3.100) and (3.101).

Since $|\beta(\tau)|$, $c(\tau)$ and $s(\tau)$ are all functions of $A_p(\tau)$ whose temporal duration is considerably long compared to $\frac{1}{\Omega}$ for typical Ω. They could be regarded as stationary with respect to t:

$$|\beta(\tau)\beta(\tau+t)| \approx |\beta(\tau)|^2 \tag{3.143}$$

$$s(\tau)s(\tau+t) \approx \eta(\tau) \tag{3.144}$$

$$c(\tau)c(\tau+t) \approx 1-\eta(\tau) \tag{3.145}$$

© 2018 Tous droits réservés.

lilliad.univ-lille.fr

Thèse de Junheng Shi, Université de Lille, 2018

The noise spectrum become

$$\begin{aligned}
(\delta i)^2_\Omega =& \int \frac{\mathrm{d}t}{\sqrt{2\pi}} \mathrm{e}^{\mathrm{i}\Omega t} \langle \hat{I}(\tau)\hat{I}(\tau+t)\rangle \\
=& \int \frac{\mathrm{d}t}{\sqrt{2\pi}} \mathrm{e}^{\mathrm{i}\Omega t} |\beta(\tau)|^2 \\
& \times \Big[\langle \hat{a}^\dagger_{out}(\tau)\hat{a}_{out}(\tau+t)\rangle \\
& + \langle \hat{a}_{out}(\tau)\hat{a}^\dagger_{out}(\tau+t)\rangle \\
& + \mathrm{e}^{-2\mathrm{i}\phi_\beta} \langle \hat{a}_{out}(\tau)\hat{a}_{out}(\tau+t)\rangle \\
& + \mathrm{e}^{2\mathrm{i}\phi_\beta} \langle \hat{a}^\dagger_{out}(\tau)\hat{a}^\dagger_{out}(\tau+t)\rangle \Big] \\
=& |\beta(\tau)|^2 \Bigg\{ \int \frac{\mathrm{d}t}{\sqrt{2\pi}} \mathrm{e}^{\mathrm{i}\Omega t} [1-\eta(\tau)]\delta(t) \\
& + \frac{\eta(\tau)}{\sqrt{2\pi}} \int \frac{\mathrm{d}t}{\sqrt{2\pi}} \mathrm{e}^{\mathrm{i}\Omega t} \int \frac{\mathrm{d}\Omega_2}{\sqrt{2\pi}} \mathrm{e}^{-\mathrm{i}\Omega_2 t} \Big[|V(\Omega_2)|^2 + |U(-\Omega_2)|^2 \\
& + \mathrm{e}^{-2\mathrm{i}\phi_\beta} U^*(-\Omega_2)V^*(\Omega_2) + \mathrm{e}^{2\mathrm{i}\phi_\beta} U(-\Omega_2)V(\Omega_2) \Big] \Bigg\} \\
=& \frac{|\beta(\tau)|^2}{\sqrt{2\pi}} \Bigg\{ 1-\eta(\tau)+\eta(\tau) \Big[\cos^2(\theta'(\Omega))\mathrm{e}^{2r(\Omega)} + \sin^2(\theta'(\Omega))\mathrm{e}^{-2r(\Omega)} \Big] \Bigg\}
\end{aligned} \tag{3.146}$$

After normalization we obtain the squeezing spectrum as

$$S_{out}(\Omega) = 1-\eta(\tau)+\eta(\tau) \Big[\cos^2(\theta'(\Omega))\mathrm{e}^{2r(\Omega)} + \sin^2(\theta'(\Omega))\mathrm{e}^{-2r(\Omega)} \Big] \tag{3.147}$$

where other parameters remain unchanged except

$$\theta'(\Omega) = \psi(\Omega) - \phi'_\beta \tag{3.148}$$

where $\phi'_\beta(\tau) = \phi_\beta(\tau) - \pi/2$. The sign of the phase of the local oscillator remains unchanged thanks to the phase-preserving nature of the time lens being used. Just an additional phase is added due to the i in front of $s(\tau)$ in Eq. (3.134).

If we also take the scaling effect of the whole temporal imaging system into consideration, the squeezing spectrum becomes

$$S_{out}(\Omega) = 1-\eta+\eta \Big[\cos^2(\theta'(\widetilde{\Omega}))\mathrm{e}^{2r(\widetilde{\Omega})} + \sin^2(\theta'(\widetilde{\Omega}))\mathrm{e}^{-2r(\widetilde{\Omega})} \Big] \tag{3.149}$$

where $\widetilde{\Omega} = M\Omega$ and M is the magnification factor. $\eta(\tau)$ is approximated as a constant because $A_p(\tau)$ barely varies during the temporal imaging process.

From Figure 3.15 we could see that the squeezing spectrum is below the shot noise for $\Omega < \widetilde{\Omega}$ indicates the presence of broadband squeezing even after passing through the temporal imaging system. That means the broadband squeezing of the input signal is preserved, if not 100% preserved. By observing the squeezing spectrum at $\Omega = 0$, we could see that PPFWM time lens based temporal imaging system still introduces noise from the input idler, but not strong enough to destroy the squeezing

© 2018 Tous droits réservés.

lilliad.univ-lille.fr

Thèse de Junheng Shi, Université de Lille, 2018

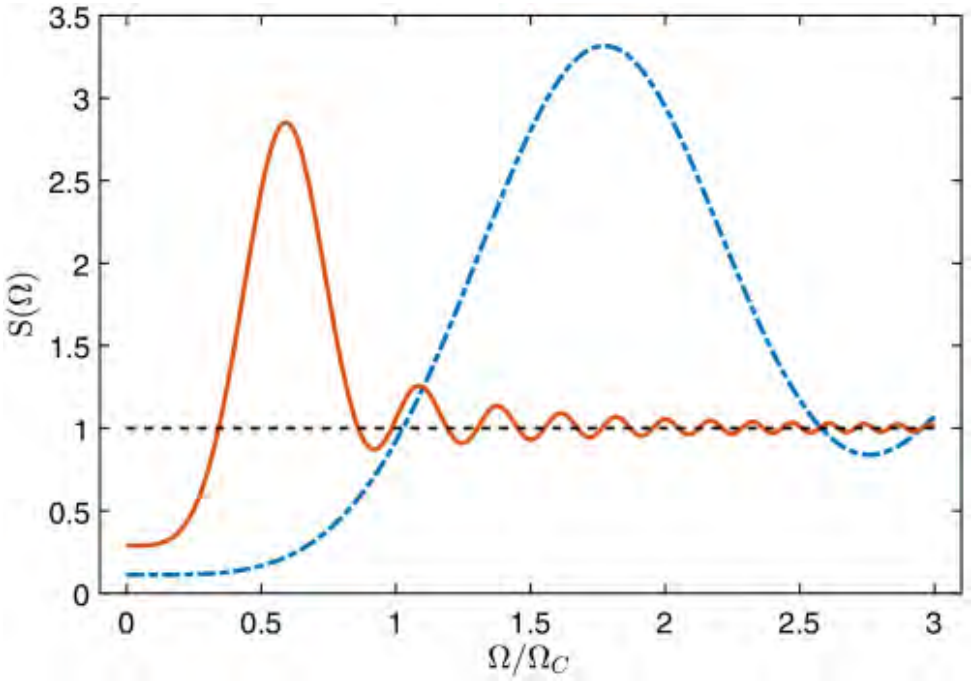

FIGURE 3.15: Squeezing spectrum of broadband squeezed light (dashed-dotted) and after a phase-preserving time lens based temporal imaging system with magnification factor $M = -3$ (solid). The conversion efficiency $\eta = 0.8$ and the maximum squeezing parameter $e^{r_m} = 3$. The ordinates are graduated in shot-noise units. Copyright 2017 Optical Society of America, reprinted with permission, from Junheng *et al.*, Optics Letters, 2017, 42(16): 3121-3124.

© 2018 Tous droits réservés.

lilliad.univ-lille.fr

Thèse de Junheng Shi, Université de Lille, 2018

completely. The amount of noise being introduced is determined by the conversion efficiency. The lower the conversion efficiency is, the more noise it introduces. As a result, PPFWM time lens based temporal imaging system is suitable for quantum temporal imaging, but the conversion efficiency should be as high as possible.

Another important issue arises from Eq. (3.149) is that how much noise would be introduced into the idler field is dependent on the conversion efficiency. So for one object signal field, it is desirable that the conversion efficiency remain unchanged during the whole duration when the signal wave is being processed by the imaging system, otherwise the squeezing property at different moments of the signal wave are preserved distinctively which is detrimental to broadband squeezed light. To prevent this from happening, the most direct measure is to ensure the temporal width of the pump wave is much larger than the total duration of the signal field. Here we define the field of view as the temporal duration of the signal field to be "imaged". According to what we came up with, the FOV of the signal field as broadband squeezed light should be much smaller than the temporal duration of the pump wave:

$$T_F \ll D_f \delta\omega_p \tag{3.150}$$

This restriction only comes from the nonclassical light, so we could name it quantum FOV.

3.4 Summary of this chapter

In this chapter we turn to quantum temporal imaging where the "object" is switched from classical field to nonclassical field. As a result, everything should be treated quantumly, for example, we develop the quantum treatment of the four-wave mixing processes the time lenses are based on. We then visit the concept of broadband squeezing and investigate the influences of FWM time lenses on broadband squeezed light. We find that the two types of FWM time lens behave distinctly in terms of quantum temporal imaging. One type is actually not suitable for quantum temporal imaging because of its destruction of the nonclassical property. The other preserves the nonclassical property with a condition. From this condition we introduce the concept of quantum FOV which only exists in quantum temporal imaging.

© 2018 Tous droits réservés.

lilliad.univ-lille.fr

Thèse de Junheng Shi, Université de Lille, 2018

Chapter 4

Resolution and Field of View in Quantum Temporal Imaging

With "imaging" in its name, temporal im aging can not escape from the same suffering that haunted his spatial brother - aberration. The basic idea behind spatial or temporal imaging is simple and elegant, just two quadratic phases, each in one of the two quadrature domains. But in reality these phase modulations could only be provided imperfectly for various reasons. Such imperfections give birth to aberrations. Consequently the quality of the image is deteriorated, or the image we are satisfied with could only be obtained under certain conditions, in other words, the performance of a temporal imaging system is limited.

Thanks to spatial imaging, there are a set of parameters that could be applied analogously to evaluating the performance of a temporal imaging system: resolution, field of View, aperture, figure of merit, etc. While the concept and purpose of each parameter remains the same, their definitions are altered due to the different causes of aberrations between spatial imaging and temporal imaging. Take a quick example, for spatial imaging, the aperture of a lens is the actual size of a lens and its pupil function could always be regarded as a rectangular function. In temporal imaging, such rectangular shaped pupil function is not common, and there is no such thing as the physical "size" of a time lens. As a result the definition of resolution needs to be modified accordingly.

Pupil function is not the only feature that differs temporal imaging from its spatial counterpart. For nonlinear process based time lens, we are also limited with the presence of dispersion inside the time lens (mainly second order dispersion). In terms of spatial imaging, it means one should be concerned with aberration brought by the Fresnel diffraction taken place inside a lens, which is never considered.

For temporal imaging a good understanding of the cause of aberration is the key to establish a fine evaluation system which includes giving appropriate definitions to the parameters for evaluation. And this is the first objective of this chapter, to investigate these two paramount aberrations mentioned above and their influences on the system performances of quantum temporal imaging, mainly through SFG time lens. Here SFG time lens is used as an example because the PP FWM time lens is similar in terms of the "beam splitter"-like transformation.

© 2018 Tous droits réservés.

lilliad.univ-lille.fr

Thèse de Junheng Shi, Université de Lille, 2018

4.1 Sum-Frequency Generation Time Lens

SFG time lens is the most commonly used nonlinear process based time lens for quantum temporal imaging. It preserves the squeezing property just like PPFWM time lens [56].

The configuration of SFG process is shown in Figure 4.1. In a nonlinear medium with second order susceptibility $\chi^{(2)}$, a signal wave with carrier frequency ω_s is mixed with a strong classical pump wave with carrier frequency ω_p and produces an idler wave with carrier frequency ω_i. They satisfy the energy conservation relation $\omega_i = \omega_s + \omega_p$ as in Figure 4.2.

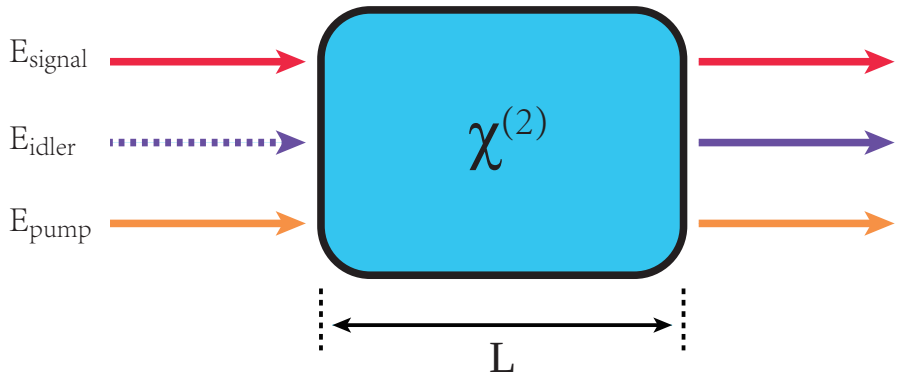

FIGURE 4.1: Configuration of sum-frequency generation.

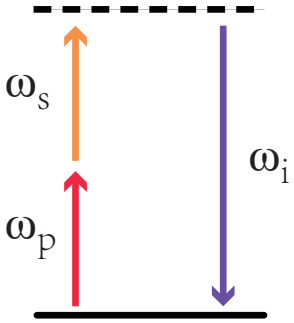

FIGURE 4.2: Energy conservation relation of sum-frequency generation.

As before, we begin by adding nonlinear polarization to Eq. (2.5) and obtain Eq. (3.1), only the nonlinear polarization term is changed from third order polarization to second order polarization for SFG process:

$$\hat{\mathbf{P}}^{NL}(z,t) = \hat{\mathbf{P}}^{(2)}(z,t) = \epsilon_0 \int_0^{+\infty} \mathrm{d}t_1 \int_0^{+\infty} \mathrm{d}t_2 \, R^{(2)}(t_1,t_2)\hat{\mathbf{E}}(z,t-t_1)\hat{\mathbf{E}}(z,t-t_2) \quad (4.1)$$

where $R^{(2)}(t_1,t_2)$ is the second order response function. It equals to zero for $t_1 < 0$ or $t_2 < 0$.

The field operator $\hat{\mathbf{E}}(z,t)$ is a mixture of three fields: signal, pump and idler.

$$\hat{\mathbf{E}}(z,t) = \sum_j \hat{E}_j(z,t) \quad (4.2)$$

© 2018 Tous droits réservés.

lilliad.univ-lille.fr

Thèse de Junheng Shi, Université de Lille, 2018

where $j \in \{s, p, i\}$.

Each field operator consists of positive and negative frequency components:

$$\hat{E}_j(z,t) = \frac{1}{2}[\hat{E}_j^{(+)}(z,t) + \hat{E}_j^{(-)}(z,t)] \tag{4.3}$$

Insert Eq. (4.1), Eq. (4.2) and Eq. (4.3) into Eq. (3.1) we obtain

$$\begin{aligned}
&\frac{\partial^2}{\partial z^2}\hat{E}_j^{(+)}(z,t) - \frac{1}{c^2}\frac{\partial^2}{\partial t^2}\hat{E}_j^{(+)}(z,t) - \frac{1}{c^2}\frac{\partial^2}{\partial t^2}\int_0^{+\infty} \mathrm{d}t'\, R^{(1)}(t')\hat{E}_j^{(+)}(z,t-t') \\
=&\sum_{k,l}\frac{1}{2c^2}\frac{\partial^2}{\partial t^2}\int_0^{+\infty}\mathrm{d}t_1\int_0^{+\infty}\mathrm{d}t_2\, R^{(2)}(t_1,t_2) \\
&\times[\hat{E}_k^{(+)}(z,t-t_1) + \hat{E}_k^{(-)}(z,t-t_1)] \\
&\times[\hat{E}_l^{(+)}(z,t-t_2) + \hat{E}_l^{(-)}(z,t-t_2)]
\end{aligned} \tag{4.4}$$

where $k, l \in \{s, p, i\}$, for simplicity we only consider the positive frequency component for $E_j(z,t)$.

Using the Fourier transform Eq. (3.6), we transform Eq. (4.4) into frequency domain:

$$\begin{aligned}
&\frac{\partial^2}{\partial z^2}\hat{E}_j^{(+)}(z,\omega_j) + \frac{\omega_j^2}{c^2}\hat{E}_j^{(+)}(z,\omega_j) + \frac{\omega_j^2}{c^2}\chi^{(1)}(\omega_j)\hat{E}_j^{(+)}(z,\omega_j) \\
=&-\sum_{k,l}\frac{\omega_j^2}{2c^2}\int\frac{\mathrm{d}\omega_k'}{\sqrt{2\pi}}[\hat{E}_k^{(+)}(z,\omega_k') + \hat{E}_k^{(-)}(z,-\omega_k')] \\
&\times\int\frac{\mathrm{d}\omega_l'}{\sqrt{2\pi}}[\hat{E}_k^{(+)}(z,\omega_l') + \hat{E}_k^{(-)}(z,-\omega_l')] \\
&\times\chi^{(2)}(\omega_k+\omega_l;\omega_k,\omega_l)\int\mathrm{d}t\,\mathrm{e}^{\mathrm{i}(\omega_j'-\omega_k'-\omega_l')t} \\
=&-\sum_{k,l}\frac{\omega_j^2}{2c^2}\int\frac{\mathrm{d}\omega_k'}{\sqrt{2\pi}}[\hat{E}_k^{(+)}(z,\omega_k') + \hat{E}_k^{(-)}(z,-\omega_k')] \\
&\times\int\frac{\mathrm{d}\omega_l'}{\sqrt{2\pi}}[\hat{E}_k^{(+)}(z,\omega_l') + \hat{E}_k^{(-)}(z,-\omega_l')] \\
&\times\chi^{(2)}(\omega_k+\omega_l;\omega_k,\omega_l)\sqrt{2\pi}\delta(\omega_j'-\omega_k'-\omega_l')
\end{aligned} \tag{4.5}$$

where the second order susceptibility equals to

$$\chi^{(2)}(\omega_k+\omega_l;\omega_k,\omega_l) = \int_0^{+\infty}\mathrm{d}t_1\int_0^{+\infty}\mathrm{d}t_2\, R^{(2)}(t_1,t_2)\mathrm{e}^{\mathrm{i}(\omega_k t_1+\omega_l t_2)} \tag{4.6}$$

All the combinations of ω_j', ω_k' and ω_l' could be found in Table 4.1.

Because of the intrinsic permutation symmetry of the nonlinear tensor, all the second order susceptibilities in this case could be considered the same and is denoted as $\chi^{(2)}$ for convenience.

© 2018 Tous droits réservés.

lilliad.univ-lille.fr

Thèse de Junheng Shi, Université de Lille, 2018

ω'_j	ω'_k	ω'_l
ω'_i	ω'_s	ω'_p
ω'_i	ω'_p	ω'_s
ω'_s	ω'_i	$-\omega'_p$
ω'_s	$-\omega'_p$	ω'_i
ω'_p	ω'_i	$-\omega'_s$
ω'_p	$-\omega'_s$	ω'_i

TABLE 4.1: All combinations of the SFG process.

According to Table 4.1, we write Eq. (4.5) into three coupled equations:

$$\frac{\partial^2}{\partial z^2}\hat{E}_i^{(+)}(z,\omega'_i)+k^2(\omega'_i)\hat{E}_i^{(+)}(z,\omega'_i)=-\frac{\omega_i'^2\chi^{(2)}}{c^2}\int\frac{\mathrm{d}\omega'_s}{\sqrt{2\pi}}\hat{E}_s^{(+)}(z,\omega'_s)\hat{E}_p^{(+)}(z,\omega'_i-\omega'_s) \tag{4.7a}$$

$$\frac{\partial^2}{\partial z^2}\hat{E}_s^{(+)}(z,\omega'_s)+k^2(\omega'_s)\hat{E}_s^{(+)}(z,\omega'_s)=-\frac{\omega_s'^2\chi^{(2)}}{c^2}\int\frac{\mathrm{d}\omega'_i}{\sqrt{2\pi}}\hat{E}_i^{(+)}(z,\omega'_i)\hat{E}_p^{(-)}(z,\omega'_s-\omega'_i) \tag{4.7b}$$

$$\frac{\partial^2}{\partial z^2}\hat{E}_p^{(+)}(z,\omega'_p)+k^2(\omega'_p)\hat{E}_p^{(+)}(z,\omega'_p)=-\frac{\omega_p'^2\chi^{(2)}}{c^2}\int\frac{\mathrm{d}\omega'_i}{\sqrt{2\pi}}\hat{E}_i^{(+)}(z,\omega'_i)\hat{E}_s^{(-)}(z,\omega'_p-\omega'_i) \tag{4.7c}$$

where $k^2(\omega_j)=\frac{\omega_j^2}{c^2}(1+\chi^{(1)}(\omega_j))$.

Under the quasi-monochromatic approximation, following the same decomposition as from Eq. (3.10) to Eq. (3.13) and approximations from Eq. (3.15) to Eq. (3.17), equations (4.7) become

$$\frac{\partial}{\partial z}\hat{a}_i(z,\Omega)=\mathrm{i}g\int\frac{\mathrm{d}\Omega'}{\sqrt{2\pi}}\hat{a}_s(z,\Omega')\hat{a}_p(z,\Omega-\Omega')\mathrm{e}^{-\mathrm{i}\Delta(\Omega,\Omega')z} \tag{4.8a}$$

$$\frac{\partial}{\partial z}\hat{a}_s(z,\Omega)=\mathrm{i}g\int\frac{\mathrm{d}\Omega'}{\sqrt{2\pi}}\hat{a}_i(z,\Omega')\hat{a}_p^\dagger(z,\Omega'-\Omega)\mathrm{e}^{\mathrm{i}\Delta(\Omega',\Omega)z} \tag{4.8b}$$

$$\frac{\partial}{\partial z}\hat{a}_p(z,\Omega)=\mathrm{i}g\int\frac{\mathrm{d}\Omega'}{\sqrt{2\pi}}\hat{a}_i(z,\Omega')\hat{a}_s^\dagger(z,\Omega'-\Omega)\mathrm{e}^{\mathrm{i}\Delta(\Omega',\Omega)z} \tag{4.8c}$$

where $g=\chi^{(2)}\frac{\epsilon_0}{\hbar}\mathcal{E}_s\mathcal{E}_p\mathcal{E}_i\propto\chi^{(2)}$ and the phase mismatch term

$$\Delta(\Omega_i,\Omega_s)=k(\omega_i+\Omega_i)-k(\omega_s+\Omega_s)-k(\omega_p+\Omega_i-\Omega_s) \tag{4.9}$$

© 2018 Tous droits réservés.

lilliad.univ-lille.fr

Thèse de Junheng Shi, Université de Lille, 2018

To be used for time lens, the pump wave could be approximated as undepleted classical wave, reducing equations (4.8) to

$$\frac{\partial}{\partial z}\hat{a}_s(z,\Omega) = \mathrm{i}g\int \frac{\mathrm{d}\Omega'}{\sqrt{2\pi}}\hat{a}_i(z,\Omega')\alpha_p^*(\Omega'-\Omega)\mathrm{e}^{\mathrm{i}\Delta(\Omega',\Omega)z} \tag{4.10a}$$

$$\frac{\partial}{\partial z}\hat{a}_i(z,\Omega) = \mathrm{i}g\int \frac{\mathrm{d}\Omega'}{\sqrt{2\pi}}\hat{a}_s(z,\Omega')\alpha_p(\Omega-\Omega')\mathrm{e}^{-\mathrm{i}\Delta(\Omega,\Omega')z} \tag{4.10b}$$

Equations (4.10) can not be solved directly because of the phase mismatch term in the phase. A common practice to resolve it is to expand the wavenumber inside the phase mismatch term with respect to Ω:

$$k(\omega_j+\Omega) = k_j + k_j'\Omega + \frac{1}{2}k_j''\Omega^2 + ... \tag{4.11}$$

Solving coupled equations (4.10) with Eq. (4.11) services as a tool for our investigations on the two aberrations mentioned before. The order of the expansion determines the level of the exploration.

If $k(\omega_j+\Omega)$ is expanded only to k_j that

$$\Delta(\Omega,\Omega') \approx k_i - k_s - k_p \tag{4.12}$$

denoted as Δ_0. Though the phase-matching is frequency independent (the dispersion of the time lens is not considered), there is limitation to the performance of the imaging scheme, brought by the pupil function. In this case, temporal imaging shall be seen in the perspective of a linear system and we summon the key instrument for analyzing it - impulse response, or point-spread function which is called in optics.

If $k(\omega_j+\Omega)$ is expanded to the first or second order. Then the dispersion inside the time lens is considered which would affect the resolution and field of view.

4.2 Temporal Resolution Defined by Impulse Response

Now let's take the approximation (4.12) and use the convolution theorem, equations (4.10) become

$$\frac{\partial}{\partial z}\hat{a}_s(z,\tau) = \mathrm{i}g\hat{a}_i(z,\tau)\alpha_p^*(\tau)\mathrm{e}^{\mathrm{i}\Delta_0 z} \tag{4.13a}$$

$$\frac{\partial}{\partial z}\hat{a}_i(z,\tau) = \mathrm{i}g\hat{a}_s(z,\tau)\alpha_p(\tau)\mathrm{e}^{-\mathrm{i}\Delta_0 z} \tag{4.13b}$$

© 2018 Tous droits réservés.

lilliad.univ-lille.fr

Thèse de Junheng Shi, Université de Lille, 2018

whose solutions are

$$\hat{a}_s(z,\tau) = \left[\cos(\gamma z) - \frac{i\Delta_0}{2\gamma}\sin(\gamma z)\right]\hat{a}_s(0,\tau)e^{i\Delta_0 z/2} + \frac{ig\alpha_p^*(\tau)}{\gamma}\sin(\gamma z)\hat{a}_i(0,\tau)e^{i\Delta_0 z/2} \tag{4.14a}$$

$$\hat{a}_i(z,\tau) = \left[\cos(\gamma z) + \frac{i\Delta_0}{2\gamma}\sin(\gamma z)\right]\hat{a}_i(0,\tau)e^{-i\Delta_0 z/2} + \frac{ig\alpha_p(\tau)}{\gamma}\sin(\gamma z)\hat{a}_s(0,\tau)e^{-i\Delta_0 z/2} \tag{4.14b}$$

where $\gamma = \sqrt{g^2|\alpha_p(\tau)|^2 + \Delta_0^2/4}$.

The pump is produced by passing a ultrashort pulse with bandwidth $\delta\omega_p$ through a dispersive medium whose GDD equals to D_f, so for $\alpha_p(\tau) = A_p(\tau)e^{i\phi_p(\tau)}$:

$$A_p(\tau) = A_p \exp\left\{-\frac{\tau^2}{2(D\delta\omega_p)^2}\right\} \tag{4.15}$$

$$\phi_p(\tau) = \frac{\tau^2}{2D_f} \tag{4.16}$$

For nonlinear medium whose length equals to L, the input signal and output idler satisfy the relation:

$$\hat{a}_i(L,\tau) = i\mathcal{Q}\left[\frac{1}{D_f}\right]s(\tau)\hat{a}_s(0,\tau) + c(\tau)\hat{a}_i(0,\tau) \tag{4.17}$$

where

$$c(\tau) = \left[\cos(\gamma L) + \frac{i\Delta_0}{2\gamma}\sin(\gamma L)\right]e^{i\Delta_0 L/2} \tag{4.18a}$$

$$s(\tau) = \frac{g|\alpha_p|}{\gamma}\sinh(\gamma L)e^{-i\Delta_0 L/2} \tag{4.18b}$$

When perfect phase-matching is achieved, these coefficients could be simplified as

$$c(\tau) = \cos[gA_p(\tau)L] \tag{4.19a}$$

$$s(\tau) = \sin[gA_p(\tau)L] \tag{4.19b}$$

For convenience, we make some changes to the notation and rewrite Eq. (4.17) as

$$\hat{a}_i(\tau) = p(\tau)\mathcal{Q}\left[\frac{1}{D_f}\right]\hat{a}_s(\tau) + p'(\tau)\hat{a}_{i,in}(\tau) \tag{4.20}$$

$p(\tau)$ could be interpreted as the pupil function and the relation (4.20) is now fitted into a big picture of a linear system. $p'(\tau)$ is the pupil function of the temporal imaging of the idler input. This was absent in the literature of classical temporal imaging.

© 2018 Tous droits réservés.

lilliad.univ-lille.fr

Thèse de Junheng Shi, Université de Lille, 2018

4.2.1 Temporal Imaging System as a Linear System

The operator algebra developed in the second chapter is a good example revealing the nature of temporal imaging system as a linear system. A system is a mapping of input functions into output functions and being linear means the total outputs of many inputs equals to the sum of each outputs resulting from every individual inputs. So if we continuously decompose the input, we could get its smallest unit - an impulse, or a point for spatial imaging. The output function for an impulse is called impulse response, or Green's function for mathematicians, or point-spread function for spatial imaging.

According to the linearity property, any output function could be regarded as a superposition of impulse responses just like its input function being decomposed into a set of impulses. So if the effect of a temporal imaging system is $\mathcal{T}$, we could write the output function as the convolution of the impulse response and the input function:

$$\begin{aligned} f_{out}(\tau) =& \mathcal{T} f_{in}(\tau_0) \\ =& \int \frac{\mathrm{d}\tau_0}{\sqrt{2\pi}} h(\tau;\tau_0) f_{in}(\tau_0) \end{aligned} \tag{4.21}$$

with $h(\tau;\tau_0)$ being the impulse response.

And if it is shift-invariant linear system, then $h(\tau;\tau_0)$ is in the form of $h(\tau-\tau_0)$

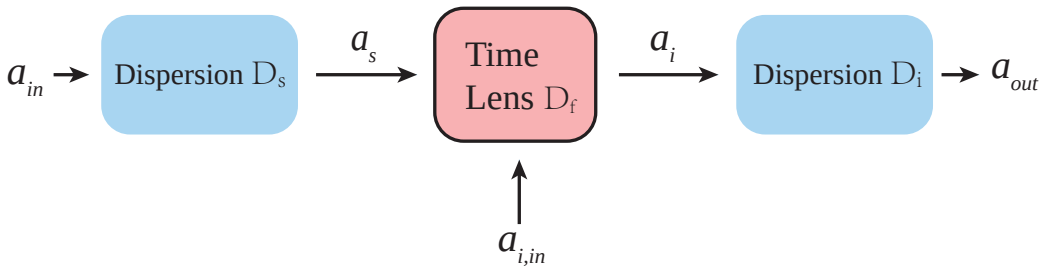

FIGURE 4.3: A single lens temporal imaging system.

With this principle in mind, let's find out the impulse response for the single-lens temporal imaging system shown in Figure 4.3. According to section 2.3.2, we have

$$\hat{a}_s = \mathcal{P}[D_s]\hat{a}_{in} \tag{4.22a}$$
$$\hat{a}_{out} = \mathcal{P}[D_i]\hat{a}_i \tag{4.22b}$$

Combining them with Eq. (4.20) we obtain

$$\hat{a}_{out}(\tau) = \mathcal{P}[D_i]p(\tau')\mathcal{Q}\left[\frac{1}{D_f}\right]\mathcal{P}[D_s]\hat{a}_{in}(\tau'') + \mathcal{P}[D_i]p'(\tau')\hat{a}_{i,in}(0,\tau') \tag{4.23}$$

Note the initial field for $\hat{a}_{i,in}$ is a vacuum which brings deterioration to the nonclassical property of the signal such as the squeezing property. Its specific effect on the noise spectrum is discussed in last chapter. And we know already the quantum temporal imaging systems would preserve the nonclassical properties though the degree of the preservation varies for different systems.

© 2018 Tous droits réservés.

lilliad.univ-lille.fr

Thèse de Junheng Shi, Université de Lille, 2018

Nevertheless, vacuum input does not affect the amplitude profile we are focus on in this chapter because

$$\langle \hat{a}_{out}(\tau)\rangle = \mathcal{P}[D_i]p(\tau')\mathcal{Q}\left[\frac{1}{D_f}\right]\mathcal{P}[D_s]\langle \hat{a}_{in}(\tau'')\rangle + \mathcal{P}[D_i]p'(\tau')\langle \hat{a}_{i,in}(0,\tau')\rangle \tag{4.24}$$

and clearly $\langle 0|\hat{a}_{i,in}(0,\tau')|0\rangle = 0$.

As a result, we could neglect it and Eq. (4.23) could be rewritten as

$$\langle \hat{a}_{out}(\tau)\rangle = \mathcal{T}_{temporal}\langle \hat{a}_{in}(\tau'')\rangle \tag{4.25}$$

with

$$\begin{aligned}
\mathcal{T}_{temporal} =& \mathcal{P}[D_i]p(\tau')\mathcal{Q}\left[\frac{1}{D_f}\right]\mathcal{P}[D_s] \\
=& \sqrt{\frac{-1}{D_sD_i}}\mathcal{Q}\left[-\frac{1}{D_i}\right]\mathcal{V}\left[\frac{1}{D_i}\right]\mathcal{F}\mathcal{Q}\left[-\frac{1}{D_i}\right]p(\tau')\mathcal{Q}\left[\frac{1}{D_f}\right]\mathcal{Q}\left[-\frac{1}{D_s}\right]\mathcal{V}\left[\frac{1}{D_s}\right]\mathcal{F}\mathcal{Q}\left[-\frac{1}{D_s}\right] \\
=& \sqrt{\frac{-1}{D_sD_i}}\mathcal{Q}\left[-\frac{1}{D_i}\right]\mathcal{V}\left[\frac{1}{D_i}\right]\mathcal{F}p(\tau')\mathcal{Q}\left[\frac{1}{D_f}-\frac{1}{D_i}-\frac{1}{D_s}\right]\mathcal{V}\left[\frac{1}{D_s}\right]\mathcal{F}\mathcal{Q}\left[-\frac{1}{D_s}\right] \\
=& \sqrt{\frac{-1}{D_sD_i}}\mathcal{Q}\left[-\frac{1}{D_i}\right]\mathcal{V}\left[\frac{1}{D_i}\right]\mathcal{F}p(\tau')\mathcal{V}\left[\frac{1}{D_s}\right]\mathcal{F}\mathcal{Q}\left[-\frac{1}{D_s}\right] \\
=& \sqrt{\frac{-1}{D_sD_i}}\mathcal{Q}\left[-\frac{1}{D_i}\right]|D_i|\mathcal{F}\mathcal{V}[D_i]p(\tau')\mathcal{V}\left[\frac{1}{D_s}\right]\mathcal{F}\mathcal{Q}\left[-\frac{1}{D_s}\right] \\
=& \sqrt{-\frac{D_i}{D_s}}\mathcal{Q}\left[-\frac{1}{D_i}\right]\mathcal{F}p(D_i\tau')\mathcal{V}[D_i]\mathcal{V}\left[\frac{1}{D_s}\right]\mathcal{V}[-1]\mathcal{F}^{-1}\mathcal{Q}\left[-\frac{1}{D_s}\right] \\
=& \sqrt{M}\mathcal{Q}\left[-\frac{1}{D_i}\right]\mathcal{F}p(D_i\tau')\mathcal{V}[M]\mathcal{F}^{-1}\mathcal{Q}\left[-\frac{1}{D_s}\right] \\
=& \sqrt{M}\mathcal{Q}\left[-\frac{1}{D_i}\right]\mathcal{F}p(D_i\tau')\frac{1}{|M|}\mathcal{F}^{-1}\mathcal{V}\left[\frac{1}{M}\right]\mathcal{Q}\left[-\frac{1}{D_s}\right] \\
=& \frac{1}{\sqrt{M}}\mathcal{Q}\left[-\frac{1}{D_i}\right]\mathcal{F}p(D_i\tau')\mathcal{F}^{-1}\mathcal{V}\left[\frac{1}{M}\right]\mathcal{Q}\left[-\frac{1}{D_s}\right]
\end{aligned} \tag{4.26}$$

There is one approximation to make. since by the definition of impulse response, the range of input function that contributes is infinitely small. So we could replace τ'' in the last operator $\mathcal{Q}[-1/D_s]$ with τ/M. So $\exp\left[-i\frac{\tau''^2}{2D_s}\right]$ now becomes $\exp\left[-i\frac{\tau^2}{2M^2D_s}\right]$ which is equivalent to moving $\mathcal{Q}[-1/(M^2D_s)]$ to the left. Consequently

$$\begin{aligned}
\mathcal{T}_{temporal} =& \frac{1}{\sqrt{M}}\mathcal{Q}\left[-\frac{1}{M^2D_s}\right]\mathcal{Q}\left[-\frac{1}{D_i}\right]\mathcal{F}p(D_i\tau')\mathcal{F}^{-1}\mathcal{V}\left[\frac{1}{M}\right] \\
=& \frac{1}{\sqrt{M}}\mathcal{Q}\left[\frac{1}{MD_f}\right]\left(\mathcal{F}p(D_i\tau')\right) * \left(\mathcal{F}\mathcal{F}^{-1}\mathcal{V}\left[\frac{1}{M}\right]\right) \\
=& \frac{1}{\sqrt{M}}\mathcal{Q}\left[\frac{1}{MD_f}\right]\left(\mathcal{F}p(D_i\tau')\right) * \left(\mathcal{V}\left[\frac{1}{M}\right]\right)
\end{aligned} \tag{4.27}$$

© 2018 Tous droits réservés.

lilliad.univ-lille.fr

Thèse de Junheng Shi, Université de Lille, 2018

We obtain the specific form of Eq. (4.25)

$$\begin{aligned}\hat{a}_{out}(\tau) =& \mathcal{T}_{temporal}\ \hat{a}_{in}(\tau'') \\ =& \frac{1}{\sqrt{M}}\mathcal{Q}\left[\frac{1}{MD_f}\right]\left(\mathcal{F}p(D_i\tau')\right) * \left(\mathcal{V}\left[\frac{1}{M}\right]\hat{a}_{in}(\tau'')\right) \\ =& \frac{1}{\sqrt{M}}\mathrm{e}^{\mathrm{i}\frac{\tau^2}{2MD_f}}\int\frac{d\tau''}{\sqrt{2\pi}}\left(\int\frac{d\tau'}{\sqrt{2\pi}}\mathrm{e}^{\mathrm{i}\tau'(\tau-\tau'')}p(D_i\tau')\right)\hat{a}_{in}(\tau''/M)\end{aligned} \tag{4.28}$$

If we let $\tau_0 = \tau''/M$ then

$$\hat{a}_{out}(\tau) = \sqrt{M}\mathrm{e}^{\mathrm{i}\frac{\tau^2}{2MD_f}}\int\frac{\mathrm{d}\tau_0}{\sqrt{2\pi}}\left(\int\frac{\mathrm{d}\tau'}{\sqrt{2\pi}}\mathrm{e}^{\mathrm{i}\tau'(\tau-M\tau_0)}p(D_i\tau')\right)\hat{a}_{in}(\tau_0) \tag{4.29}$$

But a much meaningful treatment would be assuming a magnified replica of the input waveform:

$$\hat{a}'_{in}(\tau'') = \frac{1}{\sqrt{M}}\mathcal{V}\left[\frac{1}{M}\right]\hat{a}_{in}(\tau'') \tag{4.30}$$

so it could be regarded as an impulse response of a shift-invariant system (we separate the residual phase because it's not of our concern):

$$\hat{a}_{out}(\tau) = \mathrm{e}^{\mathrm{i}\frac{\tau^2}{2MD_f}}\int\frac{\mathrm{d}\tau''}{\sqrt{2\pi}}h(\tau-\tau'')\hat{a}'_{in}(\tau'') \tag{4.31}$$

Similar to the result of spatial imaging, impulse response function is the Fourier transform of the pupil function:

$$\begin{aligned}h(\tau) =& \mathcal{F}\mathcal{V}\left[D_i\right]p(\tau') \\ =& \frac{1}{|D_i|}\mathcal{V}\left[\frac{1}{D_i}\right]\mathcal{F}p(\tau')\end{aligned} \tag{4.32}$$

Once the impulse response is obtained, it's time to define one of the main parameters of an imaging system - resolution. It is conventionally based on the concept of two-point resolution, which means how close are two impulses with equal peak amplitude located while they are still distinguishable. since what we could measure is the output function which is the sum of two impulse responses, being distinguishable or not depends on whether this output function has a dip in the middle of the two points. It is considered "barely resolved" when the dip reaches its limit, and the output function becomes "flat" in the center. The distance of two "barely resolved" points is defined as resolution.

This definition of resolution has many interpretations, in spatial imaging, it is common to use a so-called Rayleigh criterion, requires the center of the first impulse response fall the first zero of the second impulse response. In temporal imaging, the impulse response may never reaches zero, so we define the temporal resolution as the FWHM width Δ of the impulse response $h(\tau)$ divided by the magnification factor:

$$\mathcal{R} = \frac{\Delta}{|M|} \tag{4.33}$$

since Δ is the shortest resolvable temporal duration of the image, dividing it by the magnification factor we obtain the shortest resolvable temporal duration of the

© 2018 Tous droits réservés.

lilliad.univ-lille.fr

Thèse de Junheng Shi, Université de Lille, 2018

object.

4.2.2 Temporal Resolution of Sum-Frequency Generation Time Lens

Now we get the definition of temporal resolution, it's time to explore different time lenses, starting from SFG time lens.

From Eq. (4.15) and Eq. (4.19b) we obtain the pupil function for SFG time lens:

$$s(\tau') = \sin\left[\theta_0 \exp\left\{-\frac{\tau'^2}{2(D_f\delta\omega_p)^2}\right\}\right] \tag{4.34}$$

where we define $\theta_0 = gA_pL$, the temporal resolution depends on the value of θ_0.

We choose to expand the sine function in its Taylor series:

$$\begin{aligned} s(\tau') &= \sum_{n=1}^{\infty} \frac{(-1)^{(n-1)}\theta_0^{2n-1}}{(2n-1)!} \exp\left\{-\frac{(2n-1)\tau'^2}{2(D_f\delta\omega_p)^2}\right\} \\ &= \sum_{n=1}^{\infty} \frac{(-1)^{(n-1)}\theta_0^{2n-1}}{(2n-1)!} \mathcal{V}\left[\frac{\sqrt{2n-1}}{D_f\delta\omega_p}\right] \exp\left\{-\frac{\tau'^2}{2}\right\} \end{aligned} \tag{4.35}$$

and we define $s_N(\tau')$ as

$$s_N(\tau') = \sum_{n=1}^{N} \frac{(-1)^{(n-1)}\theta_0^{2n-1}}{(2n-1)!} \mathcal{V}\left[\frac{\sqrt{2n-1}}{D_f\delta\omega_p}\right] \exp\left\{-\frac{\tau'^2}{2}\right\} \tag{4.36}$$

Thanks to this expansion, we could analytically calculate the impulse response as sum of series:

$$\begin{aligned} h_{SFG}(\tau) =& \frac{1}{|D_i|}\mathcal{V}\left[\frac{1}{D_i}\right] \mathcal{F}s(\tau') \\ =& \frac{1}{|D_i|}\mathcal{V}\left[\frac{1}{D_i}\right] \mathcal{F} \sum_{n=1}^{\infty} \frac{(-1)^{(n-1)}\theta_0^{2n-1}}{(2n-1)!} \mathcal{V}\left[\frac{\sqrt{2n-1}}{D_f\delta\omega_p}\right] \exp\left\{-\frac{\tau'^2}{2}\right\} \\ =& \frac{1}{|D_i|} \sum_{n=1}^{\infty} \frac{(-1)^{(n-1)}\theta_0^{2n-1}}{(2n-1)!} \mathcal{V}\left[\frac{1}{D_i}\right] \mathcal{F}\mathcal{V}\left[\frac{\sqrt{2n-1}}{D_f\delta\omega_p}\right] \exp\left\{-\frac{\tau'^2}{2}\right\} \\ =& \frac{1}{|D_i|} \sum_{n=1}^{\infty} \frac{(-1)^{(n-1)}\theta_0^{2n-1}}{(2n-1)!} \mathcal{V}\left[\frac{1}{D_i}\right] \left|\frac{D_f\delta\omega}{\sqrt{2n-1}}\right| \mathcal{V}\left[\frac{D_f\delta\omega}{\sqrt{2n-1}}\right] \mathcal{F}\exp\left\{-\frac{\tau'^2}{2}\right\} \\ =& \sum_{n=1}^{\infty} \frac{(-1)^{(n-1)}\theta_0^{2n-1}}{(2n-1)!} \left|\frac{D_f\delta\omega}{D_i\sqrt{2n-1}}\right| \mathcal{V}\left[\frac{D_f\delta\omega}{D_i\sqrt{2n-1}}\right] \exp\left\{-\frac{\tau^2}{2}\right\} \end{aligned} \tag{4.37}$$

For large magnification $M \gg 1$

$$h_{SFG}(\tau) = \sum_{n=1}^{\infty} \frac{(-1)^{(n-1)}\theta_0^{2n-1}}{(2n-1)!} \left|\frac{\delta\omega}{M\sqrt{2n-1}}\right| \mathcal{V}\left[\frac{\delta\omega}{|M|\sqrt{2n-1}}\right] \exp\left\{-\frac{\tau^2}{2}\right\} \tag{4.38}$$

© 2018 Tous droits réservés.

lilliad.univ-lille.fr

Thèse de Junheng Shi, Université de Lille, 2018

Unfortunately it's impossible to get the FWHM of impulse response Eq. (4.38). Therefore approximations of the pupil function must be made.

When $\theta_0 \ll \frac{\pi}{2}$:

This corresponds to the situation that the conversion efficiency is very low, i.e., $\eta \ll 1$. The pupil function is then approximated as the pump amplitude profile $A_p(\tau')$, in other words, $s(\tau')$ is approximated to the first order of the expansion:

$$p_{SFG}(\tau') = s_1(\tau') \tag{4.39}$$

According to Eq. (4.38), its corresponding impulse response is

$$h_{SFG}(\tau) \approx \left|\frac{\delta\omega_p}{M}\right| \mathcal{V}\left[\frac{\delta\omega_p}{|M|}\right] \exp\left\{-\frac{\tau^2}{2}\right\} \tag{4.40}$$

Then its temporal resolution

$$\mathcal{R}_{SFG} = 2\sqrt{2\ln 2}\frac{|M|}{\delta\omega_p}/|M| \approx \frac{2.35}{\delta\omega_p} \tag{4.41}$$

When $\theta_0 \approx \frac{\pi}{2}$:

This is the situation when the peak conversion efficiency is near unity. As could be seen in Figure 4.4, expanding $s(\tau')$ to the third order is enough to achieve high approximation:

$$p_{SFG}(\tau') = s_3(\tau') \tag{4.42}$$

The corresponding impulse response is

$$\begin{aligned} h_{SFG}(\tau) \approx \frac{\delta\omega_p\theta_0}{|M|}\Bigg[&\exp\left\{-\frac{(\tau\delta\omega_p)^2}{2M^2}\right\} \\ &-\frac{\theta_0^2}{3!\sqrt{3}}\exp\left\{-\frac{(\tau\delta\omega_p)^2}{6M^2}\right\} \\ &+\frac{\theta_0^4}{5!\sqrt{5}}\exp\left\{-\frac{(\tau\delta\omega_p)^2}{10M^2}\right\}\Bigg]. \end{aligned} \tag{4.43}$$

To get the FWHM of Eq. (4.43), first we need to make it solvable. By defining a set of the parameters and variable:

$$c = \frac{\delta\omega_p\theta_0}{|M|} \tag{4.44a}$$

$$a = \frac{\theta_0^2}{3!\sqrt{3}} \tag{4.44b}$$

$$b = \frac{\theta_0^4}{5!\sqrt{5}} \tag{4.44c}$$

$$u_0(\Delta/2) = \exp\left\{-\frac{(\delta\omega_p \times \Delta/2)^2}{30M^2}\right\} \tag{4.44d}$$

© 2018 Tous droits réservés.

lilliad.univ-lille.fr

Thèse de Junheng Shi, Université de Lille, 2018

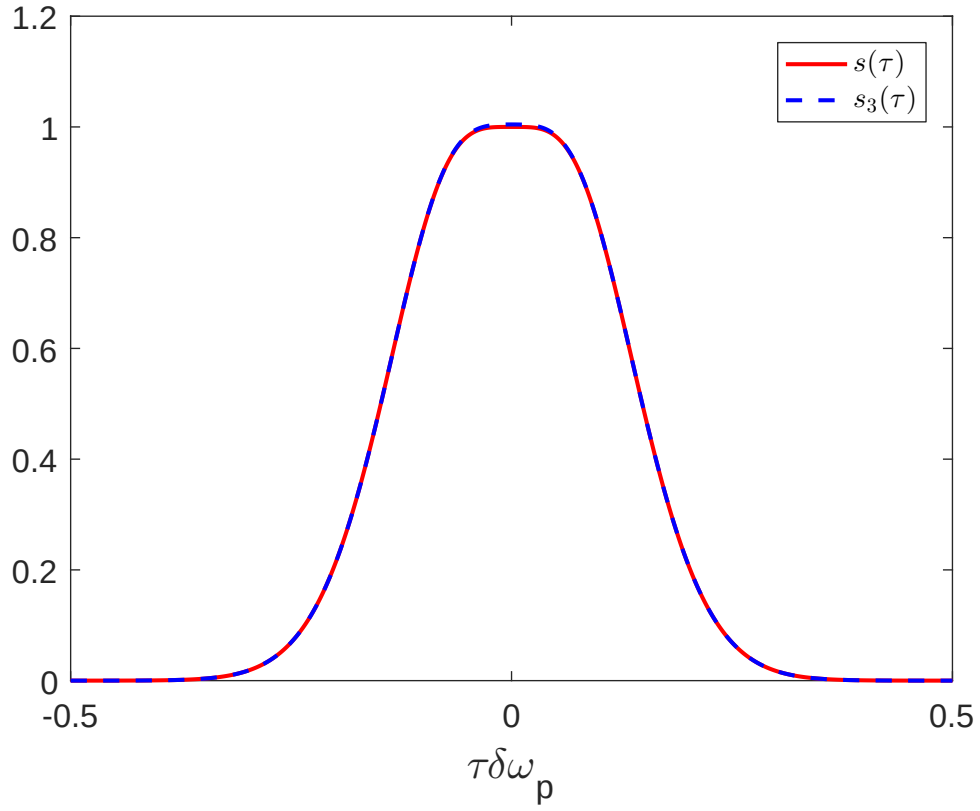

FIGURE 4.4: Comparison of the exact pupil functions $s(\tau)$ and its approximation $s_3(\tau)$ by the three first terms in the Taylor expansion.

The job has now become solving

$$u_0^{15} - au_0^5 + bu_0^3 = \frac{1-a+b}{2} \tag{4.45}$$

whose solution is $u_0 \approx 0.963$

the FWHM is

$$\begin{aligned} \Delta =& 2\sqrt{-30\ln u_0}\frac{|M|}{\delta\omega_p} \\ =& 2.12\frac{|M|}{\delta\omega_p} \end{aligned} \tag{4.46}$$

We obtain the temporal resolution

$$\mathcal{R}_{SFG} = \frac{2.12}{\delta\omega_p} \tag{4.47}$$

When $\theta_0 > \dfrac{\pi}{2}$:

If we continue increasing θ_0 to $\theta_0 > \pi/2$, the peak conversion efficiency begin to deteriorate since θ_0 has past its critical value. The central amplitude of the pupil function begins to oscillate, while the number of peaks starts increasing, which could be seen in Figure 4.5.

© 2018 Tous droits réservés.

lilliad.univ-lille.fr

Thèse de Junheng Shi, Université de Lille, 2018

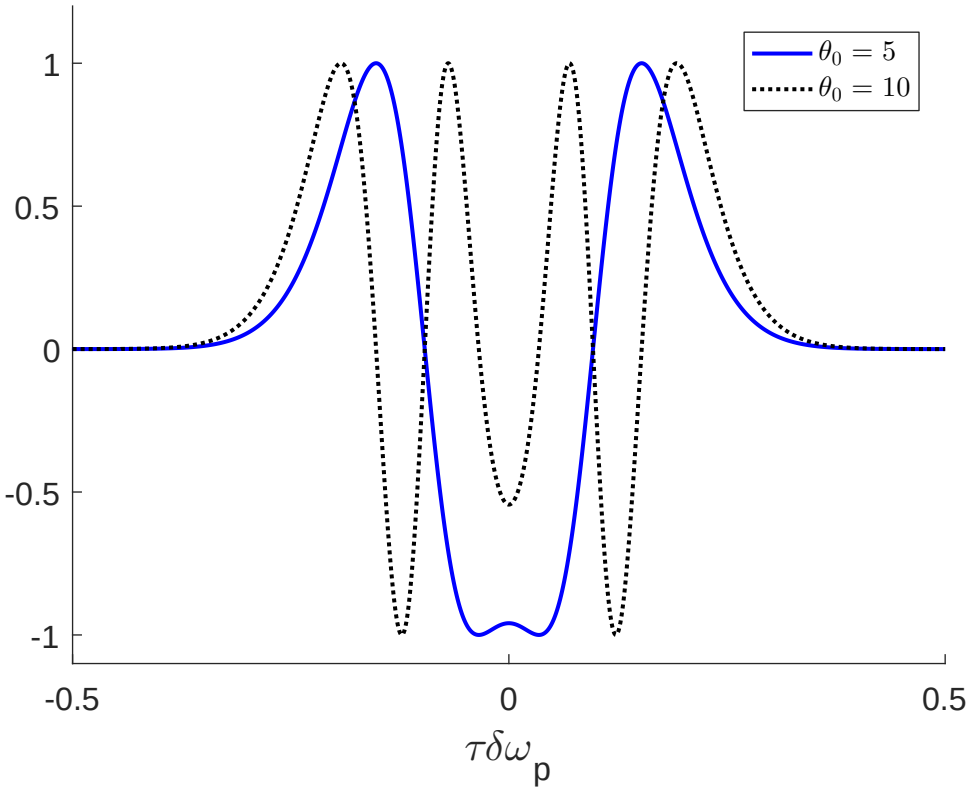

FIGURE 4.5: Pupil functions of sum-frequency generation time lens when θ_0 is larger than $\pi/2$.

Apparently, such pupil functions is less favorable for temporal imaging that these values of θ_0 are no longer worth consideration.

Now we can conclude all the temporal resolutions of SFG time lens whose pump amplitude profile is Gaussian shaped into two, one for low conversion efficiency domain Eq. (4.41), one for high conversion efficiency domain Eq. (4.47) which is also the best temporal resolution such system could achieve. Please note the temporal resolution for low conversion efficiency is what Bennett and Kolner considered "ideal resolution" for classical temporal imaging in [5].

But the definition Eq. (4.33) could also be used to evaluate nonlinear process based time lens whose pump profile is of other shapes. Take a convenient example, if we presume the pump amplitude is a rectangular function whose width is the FWHM of the Gaussian pump when Eq. (4.15):

$$A_p(\tau') = \frac{\pi}{2}\mathcal{V}\left[\frac{1}{2\sqrt{2\ln 2}D_f\delta\omega_p}\right]\Pi\left(\tau'\right) \tag{4.48}$$

Its width is defined as FWHM of a Gaussian shaped pump with peak amplitude as π is because such rectangular shaped pump wave is always obtained by reshaping a Gaussian shaped pump wave.

So its pupil function is

$$p_{SFG}(\tau') = \mathcal{V}\left[\frac{1}{2\sqrt{2\ln 2}D_f\delta\omega_p}\right]\Pi\left(\tau'\right) \tag{4.49}$$

© 2018 Tous droits réservés.

lilliad.univ-lille.fr

Thèse de Junheng Shi, Université de Lille, 2018

Its corresponding impulse response is

$$\begin{aligned} h_{SFG}(\tau) =& \frac{1}{|D_i|}\mathcal{V}\left[\frac{1}{D_i}\right]\mathcal{F}p_{SFG}(\tau') \\ =& \frac{1}{|D_i|}\mathcal{V}\left[\frac{1}{D_i}\right]\mathcal{F}\mathcal{V}\left[\frac{1}{2\sqrt{2\ln 2}D_f\delta\omega_p}\right]\Pi\left(\tau'\right) \\ =& \left|\frac{2\sqrt{2\ln 2}D_f\delta\omega_p}{D_i}\right|\mathcal{V}\left[\frac{2\sqrt{2\ln 2}D_f\delta\omega_p}{D_i}\right]\mathcal{F}\Pi\left(\tau'\right) \\ =& \left|\frac{2\sqrt{2\ln 2}D_f\delta\omega_p}{D_i\sqrt{2\pi}}\right|\mathcal{V}\left[\frac{2\sqrt{2\ln 2}D_f\delta\omega_p}{D_i}\right]\mathrm{sinc}(\tau) \\ \approx& \left|\frac{2\sqrt{2\ln 2}\delta\omega_p}{M\sqrt{2\pi}}\right|\mathcal{V}\left[\frac{2\sqrt{2\ln 2}\delta\omega_p}{|M|}\right]\mathrm{sinc}(\tau) \end{aligned} \tag{4.50}$$

Because $\mathrm{sinc}(1.895) \approx 0.5$:

$$\mathcal{R}_{SFG} = \frac{1.895 \times 2|M|}{2.355\delta\omega_p}/|M| \approx \frac{1.61}{\delta\omega_p} \tag{4.51}$$

4.2.3 Temporal Resolution of Copropagating Bragg-Scattering Time Lens

The second time lens is based on PP copropagating FWM derived in section 3.1.1, which is also named Copropagating Bragg-Scattering (CBS). Such time lens has proven to be suitable for quantum temporal imaging. According to Eq. (3.135b) and Eq. (3.136), we obtain its pupil function as

$$s'(\tau') = \sin\left[\theta_0' \exp\left\{-\frac{\tau'^2}{2(\sqrt{2}D_f\delta\omega_p)^2}\right\}\right] \tag{4.52}$$

where we define $\theta_0' = gA_p^2L$.

This pupil function shares similar form to that of SFG time lens, therefore we adopt the same method - expanding the sine function in its Taylor series:

$$s'(\tau') = \sum_{n=1}^{\infty}\frac{(-1)^{(n-1)}\theta_0^{2n-1}}{(2n-1)!}\mathcal{V}\left[\frac{\sqrt{2n-1}}{\sqrt{2}D_f\delta\omega_p}\right]\exp\left\{-\frac{\tau'^2}{2}\right\} \tag{4.53}$$

and we define $s_N(\tau')$ as

$$s_N'(\tau') = \sum_{n=1}^{N}\frac{(-1)^{(n-1)}\theta_0^{2n-1}}{(2n-1)!}\mathcal{V}\left[\frac{\sqrt{2n-1}}{\sqrt{2}D_f\delta\omega_p}\right]\exp\left\{-\frac{\tau'^2}{2}\right\} \tag{4.54}$$

© 2018 Tous droits réservés.

lilliad.univ-lille.fr

Thèse de Junheng Shi, Université de Lille, 2018

The analytical impulse response is then

$$\begin{aligned} h_{CBS}(\tau) =& \frac{1}{|D_i|}\mathcal{V}\left[\frac{1}{D_i}\right]\mathcal{F}s'(\tau') \\ =& \frac{1}{|D_i|}\mathcal{V}\left[\frac{1}{D_i}\right]\mathcal{F}\sum_{n=1}^{\infty}\frac{(-1)^{(n-1)}\theta_0^{2n-1}}{(2n-1)!}\mathcal{V}\left[\frac{\sqrt{2n-1}}{\sqrt{2}D_f\delta\omega_p}\right]\exp\left\{-\frac{\tau'^2}{2}\right\} \\ =& \sum_{n=1}^{\infty}\frac{(-1)^{(n-1)}\theta_0^{2n-1}}{(2n-1)!}\left|\frac{\sqrt{2}D_f\delta\omega}{D_i\sqrt{2n-1}}\right|\mathcal{V}\left[\frac{\sqrt{2}D_f\delta\omega}{D_i\sqrt{2n-1}}\right]\exp\left\{-\frac{\tau^2}{2}\right\} \end{aligned} \tag{4.55}$$

For large magnification $M \gg 1$

$$h_{CBS}(\tau) = \sum_{n=1}^{\infty}\frac{(-1)^{(n-1)}\theta_0^{2n-1}}{(2n-1)!}\left|\frac{\delta\omega}{M\sqrt{n-1/2}}\right|\mathcal{V}\left[\frac{\delta\omega}{|M|\sqrt{n-1/2}}\right]\exp\left\{-\frac{\tau^2}{2}\right\} \tag{4.56}$$

Similar to SFG time lens, we need to make approximations depending on the value of θ_0' in order to obtain the width of the impulse response.

When $\theta_0' \ll \frac{\pi}{2}$:

This is the situation when the conversion efficiency is very low so the pupil function is approximated with the pump profile squared. In order words, $s'(\tau')$ is expanded only to the first order:

$$p_{CBS}(\tau') = s_1'(\tau') \tag{4.57}$$

According to Eq. (4.56), its corresponding impulse response is

$$h_{CBS}(\tau) \approx \left|\frac{\sqrt{2}\delta\omega_p}{M}\right|\mathcal{V}\left[\frac{\sqrt{2}\delta\omega_p}{|M|}\right]\exp\left\{-\frac{\tau^2}{2}\right\} \tag{4.58}$$

Therefore its temporal resolution is

$$\mathcal{R}_{CBS} = 2\sqrt{2\ln 2}\frac{|M|}{\sqrt{2}\delta\omega_p}/|M| \approx \frac{1.67}{\delta\omega_p} \tag{4.59}$$

When $\theta_0' \approx \frac{\pi}{2}$:

This is the situation when the peak conversion efficiency is near unity. For the same reason as in SFG time lens, which could be seen in Figure 4.4, approximation of $s(\tau')$ with its expansion to the third order is already excellent:

$$p_{CBS}(\tau') = s_3'(\tau') \tag{4.60}$$

© 2018 Tous droits réservés.

lilliad.univ-lille.fr

Thèse de Junheng Shi, Université de Lille, 2018

According to Eq. (4.56), the corresponding impulse response is

$$\begin{aligned} h_{CBS}(\tau) \approx \frac{\sqrt{2}\delta\omega_p\theta_0'}{|M|}\Bigg[&\exp\left\{-\frac{(\tau\delta\omega_p)^2}{M^2}\right\} \\ &-\frac{\theta_0'^2}{3!\sqrt{3}}\exp\left\{-\frac{(\tau\delta\omega_p)^2}{3M^2}\right\} \\ &+\frac{\theta_0'^4}{5!\sqrt{5}}\exp\left\{-\frac{(\tau\delta\omega_p)^2}{5M^2}\right\}\Bigg]. \end{aligned} \tag{4.61}$$

With the same method as before, we obtain the FWHM of the impulse response:

$$\begin{aligned} \Delta =& 2\sqrt{-15\ln u_0}\frac{|M|}{\delta\omega_p} \\ =& 1.50\frac{|M|}{\delta\omega_p} \end{aligned} \tag{4.62}$$

Hence its temporal resolution

$$\mathcal{R}_{CBS} = \frac{1.50}{\delta\omega_p} \tag{4.63}$$

When $\theta_0' > \frac{\pi}{2}$:

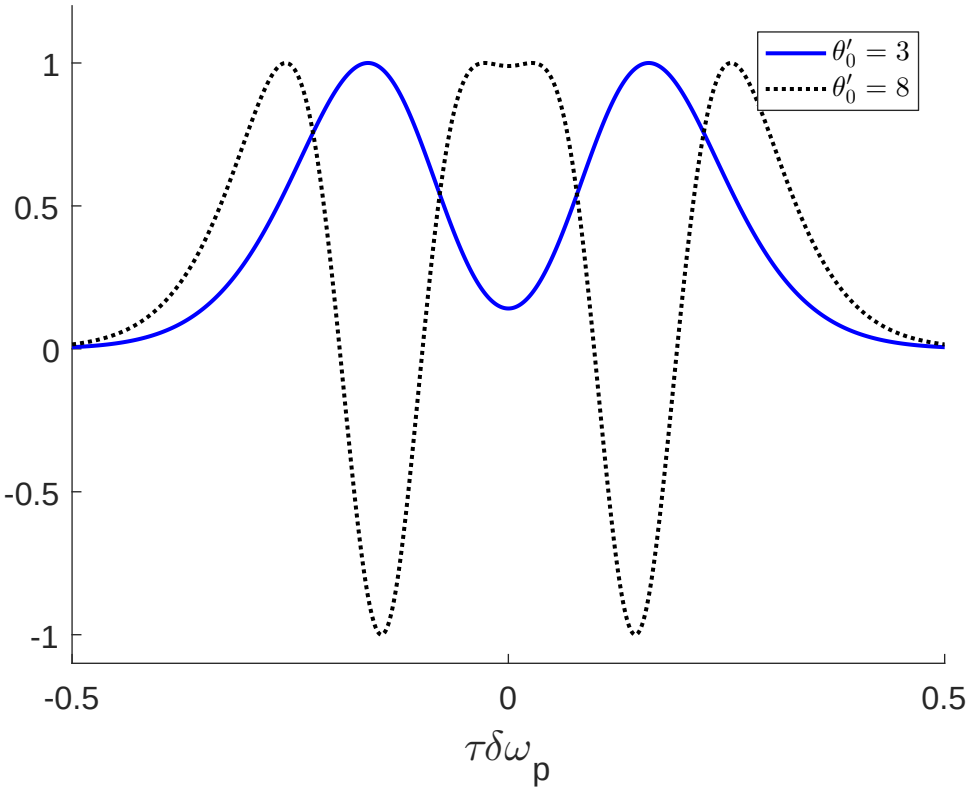

FIGURE 4.6: Pupil functions of copropagating bragg-scattering time lens when θ_0' is larger than $\pi/2$.

© 2018 Tous droits réservés.

lilliad.univ-lille.fr

Thèse de Junheng Shi, Université de Lille, 2018

If we continue increasing θ_0' to $\theta_0' > \pi/2$, the peak conversion efficiency begin to deteriorate and the pupil function begins to oscillate for the same reason as in SFG time lens, which could be seen in Figure 4.6. Therefore there is no need to consider these values of θ_0'.

By comparing the temporal resolution of SFG time lens and CBS time lens, one could conclude that if the bandwidth of the initial Gaussian pump is the same, the temporal resolution of CBS time lens is better than that of SFG time lens. And we obtained the resolution limits for both two time lenses. These limits could only only be broken by perhaps reshaping the initial Gaussian shaped pump profile.

4.2.4 Temporal Resolution of Counter-Propagating Bragg-Scattering Time Lens

Now let's take a look at something different, there is another PPFWM configuration developed in section 3.1.2, it is named Counter-Propagating Bragg-Scattering (CPBS). Its transform coefficients also satisfy the relation as a beam splitter, that it could be used for quantum temporal imaging. Yet instead of a sine function, it consists of a hyperbolic tangent function which is not periodic function.

According to Eq. (3.51) and Eq. (3.136), we obtain its pupil function as

$$s''(\tau') = \tanh\left[\theta_0' \exp\left\{-\frac{\tau'^2}{2(\sqrt{2}D_f\delta\omega_p)^2}\right\}\right] \tag{4.64}$$

where $\theta_0' = gA_p^2L$.

When $\theta_0' \ll \pi/2$, CPBS time lens behaves the same as the CBS time lens, because like sine function, $\tanh(x)$ could also be approximated with x when $x \ll 1$. Therefore, the temporal resolution is the same

$$\mathcal{R}_{CPBS} = \frac{1.67}{\delta\omega_p} \tag{4.65}$$

Nevertheless, when θ_0' is near $\pi/2$ or even larger. The situation becomes difficult since there is no appropriate expansion of hyperbolic tangent function for those values. Consequently, there is no analytical solution to the Fourier transform of the CPBS pupil function. It could be done numerically.

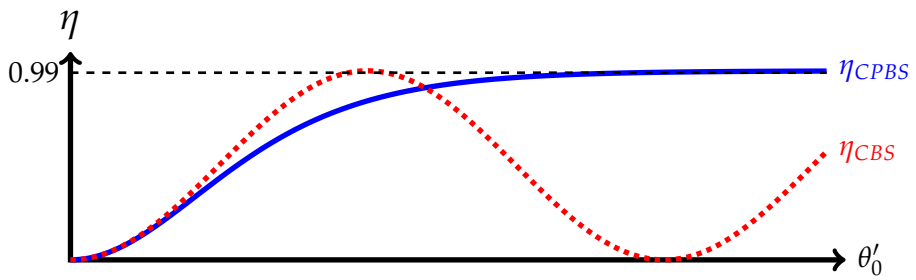

FIGURE 4.7: Comparison between the conversion efficiencies of the copropagating Bragg-scattering time lens (dotted) and the counter-propagating Bragg-scattering time lens (solid).

© 2018 Tous droits réservés.

lilliad.univ-lille.fr

Thèse de Junheng Shi, Université de Lille, 2018

Before we try to get the impulse response, let's study the property of its pupil function. It is non-periodic unlike the other two time lenses. Take CBS time lens as an example, the conversion efficiency oscillates with respect to θ_0', so the unity of conversion efficiency could only be achieved at certain values of θ_0', fluctuations around these values decrease the conversion efficiency. The conversion efficiency of CPBS time lens, however, approaches the unity monotonously with θ_0' in non-oscillating fashion. Such difference could be seen in Figure 4.7.

Another difference is that for SFG and CBS time lenses, if θ_0' is larger than $\pi/2$, then their pupil functions become unsuitable for temporal imaging which could be seen in Figure 4.6. CPBS time lens does not have such limit, on the contrary, when θ_0' is larger than $\pi/2$, its pupil function begin to resemble the shape of rectangular function, it acquires a flat-top plateau around its maximum. And its width grows with the increasing θ_0'. As could be seen in Figure 4.8, when $\theta_0' = \pi/2$, $p_{CPBS}(\tau')$ still carries the Gaussian shape, when θ_0' is larger, it gains a flat-top whose width increase with θ_0'. since the impulse response is the Fourier transform of the pupil function, consequently its width is decreasing with θ_0', thus improving the resolution.

This kind of pupil function also shed some light on the problem raised at the end of chapter 3, Eq. (3.150). With such a plateau around its center, the restriction that quantum FOV should be much smaller than the temporal width of the pump is no longer so strict.

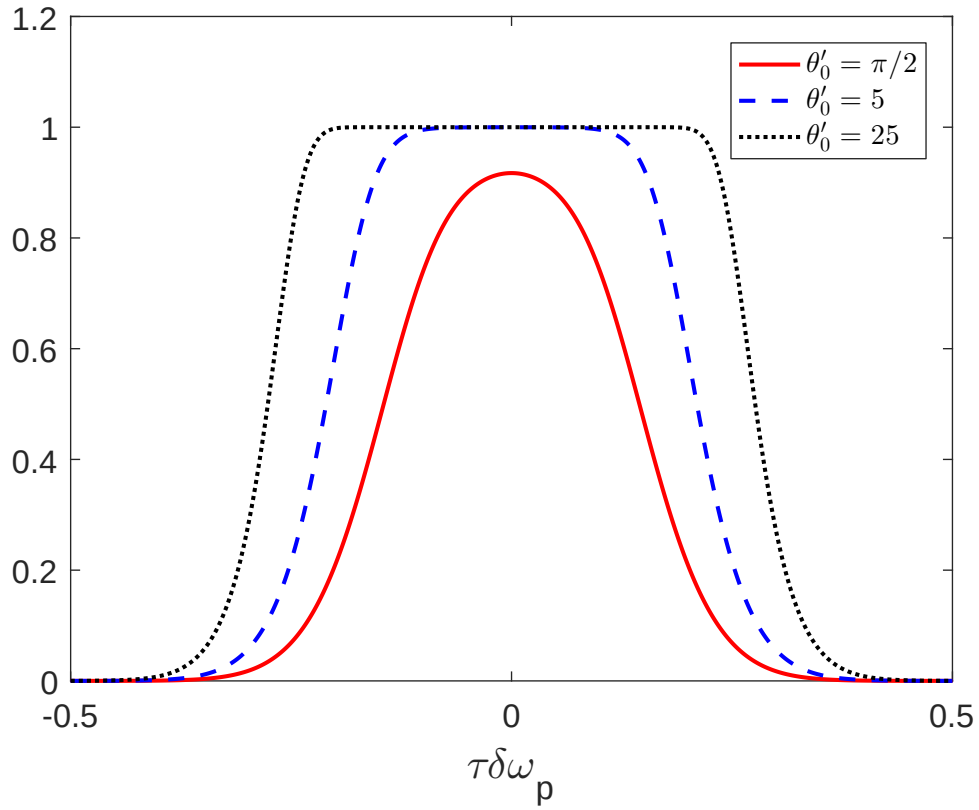

FIGURE 4.8: Pupil functions of counter-propagating Bragg-scattering time lens for different values of θ_0'.

© 2018 Tous droits réservés.

lilliad.univ-lille.fr

Thèse de Junheng Shi, Université de Lille, 2018

To obtain numerically the value of the resolution, we need to get the form of the impulse response:

$$\begin{aligned} h_{CPBS}(\tau) =& \frac{1}{|D_i|}\mathcal{V}\left[\frac{1}{D_i}\right]\mathcal{F}s''(\tau') \\ =& \frac{1}{|D_i|}\mathcal{V}\left[\frac{1}{D_i}\right]\mathcal{F}\mathcal{V}\left[\frac{1}{\sqrt{2}D_f\delta\omega_p}\right]\tanh\left[\theta_0'\exp\left\{-\frac{\tau'^2}{2}\right\}\right] \\ =& \left|\frac{\sqrt{2}D_f\delta\omega}{D_i}\right|\mathcal{V}\left[\frac{\sqrt{2}D_f\delta\omega}{D_i}\right]\mathcal{F}\tanh\left[\theta_0'\exp\left\{-\frac{\tau'^2}{2}\right\}\right] \end{aligned} \tag{4.66}$$

For large magnification $M \gg 1$

$$h_{CPBS}(\tau) = \left|\frac{\sqrt{2}\delta\omega}{M}\right|\mathcal{V}\left[\frac{\sqrt{2}\delta\omega}{|M|}\right]\mathcal{F}\tanh\left[\theta_0'\exp\left\{-\frac{\tau'^2}{2}\right\}\right] \tag{4.67}$$

Then we could use softwares such as Matlab to evaluate the FWHM of $\mathcal{F}\tanh\left[\theta_0'\exp\left\{-\frac{\tau'^2}{2}\right\}\right]$ for different θ_0'. We take $\theta_0' = \pi/2$ and $\theta_0' = 25$ as two examples.

For the typical value of $\theta_0' = \pi/2$, we could obtain the FWHM of $\mathcal{F}\tanh\left[\pi/2\exp\left\{-\frac{\tau'^2}{2}\right\}\right]$ equals to 2.08, so its temporal resolution is

$$\mathcal{R}_{CPBS} = 2.08\frac{|M|}{\sqrt{2}\delta\omega_p}/|M| = \frac{1.47}{\delta\omega_p} \tag{4.68}$$

For the value of $\theta_0' = 25$, we could obtain the FWHM of $\mathcal{F}\tanh\left[25\exp\left\{-\frac{\tau'^2}{2}\right\}\right]$ equals to 1.32, so its temporal resolution is

$$\mathcal{R}_{CPBS} = 1.32\frac{|M|}{\sqrt{2}\delta\omega_p}/|M| = \frac{0.93}{\delta\omega_p} \tag{4.69}$$

which shows 80% of improvement over the resolution for $\theta_0' \ll \pi/2$ and 61% of improvement over the best resolution for CBS time lens shown in Eq. (4.63).

More importantly, Eq. (4.69) is not the best resolution, even better resolution could be achieved by increasing θ_0' which is proportional to the peak intensity of the pump wave.

4.2.5 Resolution and Aperture of Electro-Optic Modulator Time Lens

EOM time lens is the first generation of time lens. The idea is simple, we need phase modulation, they offer phase modulation. It is based on the phenomena that certain crystal such as lithium niobate changes its refractive index when exposed to an electric field. Consequently the length of time a light passing through it is changed, introducing additional phase to the light.

© 2018 Tous droits réservés.

lilliad.univ-lille.fr

Thèse de Junheng Shi, Université de Lille, 2018

An EOM is given a sinusoidal radio-frequency (RF) signal, it introduce a phase:

$$\phi(t) = A\cos(\omega_m t) \tag{4.70}$$

$$A = \frac{\pi V_m}{V_\pi} \tag{4.71}$$

where V_m and ω_m are the amplitude and frequency of the driving voltage and V_π is the voltage needed to have phase shift equals to π. Therefore A is the amplitude of the phase-shift produced. In practice A is normally smaller than 2π because sufficiently large V_m which requires a large-nonlinear-susceptibility medium is hard to obtain.

Because the cosine function could be expanded as

$$\phi(t) = A\cos(\omega_m t) \approx A(1 - \frac{\omega_m^2}{2}t^2 + \frac{\omega^4}{4!}t^4 - ...) \tag{4.72}$$

which brings us the quadratic phase we desired if we could approximated the cosine function to the second order:

$$\phi(t) \approx A(1 - \frac{\omega_m^2}{2}t^2) \tag{4.73}$$

To make this approximation valid, the duration should be limited which gives the definition of aperture:

$$\Delta T = \frac{1}{\omega_m} \tag{4.74}$$

And it's natural to assume the pupil function of a EOM time lens is a rectangular function whose width is ΔT:

$$p_{EOM}(\tau') = \mathcal{V}\left[\frac{1}{\Delta T}\right]\Pi(\tau') \tag{4.75}$$

We also obtain the focal time of EOM time lens according to Eq. (4.73):

$$D_f = \frac{1}{A\omega_m^2} = \frac{\Delta T^2}{A} \tag{4.76}$$

© 2018 Tous droits réservés.

lilliad.univ-lille.fr

Thèse de Junheng Shi, Université de Lille, 2018

So we obtain its impulse response

$$\begin{aligned} h_{SFG}(\tau) =& \frac{1}{|D_i|}\mathcal{V}\left[\frac{1}{D_i}\right]\mathcal{F}p_{EOM}(\tau') \\ =& \frac{1}{|D_i|}\mathcal{V}\left[\frac{1}{D_i}\right]\mathcal{F}\mathcal{V}\left[\frac{1}{\Delta T}\right]\Pi(\tau') \\ =& \frac{\Delta T}{|D_i|}\mathcal{V}\left[\frac{\Delta T}{D_i}\right]\mathcal{F}\Pi(\tau') \\ =& \frac{\Delta T}{|D_i|\sqrt{2\pi}}\mathcal{V}\left[\frac{\Delta T}{D_i}\right]\mathrm{sinc}(\tau) \\ \approx& \frac{\Delta T}{|M|D_f\sqrt{2\pi}}\mathcal{V}\left[\frac{\Delta T}{|M|D_f}\right]\mathrm{sinc}(\tau) \\ =& \frac{A}{|M|\Delta T\sqrt{2\pi}}\mathcal{V}\left[\frac{A}{|M|\Delta T}\right]\mathrm{sinc}(\tau) \end{aligned} \tag{4.77}$$

Because $\mathrm{sinc}(1.895) \approx 0.5$, we obtain the resolution of EOM time lens:

$$\mathcal{R}_{EOM} = 1.895\frac{|M|\Delta T}{A}/|M| = 1.895\frac{\Delta T}{A} \tag{4.78}$$

As we could see, the resolution of EOM time lens is proportional to its aperture which is not very desirable. Usually we want the aperture to be as large as possible and the resolution to be as small as possible. But EOM time lens can not satisfy both. The only solution is have a large A which is limited by the material.

4.3 Restrictions of Quantum Temporal Imaging

After we examined the resolutions of various quantum temporal imaging systems, let's return to where we started, the coupled equations (4.10). This time we do not approximated it as in Eq. (4.12) and keep it as a function of Ω_i and Ω_s.

Then a common method to deal with equations (4.10), mainly Eq. (4.10b) is make an assumption that g is small and $\hat{a}_s(z,\Omega')$ remains unchanged during the process so we could integrate Eq. (4.10b) over z, for convenience, from $-L/2$ to $L/2$:

$$\begin{aligned} &\hat{a}_i(L/2,\Omega) - \hat{a}_i(-L/2,\Omega) \\ =& \mathrm{i}g\int\frac{\mathrm{d}\Omega'}{\sqrt{2\pi}}\hat{a}_s(L/2,\Omega')\alpha_p(\Omega-\Omega')\int_{-L/2}^{L/2}\mathrm{d}z\,\mathrm{e}^{-\mathrm{i}\Delta(\Omega,\Omega')z} \\ =& \mathrm{i}gL\int\frac{\mathrm{d}\Omega'}{\sqrt{2\pi}}\hat{a}_s(L/2,\Omega')\alpha_p(\Omega-\Omega')\mathrm{sinc}\left(\frac{\Delta(\Omega,\Omega')L}{2}\right) \end{aligned} \tag{4.79}$$

since the idler input field is vacuum, we could write Eq. (4.79) in the form of a linear system:

$$\hat{a}_i(\Omega_i) \propto \int \mathrm{d}\Omega_s K(\Omega_i,\Omega_s)\hat{a}_s(\Omega_s) \tag{4.80}$$

So this kernel $K(\Omega_i,\Omega_s)$ could be regarded as a linear filter which could provide a restriction for Ω_i and Ω_s with a range of $\delta\omega_i$ and $\delta\omega_s$. Only the signal field and idler

© 2018 Tous droits réservés.

lilliad.univ-lille.fr

Thèse de Junheng Shi, Université de Lille, 2018

field those within these ranges are imaged. Such restriction bring limitations to the resolution and FOV of the temporal imaging system.

$$K(\Omega_i, \Omega_s) = \alpha_p(\Omega_i - \Omega_s)\text{sinc}\left(\frac{\Delta(\Omega_i, \Omega_s)L}{2}\right) \tag{4.81}$$

From Eq. (4.81) we could see the main contribution to the restriction from the kernel is the phase mismatch term $\Delta(\Omega_i, \Omega_s)$L.

To evaluate these restrictions on quantum temporal imaging, we need to use the pixel pulse model in which the input field is regarded as a train of pixel pulses with identical spectrum but are separated in time.

This section includes three parts:

First, the evolution of the width and central displacement of the pixels in frequency and temporal domain which give rise to the restrictions on the temporal width and bandwidth of the pump wave;

Second, the restrictions on the FOV and resolution of signal field subsequent from the phase-matching condition $\Delta(\Omega_i, \Omega_s)$;

Third, the concept of quantum FOV.

4.3.1 Restriction on the Pump Wave

In the pixel pulse model, if the resolution of an temporal imaging system is τ_0, then the signal input field to be imaged is made up of N temporal pixels assumed to be a Gaussian function with temporal width τ_0, the temporal distance between the centers of adjacent pixels is also τ_0, all pixels is assumed to have identical spectrum with identical carrier frequency ω_s, and their bandwidth equals to $\delta\omega_s$. If all N pixels are imaged, then obviously the FOV of such input field is

$$T_F = N\tau_0 \tag{4.82}$$

On the other side, the pump wave is produced by passing a short pulse with temporal width $\delta\tau_p$ and bandwidth $\delta\omega_p$ through a dispersive medium whose GDD equals to D_f. Its temporal width becomes

$$\Delta\tau_p = D_f\delta\omega_p \tag{4.83}$$

Now let's pass the signal field through the first dispersive medium. The temporal distance between adjacent pixels remains τ_0 because of their identical spectrum. But each pixel is dispersed, its temporal width becomes $D_s\delta\omega_s$. So the total duration of the signal field is

$$T_s = D_s\delta\omega_s + (N-1)\tau_0 \tag{4.84}$$

© 2018 Tous droits réservés.

lilliad.univ-lille.fr

Thèse de Junheng Shi, Université de Lille, 2018

For quantum temporal imaging, it is important that the temporal width of the pump wave is much larger than the duration of the signal field:

$$\begin{aligned} &\Delta\tau_p \gg T_s \\ \Rightarrow &D_f\delta\omega_p \gg D_s\delta\omega_s + (N-1)\tau_0 \\ \Rightarrow &\delta\omega_p \gg \frac{D_s}{D_f}\delta\omega_s + (N-1)\frac{\tau_0}{D_f} \\ \Rightarrow &\delta\omega_p \gg \left(1+\frac{1}{|M|}\right)\delta\omega_s + (N-1)\frac{\tau_0}{D_f} \end{aligned} \tag{4.85}$$

From Eq. (4.85) we obtain the restriction on the bandwidth of the pump wave. We define this limit as active pump bandwidth:

$$\delta\omega_{pa} = \left(1+\frac{1}{|M|}\right)\delta\omega_s + (N-1)\frac{\tau_0}{D_f} \tag{4.86}$$

To understand this restriction better, we investigate the total spectral width of the idler field. We obtain that the spectral distance between adjacent pixels is τ_0/D_f, the bandwidth of the idler pixel equals to $\delta\omega_s/|M|$. So the total spectral width is

$$\delta\omega_i = \frac{\delta\omega_s}{|M|} + (N-1)\frac{\tau_0}{D_f} \tag{4.87}$$

It's not hard to find out that the restriction could be written as

$$\omega_{pa} = \omega_s + \omega_i \tag{4.88}$$

That the bandwidth of the pump wave should be much larger than sum of the spectral width of the signal wave and the idler wave.

4.3.2 Restrictions on the Resolution and Field of View

Now let's finally take a look at this phase mismatch term. The easier way is to expand it only to the first order

$$\Delta(\Omega_i, \Omega_s) \approx (k'_s - k'_p)\Omega_s + (k'_p - k'_i)\Omega_i \tag{4.89}$$

Or if we are dealing with second harmonic generation that $k'_s = k'_p$, we could expand Ω_s to the second order:

$$\Delta(\Omega_i, \Omega_s) \approx k''_s\Omega_s^2 + (k'_p - k'_i)\Omega_i \tag{4.90}$$

But this does not matter, like what was said, the purpose is to get the filtering range for Ω_s and Ω_i. Take Eq. (4.90) as an example.

© 2018 Tous droits réservés.

lilliad.univ-lille.fr

Thèse de Junheng Shi, Université de Lille, 2018

First we want to get the range for Ω_s:

$$\begin{aligned} &\Delta(\delta\omega_s, 0)L \ll 1 \\ \Rightarrow &k_s'' L \delta\omega_s^2 \ll 1 \\ \Rightarrow &\delta\omega_s \ll \frac{1}{\sqrt{k_s'' L}} \end{aligned} \tag{4.91}$$

If we define $\tau_s = \sqrt{k_s'' L}$, since ω_s is the Fourier transformed bandwidth of τ_0, we obtain the restriction on resolution:

$$\tau_0 = \frac{1}{\delta\omega_s} \gg \tau_s \tag{4.92}$$

Now we seek the range for Ω_i:

$$\begin{aligned} &\Delta(0, \delta\omega_s)L \ll 1 \\ \Rightarrow &|k_p' - k_i'| L \delta\omega_i \ll 1 \\ \Rightarrow &\delta\omega_i \ll \frac{1}{|k_p' - k_i'| L} \end{aligned} \tag{4.93}$$

If we define $\tau_i = |k_p' - k_i'|L$, then we could get the restriction for the FOV:

$$\begin{aligned} &\delta\omega_i = \frac{\delta\omega_s}{|M|} + (N-1)\frac{\tau_0}{D_f} \ll \frac{1}{\tau_i} \\ \Rightarrow &T_F \approx (N-1)\tau_0 \ll \frac{D_f}{\tau_i} - \frac{D_f}{|M|\tau_0} \\ \Rightarrow &T_F \ll \frac{D_f}{\tau_i} \end{aligned} \tag{4.94}$$

when $|M| \gg \tau_i/\tau_0$.

This restriction on FOV, along with Eq. (3.150), are all associated with the signal field being a nonclassical light. So they could be called as quantum FOV.

4.4 Summary of this chapter

In this chapter we try to establish an evaluation system for quantum temporal imaging system to assess the performances of different quantum temporal imaging schemes by understanding the limitations and aberrations. During the formalism of SFG time lens, we find these limitations are the results of the finite temporal width of the pump and the phase-matching condition. We first investigate the former limitation by regarding the pump profile as a pupil function and employ the linear system analysis to define resolution and use it to evaluate various types of time lens. We then develop a pixel pulse model where the signal field is decomposed into pixels-shortest distinguishable temporal duration. Using this model we come up with the restrictions on the bandwidth of the pump and then on the resolution and quantum FOV brought by the phase-matching conditions.

© 2018 Tous droits réservés.

lilliad.univ-lille.fr

Thèse de Junheng Shi, Université de Lille, 2018

Chapter 5

Quantum Temporal Imaging with Single Photon Source

Single-photon source is a photon source which produces one and only one photon at a time. Such source is essential to quantum information processing, for example quantum cryptography [6, 20, 71], quantum teleportation [15] or optical quantum computation [31, 32] which requires massive resources of indistinguishable photons [1, 63]. Such indistinguishability are demonstrated with the help from Hong-Ou-Mandel (HOM) interference [4, 26, 70].

One common way to generate single photon is based on parametric downconversion in a nonlinear medium that two photons are produced simultaneously. One photon is taken as the single photon and the other photon could be used to herald it. This method is simple to realize yet it's not technically a single-photon source because the photons produced still follow the Poisson distribution that there is a possibility of two photons being emitted at a time.

Another method is to use semiconductor quantum dots [9, 14, 18, 27, 36, 53, 58, 61, 64, 74] which are often regarded as "artificial atoms" that the rules for light-matter interaction could be applied. Particularly it could be seen as a two level system that it absorbs a photon to jump from the ground state with lower energy to the excited state with higher energy level. It would also emit a photon when jumping from the excited state to the ground state, such behavior is called spontaneous emission. Clearly it wouldn't emit two photons at a time otherwise the energy conservation principle would be violated. This property makes it an ideal candidate for single-photon source that we are going to investigate in this chapter.

In this chapter first we use the density operator approach to obtain the normalized second correlation function and the squeezing spectrum of the single-photon source based on quantum dot under pulsed excitation. Then we examine how quantum temporal imaging scheme would affect its nonclassical property.

5.1 Quantum Dots under Pulsed Excitation

Pulsed excitation means that this two level system would go through a process of going from the ground state to the excited state under the π pulse and then decaying back to the ground state again while emitting a photon. The π pulse is given periodically.

© 2018 Tous droits réservés.

lilliad.univ-lille.fr

Thèse de Junheng Shi, Université de Lille, 2018

Without broadening, the spectrum of the emitted photon has a Lorentzian shape which corresponds to its waveform as $g(t) = \frac{1}{2\tau_r} e^{-|t|/\tau_r}$, τ_r is the lifetime of spontaneous emission, T_0 is the period of π pulse. With the assumption that $\tau_{rad} \ll T_0$, we could approximate $g(t) \approx \delta(t)$. As each photon produced are independent to each other that we divide the whole time into time bin modes by the interval of T_0. So the density matrix of (2N+1) photon state is defined as the direct product of density operator for each time bin mode:

$$\rho = \rho_1 \otimes \rho_2 \otimes ... \otimes \rho_N = \prod_{m=-N}^{N} \rho_m \tag{5.1}$$

$$\rho_m = \int dt_m dt'_m \, f(t_m, t'_m) \hat{a}^\dagger(t_m)|0\rangle\langle 0|\hat{a}(t'_m) + (1-\eta_0)|0\rangle\langle 0| \tag{5.2}$$

$f(t_m, t'_m)$ is normalized to the quantum efficiency of the source η_s and collection efficiency η_c. In this particular case,

$$f(t_m, t_m) = \eta_0 g(t - mT_0) \tag{5.3}$$

where $\eta_0 = \eta_s \eta_c$.

Note $\mathrm{tr}(\rho_m) = 1$ is satisfied for every ρ_m.

5.1.1 Normalized Second Order Correlation Function

Using the density operator we first evaluate

$$\begin{aligned}
\tilde{G}^{(2)}(t';t'') =& \mathrm{tr}\left\{\hat{a}^\dagger(t')\hat{a}^\dagger(t'')\hat{a}(t'')\hat{a}(t')\rho\right\} \\
=& \mathrm{tr}\left\{\hat{a}(t'')\hat{a}(t') \prod_{m=-N}^{N} \rho_m \hat{a}^\dagger(t')\hat{a}^\dagger(t'')\right\} \\
=& \sum_{j=-N}^{N} \mathrm{tr}\left\{\hat{a}(t'')\left[\left(\int dt_j dt'_j f(t_j,t'_j)\left[\hat{a}^\dagger(t_j),\hat{a}(t')\right]|0\rangle\langle 0|\left[\hat{a}^\dagger(t'_j),\hat{a}(t')\right]^\dagger + 0\right)\prod_{m\neq j}\rho_m\right]\hat{a}(t'')\right\} \\
=& \sum_{j=-N}^{N} \mathrm{tr}\left\{\hat{a}(t'')\left[\left(\int dt_j dt'_j f(t_j,t'_j)\delta(t'-t_j)|0\rangle\langle 0|\delta(t'-t'_j) + 0\right)\prod_{m\neq j}\rho_m\right]\hat{a}(t'')\right\} \\
=& \eta_0 \sum_{j=-N}^{N}\sum_{j'\neq j} g(t'-jT_0) \\
& \times \mathrm{tr}\left\{\left(\int dt_{j'} dt'_{j'} f(t_{j'},t'_{j'})\left[\hat{a}^\dagger(t_{j'}),\hat{a}(t'')\right]|0\rangle\langle 0|\left[\hat{a}^\dagger(t'_{j'}),\hat{a}(t'')\right]^\dagger + 0\right)\prod_{m\neq j,j'}\rho_m\right\} \\
=& \eta_0^2 \sum_{j=-N}^{N}\sum_{j'\neq j} g(t'-jT_0)g(t''-j'T_0) \\
=& \eta_0^2 \sum_{j=-N}^{N}\sum_{j'=-N}^{N} g(t'-jT_0)g(t''-j'T_0) - \eta_0^2 \sum_{j=-N}^{N} g(t'-jT_0)g(t''-jT_0)
\end{aligned} \tag{5.4}$$

$\tilde{G}^{(2)}(t';t'')$ is illustrated in Figure 5.1 where $\tau' = t'' - t'$. We could spot the missing peak at $\tau' = 0$ which is the characteristic of a single-photon source.

© 2018 Tous droits réservés.

lilliad.univ-lille.fr

Thèse de Junheng Shi, Université de Lille, 2018

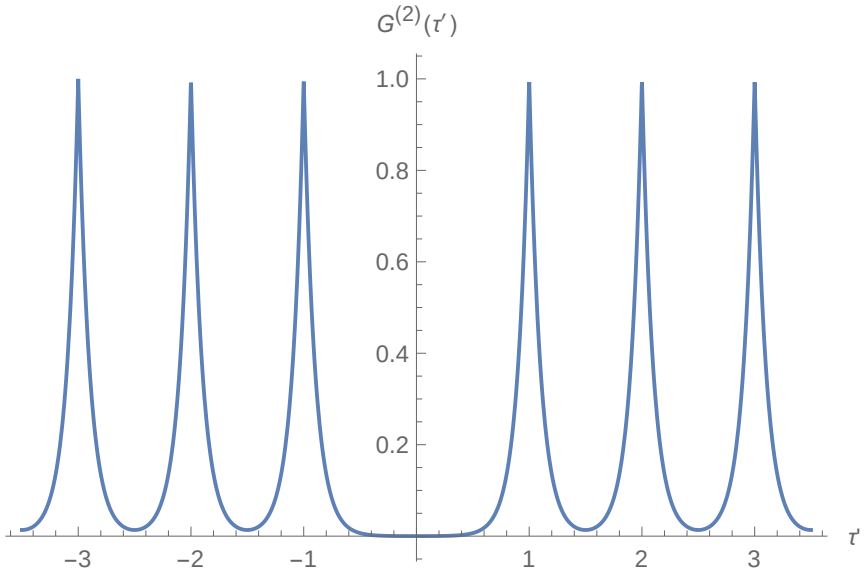

FIGURE 5.1: Second-order correlation function of single-photon source when $\tau_r = 0.1$, $T_0 = 1$, $N = 10$, $t' = 6$

However, to understand better its property, we need to integrate over the second order correlation function with help from a filter function $F(t) = \frac{1}{T}e^{-\frac{t}{T}}\theta(t)$, T could be understood as the time of observation, and we could obtain the number of time bin modes during this observation time

$$N_T = \frac{T}{T_0} \tag{5.5}$$

As a result,

$$\begin{aligned} G^{(2)}(t;\tau) &= \int_{-\infty}^{+\infty} dt' F(t-t') \int_{-\infty}^{+\infty} dt'' F(t+\tau-t'') \tilde{G}^{(2)}(t';t'') \\ &= \frac{\eta_0^2}{T^2} \int_{-\infty}^{+\infty} dt' \int_{-\infty}^{+\infty} dt'' e^{-\frac{t-t'}{T}} \theta(t-t') e^{-\frac{t+\tau-t''}{T}} \theta(t+\tau-t'') \\ &\quad \times \left[\sum_{j=-N}^{N} \sum_{j'=-N}^{N} g(t'-jT_0) g(t''-j'T_0) - \eta_0^2 \sum_{j=-N}^{N} g_j(t'-jT_0) g_j(t''-jT_0) \right] \end{aligned} \tag{5.6}$$

Now let's calculate Eq.(5.6) with the assumption that the duration of the pulsed excitation is larger than the observation time:

First we denote the time bin t is in as k_0 which satisfies $k_0 T_0 - \frac{T_0}{2} < t < k_0 T_0 + \frac{T_0}{2}$. Similarly we denote the time bin $t+\tau$ is in as k. So we have

$$k_0 = \lfloor t + \frac{T_0}{2} \rfloor \tag{5.7}$$

$$k = \lfloor t + \tau + \frac{T_0}{2} \rfloor \tag{5.8}$$

© 2018 Tous droits réservés.

lilliad.univ-lille.fr

Thèse de Junheng Shi, Université de Lille, 2018

So the first term of Eq.(5.6):

$$
\begin{aligned}
&\frac{\eta_0^2}{T^2}\int_{-\infty}^{+\infty}dt'\int_{-\infty}^{+\infty}dt''\mathrm{e}^{-\frac{t-t'}{T}}\theta(t-t')\mathrm{e}^{-\frac{t+\tau-t''}{T}}\theta(t+\tau-t'')\sum_{j=-\infty}^{+\infty}\sum_{j'=-\infty}^{+\infty}\delta(t'-jT_0)\delta(t''-j'T_0)\\
=&\frac{\eta_0^2}{T^2}\sum_{j=-\infty}^{k_0}\sum_{j'=-\infty}^{k}\int_{-\infty}^{t}dt'\int_{-\infty}^{t+\tau}dt''\mathrm{e}^{-\frac{t-t'}{T}}\mathrm{e}^{-\frac{t+\tau-t''}{T}}\delta(t'-jT_0)\delta(t''-j'T_0)\\
=&\frac{\eta_0^2}{T^2}\sum_{j=-\infty}^{k_0}\sum_{j'=-\infty}^{k}\mathrm{e}^{-\frac{t-jT_0}{T}}\mathrm{e}^{-\frac{t+\tau-j'T_0}{T}}\\
=&\frac{\eta_0^2}{T^2}\mathrm{e}^{-\frac{2t+\tau}{T}}\frac{\mathrm{e}^{k_0T_0/T}}{1-\mathrm{e}^{-T_0/T}}\frac{\mathrm{e}^{kT_0/T}}{1-\mathrm{e}^{-T_0/T}}\\
=&\frac{\eta_0^2}{T^2}\left[\frac{1}{1-\mathrm{e}^{-T_0/T}}\right]^2\exp\left\{-\left[\frac{t-k_0T_0}{T}+\frac{t+\tau-kT_0}{T}\right]\right\}\\
\approx&\frac{\eta_0^2}{T^2}\left[\frac{1}{1-(1-\frac{T_0}{T})}\right]^2\\
\approx&\frac{\eta_0^2N_T^2}{T^2}
\end{aligned}
\tag{5.9}
$$

During the process we take the assumption that

$$
\exp\left\{-\left[\frac{t-k_0T_0}{T}+\frac{t+\tau-kT_0}{T}\right]\right\}\approx 1 \tag{5.10}
$$

because according to (5.7) and (5.8), $(t-k_0T_0) < T_0 << T$ and $(t+\tau-kT_0) < T_0 << T$.

To evaluate the second term, we need to split into two conditions.

© 2018 Tous droits réservés.

lilliad.univ-lille.fr

Thèse de Junheng Shi, Université de Lille, 2018

First when $\tau < 0$ i.e. $k \leq k_0$:

$$\begin{aligned}
&\frac{\eta_0^2}{T^2}\int_{-\infty}^{+\infty}dt'\int_{-\infty}^{+\infty}dt''\mathrm{e}^{-\frac{t-t'}{T}}\theta(t-t')\mathrm{e}^{-\frac{t+\tau-t''}{T}}\theta(t+\tau-t'')\sum_{j=-\infty}^{+\infty}\delta(t'-jT_0)\delta(t''-jT_0)\\
=&\frac{\eta_0^2}{T^2}\sum_{j=-\infty}^{k}\int_{-\infty}^{t}dt'\int_{-\infty}^{t+\tau}dt''\mathrm{e}^{-\frac{t-t'}{T}}\mathrm{e}^{-\frac{t+\tau-t''}{T}}\delta(t'-jT_0)\delta(t''-jT_0)\\
=&\frac{\eta_0^2}{T^2}\sum_{j=-\infty}^{k}\mathrm{e}^{-\frac{t-jT_0}{T}}\mathrm{e}^{-\frac{t+\tau-jT_0}{T}}\\
=&\frac{\eta_0^2}{T^2}\mathrm{e}^{-\frac{2t+\tau}{T}}\frac{\mathrm{e}^{2kT_0/T}}{1-\mathrm{e}^{-2T_0/T}}\\
=&\frac{\eta_0^2}{T^2}\frac{1}{1-\mathrm{e}^{-2T_0/T}}\mathrm{e}^{-\frac{-\tau}{T}}\mathrm{e}^{-2\frac{t+\tau-kT_0}{T}}\\
\approx&\frac{\eta_0^2}{T^2}\frac{1}{1-\mathrm{e}^{-2T_0/T}}\mathrm{e}^{-\frac{-\tau}{T}}\\
\approx&\frac{\eta_0^2}{T^2}\frac{1}{1-(1-2\frac{T_0}{T})}\mathrm{e}^{-\frac{-\tau}{T}}\\
=&\frac{\eta_0^2 N_T}{2T^2}\mathrm{e}^{-\frac{-\tau}{T}}
\end{aligned}$$

Then when $\tau > 0$ i.e. $k_0 \leq k$:

$$\begin{aligned}
&\frac{\eta_0^2}{T^2}\int_{-\infty}^{+\infty}dt'\int_{-\infty}^{+\infty}dt''\mathrm{e}^{-\frac{t-t'}{T}}\theta(t-t')\mathrm{e}^{-\frac{t+\tau-t''}{T}}\theta(t+\tau-t'')\sum_{j=-\infty}^{+\infty}\delta(t'-jT_0)\delta(t''-jT_0)\\
=&\frac{\eta_0^2}{T^2}\mathrm{e}^{-\frac{2t+\tau}{T}}\frac{\mathrm{e}^{2k_0T_0/T}}{1-\mathrm{e}^{-2T_0/T}}\\
=&\frac{\eta_0^2}{T^2}\frac{1}{1-\mathrm{e}^{-2T_0/T}}\mathrm{e}^{-\frac{\tau}{T}}\mathrm{e}^{-2\frac{t-k_0T_0}{T}}\\
\approx&\frac{\eta_0^2}{T^2}\frac{1}{1-\mathrm{e}^{-2T_0/T}}\mathrm{e}^{-\frac{\tau}{T}}\\
\approx&\frac{\eta_0^2}{T^2}\frac{1}{1-(1-2\frac{T_0}{T})}\mathrm{e}^{-\frac{\tau}{T}}\\
=&\frac{\eta_0^2 N_T}{2T^2}\mathrm{e}^{-\frac{\tau}{T}}
\end{aligned}$$

Now we obtain the value of the second order correlation function:

$$G^{(2)}(t;\tau) \approx \frac{\eta_0^2 N_T^2}{T^2} - \frac{\eta_0^2 N_T}{2T^2}\mathrm{e}^{-|\tau|/T} \tag{5.11}$$

When the time delay approaches infinite, $\tau \to \infty$, any correlations would disappear, hence we obtain the average intensity

$$\begin{aligned}
\langle I\rangle^2 &= G^{(2)}(\infty)\\
&= \frac{\eta_0^2 N_T^2}{T^2}
\end{aligned} \tag{5.12}$$

© 2018 Tous droits réservés.

lilliad.univ-lille.fr

Thèse de Junheng Shi, Université de Lille, 2018

By normalizing it with $\langle I \rangle^2$, we get the normalized second order correlation function:

$$g^{(2)}(\tau) = 1 - \frac{1}{2N_T} e^{-|\tau|/T} \tag{5.13}$$

With $g^{(2)}(0) = 1 - \frac{1}{2N_T}$.

Its shape could be seen in Figure 5.2.

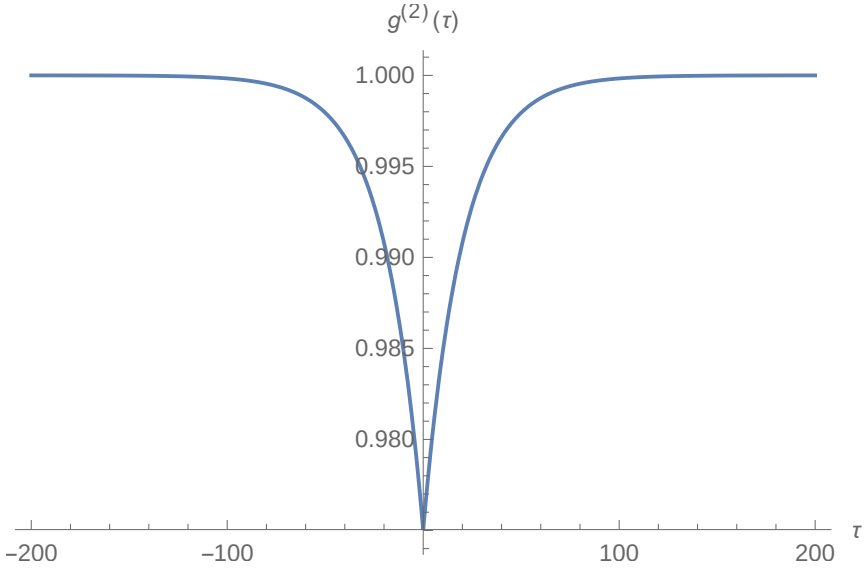

FIGURE 5.2: Normalized second-order correlation function of single-photon source when $T_0 = 1$, $T = 20$.

5.1.2 Squeezing Spectrum

Now we try to get the noise spectrum.

$$\begin{aligned}(\delta i)^2_\Omega &= \int d\tau e^{i\Omega\tau} \left[\eta_d \langle I \rangle \delta(\tau) + \eta_d^2 (G^{(2)}(\tau) - \langle I \rangle^2)\right] \\ &= \eta_d \frac{\eta_0 N_T}{T} \int d\tau e^{i\Omega\tau} \delta(\tau) - \eta_d^2 \frac{\eta_0^2 N_T}{2T^2} \int d\tau e^{i\Omega\tau} e^{-\frac{|\tau|}{T}} \\ &= \eta_d \frac{\eta_0 N_T}{T} - \eta_d^2 \frac{\eta_0^2 N_T}{2} \frac{2/T^2}{(1/T)^2 + \Omega^2}\end{aligned} \tag{5.14}$$

where η_d is the quantum efficiency of photon detector

We could also obtain the squeezing spectrum

$$\begin{aligned}S(\Omega) &= \frac{(\delta i)^2_\Omega}{\langle i \rangle} \\ &= 1 - \eta_0' \frac{1}{2} \frac{2/T^2}{(1/T)^2 + \Omega^2} \\ &= 1 - \eta_0' \frac{1}{1 + (\Omega T)^2}\end{aligned} \tag{5.15}$$

© 2018 Tous droits réservés.

lilliad.univ-lille.fr

Thèse de Junheng Shi, Université de Lille, 2018

where $\eta_0' = \eta_d \eta_0$,
When $\Omega = 0$, $S(\Omega) = 1 - \eta_0'$. As could be seen in Figure 5.3, $S(\Omega)$ is below shot-noise which indicates the presence of squeezing.

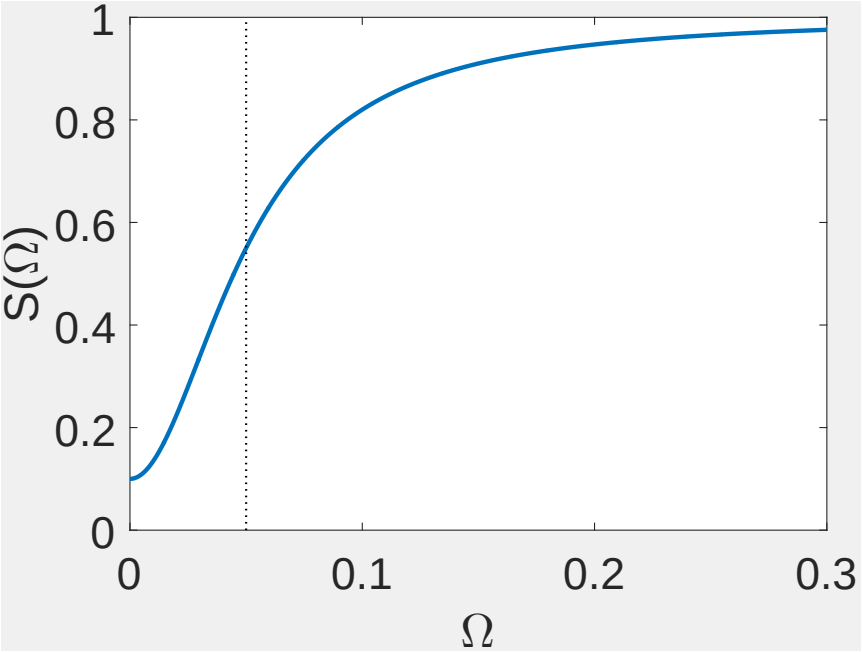

FIGURE 5.3: Squeezing spectrum of single-photon source when $\eta_0' = 0.9$, $T_0 = 1$, $T = 20$, the dashed line is the location of the characteristic time, $\frac{1}{T}$.

5.2 Four-Wave Mixing Time Lens with Single-Photon Source

Now we pass the photons produced by the single-photon source through the FWM time lens just like what we did with broadband squeezed light and check how it would affect its nonlinear property.

First we need to expand the density operator by direct multiplication with the density operator for idler vacuum input:

$$\rho = \prod_{m=-N}^{N} \rho_{s,m} \otimes \rho_i \tag{5.16}$$

$$\rho_{s,m} = \int dt_m dt_m' \, f(t_m, t_m') \hat{a}_{s,in}^{\dagger}(t_m) |0\rangle\langle 0|_s \hat{a}_{s,in}(t_m') + (1 - \eta_0) |0\rangle\langle 0|_s \tag{5.17}$$

$$\rho_i = |0\rangle\langle 0|_i \tag{5.18}$$

According to what we had obtained in Chapter 3, we already know that PC FWM time lens would destroy the nonclassical property by introducing vacuum noise.

So here we are interested in how the other quantum temporal scheme - PP FWM time lens would affect the nonclasscial property of single photons.

© 2018 Tous droits réservés.

lilliad.univ-lille.fr

Thèse de Junheng Shi, Université de Lille, 2018

According to Eq.(3.134), the transformation of the annihilation operator brought by the PP FWM time lens is

$$\hat{a}_{out}(\tau) = \mathrm{i}e^{\mathrm{i}\phi_p(\tau)}\sqrt{\eta}\,\hat{a}_{s,in}(\tau) + \sqrt{1-\eta}\,\hat{a}_{i,in}(\tau) \tag{5.19}$$

So the second order correlation function becomes

$$\begin{aligned}
\tilde{G}^{(2)}(t';t'') =& \mathrm{tr}\left\{\hat{a}^\dagger_{out}(t')\hat{a}^\dagger_{out}(t'')\hat{a}_{out}(t'')\hat{a}_{out}(t')\rho\right\} \\
=& \mathrm{tr}\Bigg\{\left[-\mathrm{i}e^{-\mathrm{i}\phi_p(t')}\sqrt{\eta}\,\hat{a}^\dagger_{s,in}(t') + \sqrt{1-\eta}\,\hat{a}^\dagger_{i,in}(t')\right] \\
&\times\left[-\mathrm{i}e^{-\mathrm{i}\phi_p(t'')}\sqrt{\eta}\,\hat{a}^\dagger_{s,in}(t'') + \sqrt{1-\eta}\,\hat{a}^\dagger_{i,in}(t'')\right] \\
&\times\left[\mathrm{i}e^{\mathrm{i}\phi_p(t'')}\sqrt{\eta}\,\hat{a}_{s,in}(t'') + \sqrt{1-\eta}\,\hat{a}_{i,in}(t'')\right] \\
&\times\left[\mathrm{i}e^{\mathrm{i}\phi_p(t')}\sqrt{\eta}\,\hat{a}_{s,in}(t') + \sqrt{1-\eta}\,\hat{a}_{i,in}(t')\right]\rho\Bigg\} \\
=& \eta^2\mathrm{tr}_s\left\{\hat{a}^\dagger_{s,in}(t')\hat{a}^\dagger_{s,in}(t'')\hat{a}_{s,in}(t'')\hat{a}_{s,in}(t')\prod_{m=-N}^{N}\rho_{s,m}\right\}\mathrm{tr}_i\left\{\rho_i\right\} \\
=& \eta^2\mathrm{tr}_s\left\{\hat{a}^\dagger_{s,in}(t')\hat{a}^\dagger_{s,in}(t'')\hat{a}_{s,in}(t'')\hat{a}_{s,in}(t')\prod_{m=-N}^{N}\rho_{s,m}\right\}
\end{aligned} \tag{5.20}$$

Compared to Eq.(5.4), the result is not so much different from before, the only difference is that it is now multiplied by η^2 which could be understood as conversion efficiency.

As a result we could follow the same process and obtain the second-order correlation function:

$$G^{(2)}(t;\tau) \approx \frac{\eta^2\eta_0^2 N_T^2}{T^2} - \frac{\eta^2\eta_0^2 N_T}{2T^2}e^{-|\tau|/T} \tag{5.21}$$

The normalized second order correlation function remains the same as Eq.(5.13) however the squeezing spectrum is changed:

$$\begin{aligned}
S(\Omega) &= \frac{(\delta i)^2_\Omega}{\langle i\rangle} \\
&= 1 - \eta_0'\eta\frac{1}{1+(\Omega T)^2}
\end{aligned} \tag{5.22}$$

as could be seen in Figure 5.4.

5.3 Summary of this chapter

This chapter falls n the same category as Chapter 3 where we investigate the temporal imaging of nonclassical field. We focus on its influence on the single-photon source. We use the a simple and typical model of single-photon source in density operator approach to calculate the second order correlation function and then the

© 2018 Tous droits réservés.

lilliad.univ-lille.fr

Thèse de Junheng Shi, Université de Lille, 2018

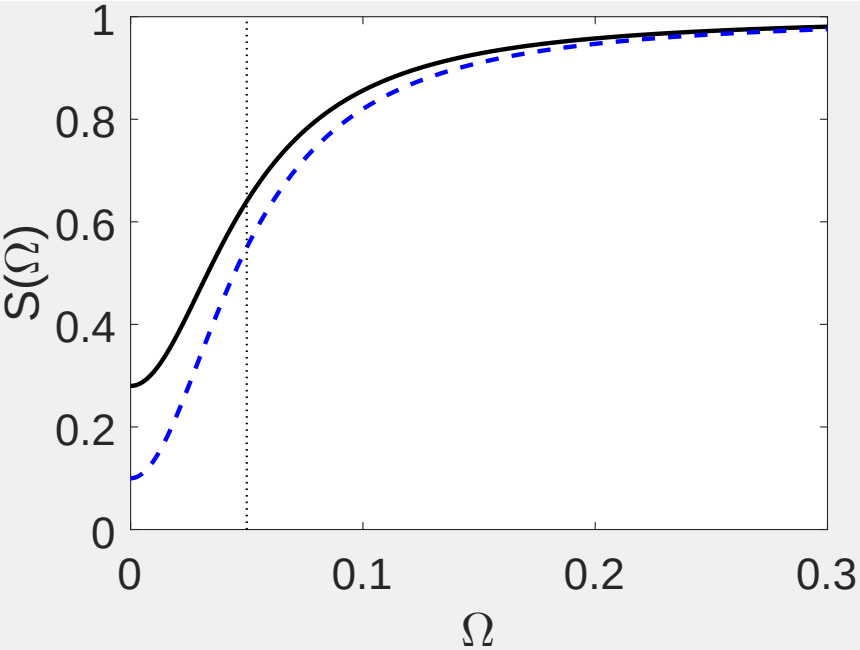

FIGURE 5.4: Squeezing spectrum of single-photon source after a four-wave mixing time lens when $\eta_0' = 0.9$, $\eta = 0.8$ $T_0 = 1$, $T = 20$.

squeezing spectrum. We then study the influence of FWM time lens on the squeezing spectrum of such source and find the decrease of nonclassical property depending on the conversion efficiency of nonlinear-process based time lens.

© 2018 Tous droits réservés.

lilliad.univ-lille.fr

© 2018 Tous droits réservés.

lilliad.univ-lille.fr

Thèse de Junheng Shi, Université de Lille, 2018

Chapter 6

Prospects

Quantum temporal imaging has a variety of applications in quantum optics and quantum information, especially serves as an efficient interface between physical systems for transmitting information in a quantum network. Not only could it translate the carrier frequency of the quantum optical signal, it could also modify its characteristic time or bandwidth, in order to fit it into other part of the quantum network such as a detector. Quantum temporal imaging could change the characteristic frequency of a broadband squeezed light, such experiments has not been reported.

From theoretical point of view, quantum temporal imaging combines the studies on linear system for the evaluation of the imaging system, on quantum optics for the nonclassical light as the "object" and on nonlinear optics for the time lens. More researches on how to achieve higher conversion efficiency for the time lens, especially the PPFWM time lens are needed since the present focus of nonlinear-process based time lens is on PCFWM time which is not suitable for quantum temporal imaging. When near-unity conversion efficiency is achievable, mathematical studies on coupled equations of the nonlinear equations should move forward, enabling first more analytical analysis of the effect of e.g. phase-matching condition on the imaging performance, second better understanding of the nonlinear transformation relations and using different shapes of pump to improve the imaging performance.

© 2018 Tous droits réservés.

lilliad.univ-lille.fr

© 2018 Tous droits réservés.

lilliad.univ-lille.fr

Thèse de Junheng Shi, Université de Lille, 2018

Bibliography

[1] N Akopian et al. "Entangled photon pairs from semiconductor quantum dots". In: *Physical review letters* 96.13 (2006), p. 130501.

[2] Abhishek Anchal et al. "Frequency-shift free optical phase conjugation using counter-propagating dual pump four-wave mixing in fiber". In: (2016).

[3] John AuYeung et al. "Continuous backward-wave generation by degenerate four-wave mixing in optical fibers". In: *Optics Letters* 4.1 (1979), p. 42.

[4] AJ Bennett et al. "Influence of exciton dynamics on the interference of two photons from a microcavity single-photon source". In: *Optics express* 13.20 (2005), pp. 7772–7778.

[5] Corey V Bennett and Brian H Kolner. "Principles of parametric temporal imaging. II. System performance". In: *IEEE journal of quantum electronics* 36.6 (2000), pp. 649–655.

[6] Alexios Beveratos et al. "Single photon quantum cryptography". In: *Physical review letters* 89.18 (2002), p. 187901.

[7] Benjamin Brecht et al. "From quantum pulse gate to quantum pulse shaper—engineered frequency conversion in nonlinear optical waveguides". In: *New Journal of Physics* 13.6 (2011), p. 065029.

[8] Jun Chen et al. "Fiber-based telecom-band degenerate-frequency source of entangled photon pairs." In: *Optics letters* 31.18 (2006), pp. 2798–2800.

[9] Julien Claudon et al. "A highly efficient single-photon source based on a quantum dot in a photonic nanowire". In: *Nature Photonics* 4.3 (2010), p. 174.

[10] T Corti, E Brambilla, and A Gatti. "Critical behavior of coherence and correlation of counterpropagating twin beams". In: *Physical Review A* 93.2 (2016).

[11] Jean-Claude Diels and Wolfgang Rudolph. *Ultrashort laser pulse phenomena: fundamentals, techniques, and applications on a femtosecond time scale*. Elsevier, 2006.

[12] John M Donohue, Michael D Mazurek, and Kevin J Resch. "Theory of high-efficiency sum-frequency generation for single-photon waveform conversion". In: *Physical Review A* 91.3 (2015), p. 033809.

[13] S Tefan W Eber et al. "Time-stretched real-time measurement technique for ultrafast absorption variations with TS / s sampling-rate". In: 25.13 (2017), pp. 3618–3622.

[14] Dirk Englund et al. "Controlling the spontaneous emission rate of single quantum dots in a two-dimensional photonic crystal". In: *Physical review letters* 95.1 (2005), p. 013904.

[15] David Fattal et al. "Quantum teleportation with a quantum dot single photon source". In: *Physical review letters* 92.3 (2004), p. 037904.

[16] Mark A Foster et al. "Silicon-chip-based ultrafast optical oscilloscope". In: *Nature* 456.7218 (2008), p. 81.

[17] Mark A Foster et al. "Ultrafast waveform compression using a time-domain telescope". In: *Nature Photonics* 3.10 (2009), p. 581.

© 2018 Tous droits réservés.

lilliad.univ-lille.fr

Thèse de Junheng Shi, Université de Lille, 2018

[18] JM Gérard et al. "Enhanced spontaneous emission by quantum boxes in a monolithic optical microcavity". In: *Physical review letters* 81.5 (1998), p. 1110.
[19] J Giordmaine, M Duguay, and J Hansen. "Compression of optical pulses". In: *IEEE Journal of Quantum Electronics* 4.5 (1968), pp. 252–255.
[20] Nicolas Gisin et al. "Quantum cryptography". In: *Reviews of modern physics* 74.1 (2002), p. 145.
[21] Roy J Glauber. "Coherent and incoherent states of the radiation field". In: *Physical Review* 131.6 (1963), p. 2766.
[22] K Goda and B Jalali. "Dispersive Fourier transformation for fast continuous single-shot measurements". In: *Nature Photonics* 7.2 (2013), pp. 102–112.
[23] Joseph W Goodman. *Introduction to Fourier optics*. Roberts and Company Publishers, 2005.
[24] D. Grischkowsky. "Optical pulse compression". In: *Applied Physics Letters* 25.10 (1974), pp. 566–568.
[25] D Grischkowsky and AC Balant. "Optical pulse compression based on enhanced frequency chirping". In: *Physics of New Laser Sources*. Springer, 1982, pp. 109–116.
[26] R Hafenbrak et al. "Triggered polarization-entangled photon pairs from a single quantum dot up to 30 K". In: *New Journal of Physics* 9.9 (2007), p. 315.
[27] T Heindel et al. "Electrically driven quantum dot-micropillar single photon source with 34% overall efficiency". In: *Applied Physics Letters* 96.1 (2010), p. 011107.
[28] Kyo Inoue. "Tunable and selective wavelength conversion using fiber four-wave mixing with two pump lights". In: *IEEE Photonics Technology Letters* 6.12 (1994), pp. 1451–1453.
[29] D Kielpinski, JF Corney, and HM Wiseman. "Quantum optical waveform conversion". In: *Physical review letters* 106.13 (2011), p. 130501.
[30] John R Klauder et al. "The theory and design of chirp radars". In: *Bell Labs Technical Journal* 39.4 (1960), pp. 745–808.
[31] Emanuel Knill, Raymond Laflamme, and Gerald J Milburn. "A scheme for efficient quantum computation with linear optics". In: *nature* 409.6816 (2001), p. 46.
[32] Pieter Kok et al. "Linear optical quantum computing with photonic qubits". In: *Reviews of Modern Physics* 79.1 (2007), p. 135.
[33] Mikhail I Kolobov. "The spatial behavior of nonclassical light". In: *Reviews of Modern Physics* 71.5 (1999), p. 1539.
[34] Katarzyna Krupa et al. "Bragg-Scattering conversion at telecom wavelengths towards the photon counting regime". In: *Optics Express* 20.24 (2012), pp. 27220–27225.
[35] Jonathan Lavoie et al. "Spectral compression of single photons". In: *Nature Photonics* 7.5 (2013), p. 363.
[36] Kristian Høeg Madsen et al. "Efficient out-coupling of high-purity single photons from a coherent quantum dot in a photonic-crystal cavity". In: *Physical Review B* 90.15 (2014), p. 155303.
[37] Leonard Mandel and Emil Wolf. *Optical coherence and quantum optics*. Cambridge university press, 1995.
[38] H J McGuinness, M G Raymer, and C J McKinstrie. "Theory of quantum frequency translation of light in optical fiber: application to interference of two photons of different color." In: *Optics express* 19.19 (2011), pp. 17876–907.
[39] H. J. McGuinness et al. "Quantum frequency translation of single-photon states in a photonic crystal fiber". In: *Physical Review Letters* 105.9 (2010), pp. 1–4.

© 2018 Tous droits réservés.

lilliad.univ-lille.fr

Thèse de Junheng Shi, Université de Lille, 2018

[40] HJ McGuinness et al. "Quantum frequency translation of single-photon states in a photonic crystal fiber". In: *Physical review letters* 105.9 (2010), p. 093604.
[41] C McKinstrie et al. "Quantum noise properties of parametric processes." In: *Optics express* 13.13 (2005), pp. 4986–5012.
[42] C. J. McKinstrie. "Stokes-space formalism for Bragg scattering in a fiber". In: *Optics Communications* 282.8 (2009), pp. 1557–1562.
[43] C. J. McKinstrie. "Unitary and singular value decompositions of parametric processes in fibers". In: *Optics Communications* 282.4 (2009), pp. 583–593.
[44] C J McKinstrie et al. "Four-wave mixing in fibers with random birefringence". In: *Opt.\ Exp.* 12.10 (2004), pp. 2033–2055.
[45] C J McKinstrie et al. "Multicolor multipartite entanglement produced by vector four-wave mixing in a fiber." In: *Optics express* 16.4 (2008), pp. 2720–2739.
[46] C. J. McKinstrie et al. "Quantum-state-preserving optical frequency conversion and pulse reshaping by four-wave mixing". In: *Physical Review A - Atomic, Molecular, and Optical Physics* 85.5 (2012), pp. 3–6.
[47] C J McKinstrie et al. "Translation of quantum states by four-wave mixing in fibers". In: *Opt.\ Exp.* 13.22 (2005), pp. 9131–9142.
[48] CJ McKinstrie et al. "Translation of quantum states by four-wave mixing in fibers". In: *Optics Express* 13.22 (2005), pp. 9131–9142.
[49] Colin J McKinstrie et al. "Quantum-state-preserving optical frequency conversion and pulse reshaping by four-wave mixing". In: *Physical Review A* 85.5 (2012), p. 053829.
[50] D Méchin et al. "180-nm wavelength conversion based on Bragg scattering in an optical fiber." In: *Optics express* 14.20 (2006), pp. 8995–9.
[51] L Mejling et al. "Effects of nonlinear phase modulation on Bragg scattering in the low-conversion regime". In: *Optics Express* 20.24 (2012), pp. 27454–27475.
[52] L Mejling et al. "Quantum frequency translation by four-wave mixing in a fiber: low-conversion regime". In: *Optics express* 20.8 (2012), pp. 8367–8396.
[53] P Michler et al. "A quantum dot single-photon turnstile device". In: *science* 290.5500 (2000), pp. 2282–2285.
[54] Moshe Nazarathy and Joseph Shamir. "Fourier optics described by operator algebra". In: *JOSA* 70.2 (1980), pp. 150–159.
[55] Y Okawachi et al. "High-resolution spectroscopy using a frequency magnifier". In: *Optics Express* 17.7 (2009), pp. 5691–5697.
[56] Giuseppe Patera and Mikhail I Kolobov. "Temporal imaging with squeezed light". In: *Optics letters* 40.6 (2015), pp. 1125–1128.
[57] Avi Pe'Er et al. "Temporal shaping of entangled photons". In: *Physical review letters* 94.7 (2005), p. 073601.
[58] Matthew Pelton et al. "Efficient source of single photons: a single quantum dot in a micropost microcavity". In: *Physical review letters* 89.23 (2002), p. 233602.
[59] Reza Salem, Mark A Foster, and Alexander L Gaeta. "Application of space–time duality to ultrahigh-speed optical signal processing". In: *Advances in Optics and Photonics* 5.3 (2013), pp. 274–317.
[60] Reza Salem et al. "High-speed optical sampling using a silicon-chip temporal magnifier". In: *Optics express* 17.6 (2009), pp. 4324–4329.
[61] Charles Santori et al. "Triggered single photons from a quantum dot". In: *Physical Review Letters* 86.8 (2001), p. 1502.
[62] Erwin Schrödinger. "The steady transition from micro to macro mechanics". In: *science* 14.28 (1926), pp. 664–666.
[63] R Mark Stevenson et al. "A semiconductor source of triggered entangled photon pairs". In: *Nature* 439.7073 (2006), p. 179.

© 2018 Tous droits réservés.

lilliad.univ-lille.fr

Thèse de Junheng Shi, Université de Lille, 2018

[64] Stefan Strauf et al. "High-frequency single-photon source with polarization control". In: *Nature photonics* 1.12 (2007), p. 704.

[65] Yifan Suen et al. "Time-frequency representation measurement based on temporal Fourier transformation". In: *Optics Communications* 376 (2016), pp. 86–91.

[66] Pierre Suret et al. "Single-shot observation of optical rogue waves in integrable turbulence using time microscopy". In: *Nature communications* 7 (2016), p. 13136.

[67] C Szwaj et al. "High sensitivity photonic time-stretch electro-optic sampling of terahertz pulses". In: *Citation: Review of Scientific Instruments* 87 (2016).

[68] Hiroki Takesue and Kyo Inoue. "Generation of polarization-entangled photon pairs and violation of Bell's inequality using spontaneous four-wave mixing in a fiber loop". In: *Physical Review A* 70.3 (2004), pp. 1–4.

[69] E. B. Treacy. "Optical Pulse Compression With Diffraction Gratings". In: *IEEE Journal of Quantum Electronics* 5.9 (1969), pp. 454–458.

[70] S Varoutsis et al. "Restoration of photon indistinguishability in the emission of a semiconductor quantum dot". In: *Physical Review B* 72.4 (2005), p. 041303.

[71] Edo Waks et al. "Secure communication: Quantum cryptography with a photon turnstile". In: *Nature* 420.6917 (2002), p. 762.

[72] Ian A. Walmsley and Christophe Dorrer. "Characterization of ultrashort electromagnetic pulses". In: *Advances in Optics and Photonics* 1.2 (2009), p. 308.

[73] Andrew M. Weiner. "Ultrafast optical pulse shaping: A tutorial review". In: *Optics Communications* 284.15 (2011), pp. 3669–3692.

[74] Zhiliang Yuan et al. "Electrically driven single-photon source". In: *science* 295.5552 (2002), pp. 102–105.

[75] Horace P Yuen and Vincent WS Chan. "Noise in homodyne and heterodyne detection". In: *Optics letters* 8.3 (1983), pp. 177–179.

[76] Yunhui Zhu, Jungsang Kim, and Daniel J Gauthier. "Aberration-corrected quantum temporal imaging system". In: *Physical Review A* 87.4 (2013), p. 043808.

© 2018 Tous droits réservés.

lilliad.univ-lille.fr